Lecture 9

Review 196

Solidification Structures and Properties of Fusion Welds

by G. J. Davies and J. G. Garland

To an increasing extent the wide range of fundamental knowledge of solidification processes is being applied to the study of fusion-weld solidification. Initially this fundamental knowledge is surveyed concisely and those areas of particular importance to weld-pool solidification are indentified. This is followed by an examination of phenomenological studies of the solidification behaviour of fusion welds in which particular attention is given to factors influencing the development of the fusion-zone structure. Then, the ways in which the metallurgical structure of the fusion zone influences the mechanical properties of the weldment are reviewed. Attention is then given to methods of controlling the fusion-zone structure by using inoculants, stimulated surface nucleation, dynamic grain refinement, and arc modulation. The gains and advantages which accrue from the way in which structure control affects properties are then considered. The review concludes with a discussion of likely future developments, paying specific attention to those areas where it is considered that fundamental research is most necessary, e.g. applications of arc-modulation processes and development of inoculation procedures.

Although over a number of years the understanding of the fundamental aspects of the solidification of cast metals has increased to a very substantial degree, this increased understanding has not been widely directed to the study of weld-pool solidification. When it is recognized that there have been enormous economic gains from the development of a foundry technology based on a fundamental understanding of solidification, it is most surprising that the control of weld-pool solidification to produce weldments with enhanced properties has been so neglected despite the potential rich rewards. (Efforts have been made, however, to develop empirical methods of control involving varying the process variables and these have dealt with some of the practical difficulties encountered in fusion welds, e.g. weld solidification cracking, porosity, etc.) Only recently has research been concentrated on using the wide range of fundamental solidification knowledge in the study of fusion weld-pool solidification. Then, not only has it proved possible to interpret phenomenological observations of the solidification behaviour of weld pools, but also it has led to the development of methods of structure control. These, in turn, offer great promise of significant improvements in weldment properties. In this review these three aspects of weld-pool solidification will be considered in turn. Initially, however, it is necessary to present a concise survey of the basic principles of solidification to indicate the current state of theory and experiment, to emphasize those areas of particular importance in the study of weld-pool solidification, and to establish the relationship between ingot solidification and weld-pool solidification.

This first section is followed by a review of the phenomenological observations of the solidification behaviour of fusion welds paying particular attention to the development of the fusion-zone structure. Throughout, the various observations are correlated with the fundamental data reported in the previous section. Subsequently, the ways in which the metallurgical structure of the fusion zone influences the mechanical properties of the weldment, are reviewed. Here, although the intention is to define general principles, some reference to the behaviour of specific alloys must necessarily be made.

A most important aspect is considered in the following section, namely, the definition of methods whereby the fusion-zone structure (and, therefore, the associated properties) can be controlled. A series of methods employing basic principles is described and discussed and some attention is given to current developments in practice. The gains and advantages accruing from fusion-zone structure control exerted by using these methods are described in the next section. This review concludes with a discussion of likely future developments in those areas where a lack of knowledge is hindering progress. Specific attention is given to those areas where it is considered that fundamental research effort is most necessary.

1. Basic Solidification Principles

Extensive details of the current state of theoretical and experimental knowledge of the solidification of metals can be found in recent monographs.[1-3] Only those fundamentals essential to an understanding of weld-pool solidification and relevant in assessing procedures for structure control will be described here.

1.1 Nucleation

Traditionally, nucleation phenomena are classified as homogeneous or as heterogeneous depending upon whether the nucleation events occur without or under the influence of impurities, inoculants, or external surfaces. In practice, homogeneous nucleation in liquid metals only occurs under the most carefully controlled experimental conditions and is a laboratory phenomenon. Heterogeneous nucleation is the norm and in castings, undercoolings of 5 –20 C are sufficient to provide the driving energy for nucleation. For nucleation on a planar substrate (Fig.1) the critical radius r^* and the work of nucleation ΔG^* are given by[1]

G. J. Davies BE, MA, PhD, CEng, MIMechE, AIM, is in the Department of Metallurgy and Materials Science, University of Cambridge. J. G. Garland, MA, PhD, AIM, MWeldI, was with the Welding Institute, Abington, Cambridge, and is now with the British Steel Corporation, General Steels Division, Research Centre, Middlesbrough.

$$r^* = \frac{2\gamma_{l,c} \cdot T_m}{L_m \cdot \Delta T},$$

and

$$\Delta G^* = \frac{4\pi\gamma_{l,c}^3 \cdot T_m^2}{3(L_m \cdot \Delta T)^2} \cdot (2 - 3\cos\theta + \cos^3\theta)$$

where $\gamma_{l,c}$ is the surface energy of the liquid-crystal interface, T_m is the equilibrium melting temperature, L_m is the latent heat of melting, ΔT is the undercooling below T_m, and θ is the contact angle. It is clear from these equations that the critical radius decreases rapidly with decreasing temperature as does the work of nucleation. In systems where the contact angle is small, it is apparent that the barrier to nucleation is small and the rate of nucleation I given by

$$I = K \exp[-(\Delta G^* - \Delta G_A)/kT]$$

where K is a constant, ΔG_A is the energy of activation for addition of atoms to the nucleus, and T is the temperature ($= T_m - \Delta T$), is then correspondingly rapid.

In fusion welds the weld pool is formed by melting regions of the base metal and thus there is always a region of solid in contact with the liquid.† This effectively reduces ΔG^* to a point where the nucleation barrier disappears. Only in those cases where artificial nucleating agents (inoculants) are introduced into the weld pool must the basic constraints of heterogeneous nucleation theory be taken into account. The use of inoculants is of great importance in casting technology. The factors determining inoculant effectiveness have been reviewed by Chadwick[5] and Hughes,[6] who have shown that both chemical and crystallographic parameters are important.

The above considerations treat nucleation as a quasi-static phenomenon. It is also possible to induce nucleation by subjecting the solidifying melt to dynamic stimuli. The most significant effects are achieved by introducing disturbances, e.g. vibrations, which fragment the interface of the growing solid and produce a grain-refining action. Here we have crystal multiplication and this is *not* a nucleation event in the normal sense. It is, however, an important means of exerting control over the grain structure, particularly with fusion welds since the interface is always present. Dynamic grain refinement is considered further in Section 1.5.

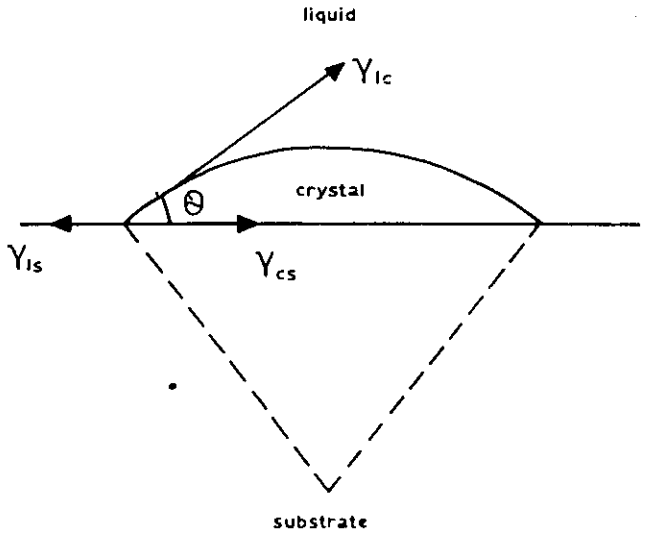

1 *Spherical cap of solid formed on planar substrate*

† This is discussed in greater detail in Section 3.1

1.2 Growth

After nucleation or in the presence of a pre-existing solid/liquid interface, growth occurs by the addition of atoms to the solid. Although three mechanisms for growth are normally considered, namely,

(i) normal growth[7]
(ii) growth by repeated surface nucleation[8]
(iii) growth on imperfections,[9]

only the first of these is important in casting and weld-pool solidification. For normal growth the interface advances by the continuous random addition of atoms and rapid growth rates are comparatively easily sustained. During normal growth the macroscopic form of the interface is determined by conditions adjacent to the interface and the interface may vary from being planar, through a cellular form, to being dendritic as the growth conditions alter. Conditions which give rise to constitutional supercooling[10] promote interface breakdown. These conditions are:

(i) low temperature gradients in the liquid
(ii) fast growth rates
(iii) for alloys, steep liquidus lines
(iv) high alloy contents (for castings and weldments constitutional supercooling normally will exist for alloy contents greater than ~0·2%)
(v) extreme values of the distribution coefficient k_0 given by the ratio of the solute concentration in the solid at a given temperature to the corresponding solute concentration in the liquid at the same temperature.

For low degrees of supercooling the interface is cellular[11,12] As the degree of supercooling increases a dendritic interface develops.[11] Dendritic growth is strongly crystallographic and the primary arms and side branches lie parallel to specific crystallographic directions,[12,13] e.g. the <100> directions in fcc and bcc metals and alloys. These are the rapid easy-growth directions. An extensive series of studies by Flemings and his co-workers[14-16] have shown that these cellular dendrites form a characteristic plate-like array with an arm spacing determined by the *local solidification time*. The local solidification time has been defined[14] as the time at a given location in a solidifying metal between initiation and completion (or near completion) of solidification. As the local solidification time decreases so does the dendrite arm spacing.

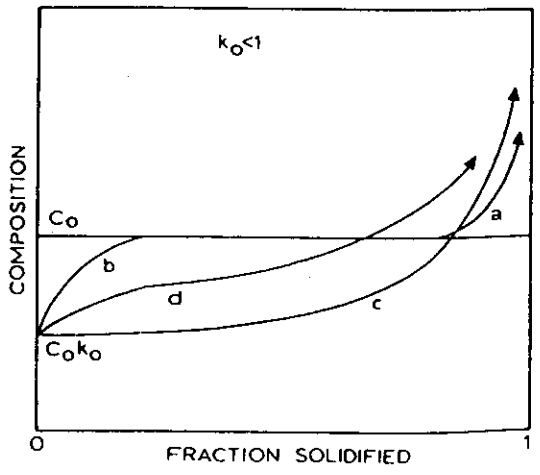

2 *Solute distributions in a solid bar frozen from liquid of concentration C_0: a equilibrium freezing, b solute mixing in the liquid by diffusion only, c complete solute mixing in the liquid, and d partial solute mixing in the liquid*

In most castings or weld pools conditions will be such that growth is cellular or cellular dendritic. Under these conditions the simplified concept of constitutional supercooling[19] is no longer applicable and attention must be given to the various contributions to the total undercooling near the liquid/solid interface. This undercooling is not only a function of the structure of the interface but is also dependent on the growth rate and temperature gradient in the liquid ahead of the growing interface.[20-22] Then the total *measured* undercooling ΔT is given by

$$\Delta T = \Delta T_C + \Delta T_r + \Delta T_K$$

where ΔT_C is the contribution due to the solute layer, ΔT_r is due to interface curvature, and ΔT_K is a kinetic contribution. Constitutional supercooling normally refers to ΔT_C only. ΔT_r is, for metals, usually assumed to be negligibly small compared with the other contributions. One important consequence of these considerations is that it is feasible under certain conditions for crystals to grow in the liquid ahead of the interface.

1.3 Redistribution of Solute

As alloys solidify there are marked effects resulting from the concurrent redistribution of solute. These are not only responsible for the changes in growth morphology referred to above but also lead to solute segregation on both a microscale and a macroscale (*see* Section 1.6). As a bar of initial composition C_0 solidifies directionally under conditions varying from equilibrium freezing to complete solute mixing in the liquid a range of solute distributions are produced[16, 21, 22] (Fig.2). These distributions are derived assuming the interface is macroscopically planar and experimental evidence[23] supports this assumption. In the presence of cellular or dendritic growth these will be *average* values only and substantial localized microscopic fluctuations in composition in both longitudinal and transverse directions are to be expected. If a change in the growth rate occurs during solidification macroscopic fluctuations in composition occur (Fig.3). These are usually associated with structural banding. Banding is very common in fusion welds because of the periodicity of the heat input and is apparent as both substructural bands (Fig.4) and as surface rippling.[24]

Frequently the expected average solute distributions are complicated by fluid-flow effects. For example, because of the contraction normally associated with solidification at the latter stages of solidification, solute-rich liquid can flow along the interdendritic channels in a direction opposite to the growth direction. This gives rise to a local solute distribution opposite to that predicted and this is known as inverse segregation.[25, 26]

1.4 Solidification of Multiphase Alloys

The solidification of alloys in which two or more phases are present is a complex process. In normal fusion welding eutectic alloys are rarely encountered. Peritectic alloys are

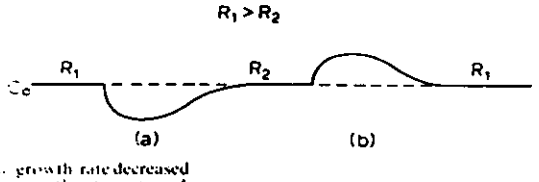

a growth rate decreased
b growth rate increased

3 *Effect of changes in growth rate on localized solute distribution in the solid*

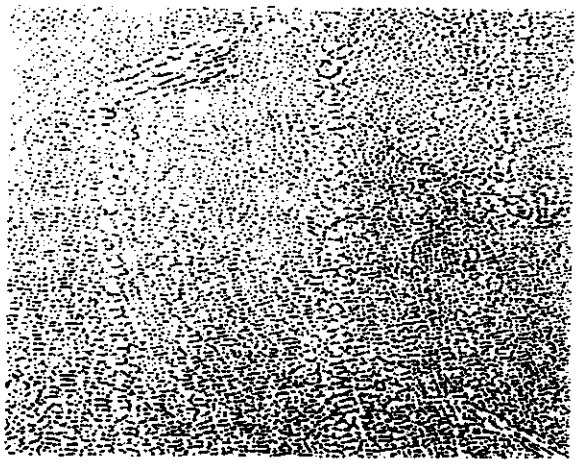

4 *Structural banding in an aluminium alloy fusion weld (Garland and Davies[24])* 80/

slightly more common and for virtually all compositions the solidified microstructure consists of cored primary dendrites of one phase surrounded by the other phases.[27] The peritectic reaction seldom proceeds to completion because it becomes stifled by the need for diffusion through the solid layer which rapidly encapsulates the primary phase.[28]

Insoluble particles and inclusions are common in weld pools and a knowledge of their behaviour during solidification is important. Although it is possible for the growing interface to push suspended particles before it, the conditions in a weld pool are such that particle entrapment is to be expected,[29] either by the advancing interface or by particles becoming isolated in regions between growing dendrite branches.

Gas porosity produced by the evolution of dissolved gas in metals is common because of the marked differences in the solubility of gases in liquid and solid metals. For example, at the melting temperature liquid aluminium dissolves 9·036 cm³ of hydrogen per 100 g whereas solid aluminium dissolves 0·69 cm³ per 100 g.[30] The high supersaturations that occur near the solid liquid interfaces lead to bubble nucleation and after this the bubble[31] (a) floats away collecting more gas and escapes at the free surface, or (b) moves with the interface,

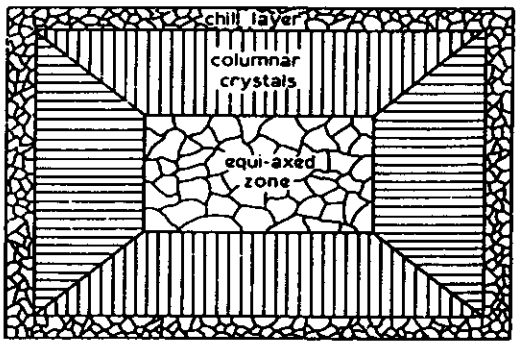

5 *Transverse section of an as-cast structure showing the chill zone, columnar zone, and equiaxed zone (Walker[33])*

growing at the same time and in due course becoming entrapped, or (c) becomes incorporated in the interface to form an elongated blowhole, or (d) is rapidly overgrown and entrapped.

In fusion welds dissolved gases are not uncommon and although in principle all the above modes of behaviour are possible the high growth rates make modes (c) and (d) the most probable. It means that steps are generally taken to eliminate dissolved gas from the weld pool, e.g. by the incorporation of oxygen scavenging agents into the welding flux.

1.5 Ingot Solidification

The macrostructure of a cast ingot normally consists of a chill zone, a columnar zone, and an equiaxed zone (Fig.5). The chill zone is produced by heterogeneous nucleation in the region adjacent to the mould wall as a result of thermal undercooling.[32, 33] Since heterogeneous nucleation is not expected in weld pools (*see* Section 1.1) this zone is absent. The columnar zone of an ingot develops by competitive growth from crystals at the initial solid liquid interface. These correspond to the partially melted crystals at the boundary of the fusion zone in a weld pool (*see* Section 2.1). The columnar crystals show a strong preferred orientation which corresponds with the preferred crystallographic directions of dendritic growth, i.e. <100> in cubic metals.[13] The columnar zone persists until conditions become favourable for the formation of equiaxed crystals which then grow, obstructing further columnar growth.

There are three major sources of nuclei for the equiaxed crystals.

(i) apparently isolated heterogeneous nucleation events in the melt[34]

(ii) fragmentation of the growing columnar zone[35]

(iii) nucleation events at the free surface.[36]

In ingot solidification all three sources are normally contributory to various degrees and it is manipulation of conditions to favour these different mechanisms which is foremost in the control of the cast structure.

Heterogeneous nucleation occurs in the initially chilled liquid on pouring and some of these nuclei can be swept into the bulk of the liquid and survive there.

Fragmentation occurs by dendrite remelting and is a consequence of thermal fluctuations associated with convection[35] (*see* Fig.6). Nuclei are produced at the free surface because of preferential heat loss and shower down into the liquid ahead of the columnar zone.[36] In all cases, however, it is important to note that it is *not* sufficient merely to generate nuclei but that these nuclei must survive without completely melting.

The morphology of the solidification front and the conditions and velocities of dendritic growth at and in front of the interface depend significantly on the rate of heat extraction and on the magnitude of the local supercooling.[37, 38] As mentioned in Section 1.2 thermal conditions can exist ahead of the columnar interface which favour the growth of 'nuclei' which exist ahead of the interface. The interruption of columnar growth occurs when the growing dendrite fragments floating in the liquid adhere to the solidification front. The effectiveness of the interruption process depends upon an interplay between the number and size of the floating crystals and on the shape of the solidification front.[39] The structure produced under given conditions in any system is logically dependent on the constitution of the system and the composition of the particular alloy under examination.[37]

In weld pools the very high temperatures in the liquid make fragment survival difficult and so normally only the columnar zone appears (*see* Section 3.3).

In casting practice structure control is normally exerted by introducing heterogeneous nucleants (inoculants)[7, 8] or by encouraging dynamic fragmentation of the growing dendrites (dynamic grain refinement) using, for example, mechanical stirring[41, 42] or ultrasonic vibrations.[43]

1.6 Segregation

Segregation is classified as either microsegregation (extending over distances of the grain diameter or less) or macrosegregation (extending over more than several grain diameters). In turn microsegregation is subdivided into cellular, dendritic, and grain-boundary segregation. The short-range effects occurring when an interface is growing in a cellular form[44] produce compositional variations which although large[11, 45] can readily be eliminated by heat treatment. Dendritic segregation either as coring or by the accumulation of solute in interdendritic spaces[46] is more difficult to eliminate. Grain-boundary segregation occurs either by solute accumulation in grain-boundary grooves (Fig.7*a*) or by the impingement of two interfaces growing with a growth component normal to each other (Fig.7*b*). This latter type of segregation is more properly considered as macrosegregation and centre-line solute accumulations can be very marked when columnar growth predominates.[47] The detailed nature of the segregation pattern is dependent on the growth conditions and morphology of the growing dendrites and is largely a manifestation of liquid flow in the semi-solid region.[48, 49, 50] Of the

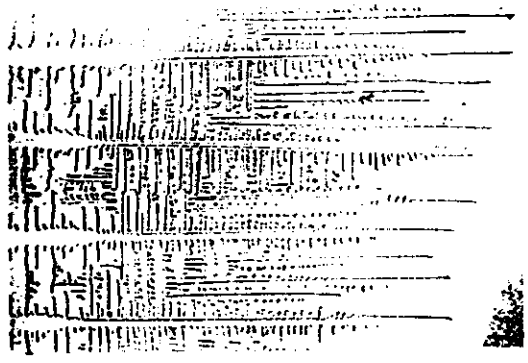

6 *Dendrite structure in transparent organic metal-analogue after a growth-rate fluctuation, the detachment by melting of dendrite arms can be clearly seen (Jackson et al.[30])*

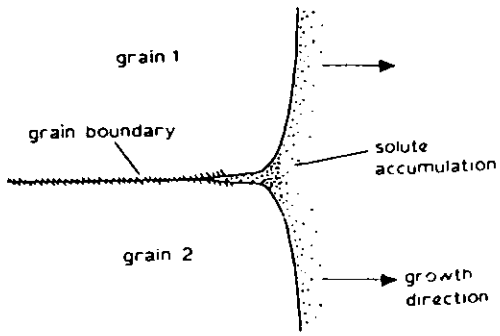

7*a* *Schematic representation of section through a grain-boundary groove*

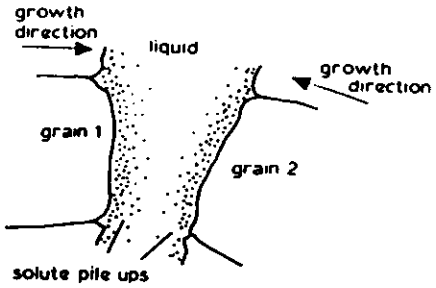

7b *Formation of grain boundary by impingement (schematic)*

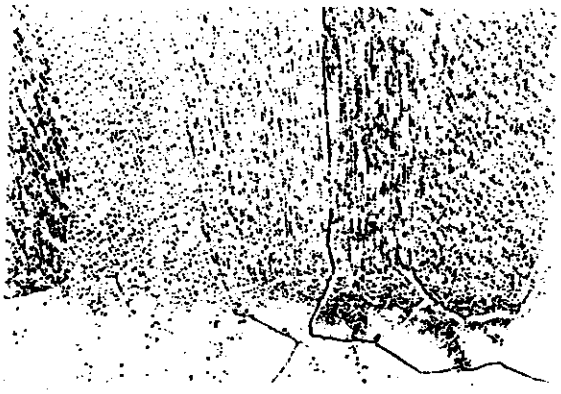

8 *Growth from the fusion boundary of TIG melt run in Al 4·5Cu sheet; the fusion-zone boundary is clearly defined in the partially melted grains* · 150

other main forms of macrosegregation, gravity segregation and inverse segregation are normally only expected in relatively large systems. They are not of particular relevance when considering weld-pool solidification and do not warrant further consideration here.

Normal macroscopic segregation can be described in terms of average compositions and directional growth leads to solute distributions broadly similar to those observed in directionally solidified bars,[42] e.g. as in Fig.2, when allowance is made for the influences of fluid flow.

1.7 Solidification Defects

Although a wide range of solidification defects commonly occur in castings[43] many of them are the result of deficiencies in casting practice. The three most important in the present context are:

(i) gas blowholes (porosity) produced by entrapment or generation of gas bubbles in the liquid (*see* Section 1.4)

(ii) contraction cracks (hot tears) formed when the metal pulls itself apart on cooling under the influence of thermal stress

(iii) shrinkage cavities which appear as a result of the volume contraction associated with the transformation from liquid to solid.

These can be avoided by degassing, control of thermal gradients, and promotion of directional solidification, respectively. In weld-pool solidification each of these three defects could possibly occur and similar remedies must, if possible, be adopted to eliminate them. It should be noted, however, that shrinkage cavities are only to be expected when the pool is very large.

2. Relationship between Ingot Solidification and Weld-Pool Solidification

While the process of weld-pool solidification is frequently compared with that of an ingot in miniature, a number of basic differences, already mentioned, exist which markedly influence the structure and ultimately the properties of the final weld deposit. These can be summarized as:

(a) during ingot solidification, the nucleation and growth of metal crystals takes place on pouring, generating the characteristic chill zone observed in most castings (*see* Section 1.5); in contrast, no nucleation event is necessary to initiate weld-pool solidification; the molten weld pool readily wets partially melted grains in the base material, which is usually similar in chemical composition to the weld pool itself; as the weld pool cools past its liquidus, a solidification interface is thus effectively present at the fusion boundary and growth takes place from partially melted grains in the base metal into the receding weld pool (Fig.8) with a minimum of supercooling

(b) macroscopic solidification rates in weldments are orders of magnitude greater than those found in ingots, being determined by the speed of welding, e.g. they vary from 100 mm/min in tungsten inert gas (TIG) welding up to as high as 1000 mm/min in electron beam welding; very steep thermal gradients in the weld pool are associated with these high solidification rates; the distance of the welding heat source from the solidification interface may vary from 2 mm up to more than 70 mm depending on the speed of welding and process considered; average thermal gradients of 72 °C/mm in the weld pool have been claimed during TIG welding,[53] while gradients of 40°C/mm have actually been measured near the trailing edge of a submerged arc weld pool[54]

(c) the overall macroscopic shape of the solid/liquid interface changes progressively with time during ingot solidification; in welding, however, a continuously moving interface bounds the weld pool, the shape of which remains constant over the major portion of the weld length; this is disturbed in general only by weld start and finish effects or external perturbations to the welding process by, for example, variations in arc behaviour

(d) the motion of the molten metal within a weld pool is typically much greater than that experienced in a solidifying ingot; this is particularly true of arc welding, where electromagnetic stirring of the weld pool generated by Lorentz forces creates conditions of considerable turbulence within the pool.[55]

To appreciate fully the implications of these differences in general solidification behaviour between a weld pool and an ingot, it is necessary to consider in detail the sequence of events taking place in a solidifying pool beginning with the initiation of growth at the fusion boundary.

3. Weld-Pool Solidification

3.1 Growth Initiation in a Weld Pool

The influence of base-metal grain size and orientation upon the initiation of solidification in a molten weld pool was first recognized and studied systematically by Savage and his co-workers,[56, 57] who concluded from the continuity of grains across the fusion boundary observed in melt runs on a range

of materials that solidification had begun by 'epitaxial' growth* on the parent plate (e.g. Fig.8). Such a process of growth at the fusion boundary must generate grains in the weld metal having the same crystallographic orientation as the immediately contiguous parent-plate grains across the fusion boundary, and this orientation relationship has been confirmed by Savage and Aronson[57] and a number of other investigators for both bcc[60] and fcc[33, 61, 62] metals using the Laue X-ray back-reflection technique. On the basis of these results, it thus seems well established that the growth initiation event in weld-pool solidification does not present a significant energy barrier. As mentioned above, the weld metal almost perfectly wets melted grains in the heat-affected zone (HAZ) of the parent plate and growth takes place from these grains into the weld pool after the passage of the welding heat source.

Since growth during weld-pool solidification begins from grains in the parent plate, the width of a weld-metal grain at the fusion boundary will be determined by the width of that grain in the HAZ acting as the growth substrate. This was observed in passing by Savage *et al.*[58] and has subsequently been studied in more detail by Matsuda *et al.*[33] and Loper *et al.*[63]

The size of a grain in the HAZ of a given base material depends on the magnitude and duration of the thermal cycle experienced during welding and the metallurgical characteristics of the material. Thus it might be expected that the size of the HAZ grains at the fusion boundary, and hence the immediately adjacent weld-metal grains, would depend upon those welding parameters which determine the extent of the thermal cycle in the base material. Loper *et al.*[63] have found, however, that the average width of both the HAZ grains and the weld-metal columnar grains at the fusion boundary remain approximately constant over a range of heat inputs up to 0·4 kJ/mm in TIG melt runs on 6·35 mm thick commercial aluminium plate. This research confirmed the results of Matsuda *et al.*[33] for commercially pure titanium, niobium, and tantalum, but not their results for zirconium, which showed some correlation between the width of the fusion boundary, weld-metal grains, and the welding speed at a fixed current level. Both these investigations were directed at unrealistically low heat-input situations compared with current trends in welding, however, and it is worth noting that under the higher heat-input conditions found in the electroslag and submerged arc welding of ferrous alloys, e.g. 8 kJ/mm, HAZ grain growth ahead of the molten zone could be a factor in determining the number of weld-metal grains at the fusion boundary and consequently the overall structure of the weld bead. The significance of such an effect has yet to be satisfactorily studied.

It has been tacitly assumed in the above discussion on the initiation of growth in weld-pool solidification that the fusion boundary can be located precisely as the point where complete melting has taken place. In general, this is not strictly true and it is not always possible to determine the boundary of melting with complete confidence. Savage and Szekeres[64] have shown that the apparent position of the fusion boundary in steel weldments made using filler wire additions to the pool depends on the method of etching of prepared metallographic specimens, and they suggest that this may be due to the existence of a region of melted base metal which has resolidified without mixing with the main body of the pool. This effect would not apply to simple melt runs, where the pool and the base plate were identical in composition, but would be significant in the realistic welding situation where filler metal of a different composition is used. Neither Duval and Owczarski[65] nor Makara and Rossoshinskii[66] were able to locate this region of completely unmixed, melted base metal in more quantitative studies but found instead a zone of incomplete mixing of filler and melted base metal at the extremities of the weld bead. Using electron microprobe analysis on the fusion boundary of a steel weldment, Duvall and Owczarski[65] identified a composition gradient extending from the average weld-metal composition into the HAZ for 80–150 μm until the average base-metal composition was reached. When considering welds made with filler metal additions it is, therefore, more appropriate to look upon the area of the bead immediately adjacent to the general fusion boundary as an ill defined region extending from the true weld metal, through the regions of incomplete mixing and of partial melting, eventually to the HAZ proper. This does not affect in any way, however, the validity of the conclusions discussed above on the nature of the initiation of growth in a solidifying weld bead.

3.2 Development of Grain Structure During Weld-Pool Solidification

The initial growth of partially melted grains in the parent plate is followed in weld-pool solidification by a period of columnar grain development during which a process of competitive growth occurs in an exactly analogous manner to that taking place in ingot solidification (*see* Section 1.5). This period of columnar solidification normally dominates the remainder of the weld-pool solidification since, as will be seen later, columnar-to-equiaxed growth transitions are comparatively rare during welding unless specific steps are taken to suppress columnar growth. Consequently, the overall solidification macrostructure of a weld bead is determined in general solely by the nature of the competitive growth process between adjacent columnar grains, and this therefore has a very significant influence upon the final properties of the fusion zone.

As described in Section 1.5 both fcc and bcc materials have as preferred easy-growth directions the <100> directions. Solidification usually proceeds along that easy-growth direction oriented most closely to the direction of the maximum thermal gradient in the melt. During welding the maximum thermal gradient in a weld pool is normal to the pool boundary at all points on the boundary and thus the form of the competitive growth process in a given material is uniquely controlled by the weld-pool geometry. Furthermore, the grain orientation in the weld metal at the fusion boundary is determined by the orientations of the partially melted grains and will therefore be most favourable for those grains growing from substrate grains with a <100> direction most nearly aligned parallel to the direction of the normal to the pool boundary at the moment of solidification being considered. This interaction between parent-plate grain orientation and the anisotropy of crystal growth and its effect upon the competitive grain-growth mechanism in welds of varying geometry, has been studied in detail by Bray *et al.*[62] They made full penetration TIG melt runs on deoxidized copper sheet in such a way that the fusion boundary of the welds ran through particular grains and twins whose local orientations had been previously determined. From considerations of the process of growth on these substrates of known orientation and the ensuing competitive growth in a pool of selected geometry, Bray and his co-workers were able to apply the general concepts discussed above to predict correctly which grain or twin would dominate the solidification in particular welds. This work

* Epitaxy or oriented overgrowth is usually reserved as a description for oriented crystallization on *foreign* substrates from the vapour[34] or liquid.[35] Growth from partially melted crystals without a nucleation event as in the case under consideration here cannot, therefore, strictly be described as epitaxial.

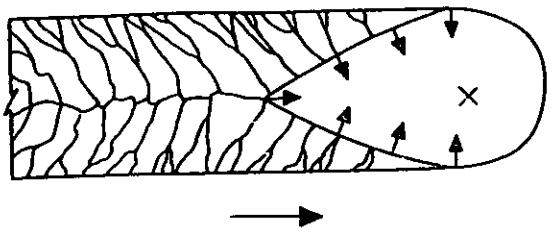

9 *Columnar development in a tear-shaped weld pool: arrows in the weld pool show the almost invariant direction of the maximum thermal gradient throughout a large proportion of the solidification time, this results in the early elimination of unfavourably oriented grains and few columnar grains survive to reach the centre line*

confirmed the results of earlier similar investigations by Savage *et al.*[58] and Chase,[61] and also showed that the theories developed to explain competitive growth in ingot solidification could be applied with confidence to the particular conditions of weld-pool solidification.

3.3 Influence of Weld-Pool Geometry

It is evident from the above discussion that a change in weld-pool shape caused by variations in welding parameters may markedly alter the structure of a fusion weld in a given material. Considering the two-dimensional shape of a weld pool, as seen on the weld surface, a tear-shaped weld pool has an almost invariant direction of maximum thermal gradient at all points on the pool edge from the fusion boundary to the weld centre (Fig.9). This results in any grain favourably oriented for growth at the fusion boundary being able to grow at optimum speed and expand at the expense of less favourably oriented grains. Relatively few grains thus survive to reach the weld centre. In contrast, in an elliptically shaped pool, formed at either lower welding speeds or higher welding currents than a tear-shaped pool, the direction of the maximum thermal gradient, i.e. the direction of the perpendicular to the pool trailing edge, changes continually from the fusion boundary to the weld centre (Fig.10). In consequence, no one grain experiences favoured growth for any extended period and very many more survive to reach the centre of the weld. This difference in macroscopic grain development for tear-shaped and elliptical weld pools has been demonstrated experimentally in a number of papers[37, 60, 67, 69] and, as will be seen in a later section, can have an important effect upon the properties of the weld bead.

A columnar grain which survives over any great distance in an elliptical weld pool exhibits considerable curvature (Fig. 11) due to the progressive change in the favoured growth

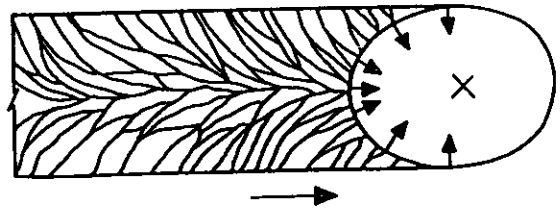

10 *Columnar development in an elliptical weld-pool, the progressive change in direction of the maximum thermal gradient is reflected in the survival of many more columnar grains*

11 *Curved columnar grain development in an elliptically shaped weld pool in an Al–2·5Mg alloy* ·30

direction. The crystallographic orientation of this grain remains constant, however, the curvature observed being generated by the repeated side-branching of the solidification substructure.[69, 70] As such columnar grains develop, a situation may be reached when growth by side-arm branching becomes difficult for a number of adjacent grains due to the relative orientation of the easy-growth direction and the continually changing direction of the maximum thermal gradient. Under these circumstances, a new columnar grain may be initiated from a random solid fragment which has been incorporated into the advancing interface from the melt with a <100> direction oriented parallel to the direction of the maximum thermal gradient at that particular moment of solidification.[67, 69, 71] This fragment is thus able to grow more rapidly than neighbouring grains and rapidly expands to dominate the local solidification process. The source of these solid fragments during welding has yet to be investigated, but it would seem clear that they are generated by some process of interface fragmentation similar to that which can occur in ingot solidification due to either thermal fluctuations in the melt or mechanical disturbances at the solid/liquid interface. Indeed, it is important to note in this context that recent work on grain refinement during weld-pool solidification[34] has demonstrated that variations in arc behaviour, such as arc vibration or periodicity in the heat input to the pool associated with cyclic current characteristics, can promote such interface fragmentation (*see* Sections 4.2 and 4.3).

The nature of the solid fragments which initiate new columnar grains during normal solidification in an elliptical weld pool may vary from apparently minute dendrite fragments[67, 71] to relatively large grains exhibiting free dendritic growth morphologies[31, 71] similar to those observed by Southin[36] in the heads of the characteristically comet-shaped grains found in the equiaxed and columnar zones of a solidified ingot. The occurrence of solid fragments within the body of columnar development in a weld pool is promoted, as in ingot solidification, by conditions which enhance constitutional supercooling and dendrite remelting in the melt.[67, 71] This is substantiated by the increased tendency to observe large fragments showing evidence of free dendritic growth at high alloy contents.[71] Solid fragments of the type described above are also found in tear-shaped as well as elliptical weld pools, but under these conditions of invariant direction of maximum thermal gradient, they tend to be grown out by the already

12 *Small comet-shaped grains in the body of the columnar region developing from a tear-shaped weld pool in an Al 2·5Mg alloy* · 60

well established columnar grains (Fig.12). The existence of solid fragments ahead of the growing interface has important implications in both the columnar-to-equiaxed growth transition during welding and the control of weld-pool solidification, and these are considered in more detail in subsequent sections.

The importance of weld-pool geometry in determining the form of the solidification macrostructure has encouraged a number of research workers to try and develop mathematical equations capable of predicting the two-dimensional, weld-pool shape for a range of welding conditions and materials.[54, 55] All of this work has built into it a number of very arbitrary assumptions made to simplify the heat-flow problems associated with the welding situation under study. In particular, the fundamental assumptions are made that weld-pool shape is dependent solely upon the heat-flow pattern in the base material and that the welding arc can be considered as a moving point heat source. Weld-pool shape is critically affected by the turbulence pattern in the melt, however, which depends in turn upon current paths in the pool.[56, 57] The equations obtained have thus had little appreciable success in predicting actual weld-pool shape. Zanner[58] has attempted a more realistic approach to the problem, using impulse decanting to reveal the three-dimensional pool shape in the TIG welding of mild steel. With the aid of regression analysis, he succeeded in developing a computer model simulating the welding process which enabled predictions to be made of the weld speed and current necessary to produce a weld pool of specified length, width, and depth. Despite this sophisticated approach, however, considerable error still remained, particularly in the prediction capability for speed.

The geometry of the weld pool places certain requirements upon local solidification rates at different points along the pool interface if the shape of the pool is to remain constant. Over a given time interval, the interface at the centre of the weld pool must, by the nature of the shape of the pool, travel a greater distance than the growing interface at any other position on the pool boundary. This led a number of workers[59, 54, 55] to propose that the local solidification rate at any position on the pool boundary should be given by $V\cos\theta$, where V is the welding speed and θ is represented diagrammatically as the angle between the normal to the tangent to the pool at the point considered and the welding direction (Fig. 13*a*). This assumes, however, that crystal growth is isotropic

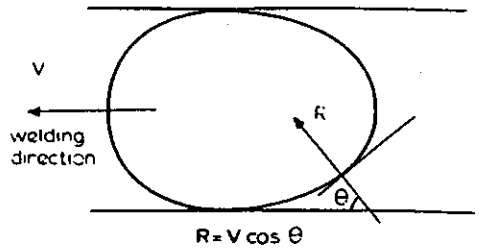

13*a* *Solidification rates at different positions on the trailing edge of the weld pool (assuming isotropic growth)*

and takes place along the direction of the maximum thermal gradient, i.e. in the direction of the normal to the fusion boundary. In fact, as discussed above, rapid growth takes place along that favoured growth direction most nearly aligned with the direction of the maximum thermal gradient. Accordingly, some adjustment to the expression for local solidification rates is required to allow for this anisotropy of crystal growth. Nakagawa *et al.*[60] were the first investigators fully to appreciate this and their expression for local solidification rates makes the necessary corrections to the above work (Fig.13*b*). Thus, the local solidification rate is given by

$$R = \frac{R_n}{\cos(\theta' - \theta)} = \frac{V\cos\theta}{\cos(\theta' - \theta)}$$

where R_n is the growth rate in a direction normal to the isotherm and θ' is the angle between the welding direction and the direction of favoured growth. Thus, in welding the solidification rate is greatest on the weld-pool centre line where $\theta = 90$. At this point the temperature gradients are most shallow because of the distance from the welding heat source. The lowest growth rates are found at the weld-pool edge ($\theta = 0$) where the gradients are steepest because of the proximity of the heat source. This is in contrast to the situation in castings where maximum solidification rates are normally associated with maximum temperature gradients and vice versa.

3.4 Columnar-to-Equiaxed Growth Transition

In contrast to ingot solidification, natural transitions from columnar to equiaxed growth are comparatively rare during weld-pool solidification. As discussed in Section 1.5 some

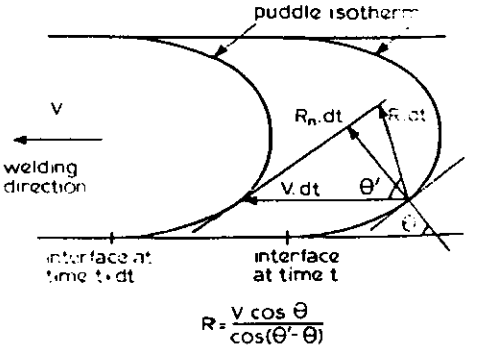

13*b* *Relationship between welding speed and actual growth rate (Nakagawa et al.[60])*

limited generation of nuclei can take place during welding associated with either arc instabilities or periodicity in heat input. The thermal conditions in the melt are so severe during welding, however, that nuclei survival is very limited unless either the mechanisms promoting nuclei generation are particularly effective, which is normally only the case when steps are specifically taken to obtain equiaxed growth (*see* below), or the conditions of welding are such as to produce a high level of cellular or dendritic undercooling in the pool. Accordingly, nuclei are rarely present in sufficient size and number to physically block columnar development and promote true equiaxed growth. At best some refinement of overall columnar grain size is achieved by the repeated incorporation of individual isolated nuclei into the overall growth pattern.

Equiaxed weld-pool solidification thus tends to occur unaided in the region of the centre line of the pool, where solidification rates are highest and the thermal gradients flattest due to the distance of the arc, and is generally associated with high welding speeds[53, 58] and high alloy contents.[58, 81] For example, Matsuda *et al.*[53] only succeeded in generating equiaxed grains at the centre of full penetration melt runs in 0·32"„ steel sheet, 1·0 mm thick, when the welding speed reached 1 m/min and Miller[81] found that equiaxed dendrites were formed in welds made on 70Cu–30Ni sheet only with welding conditions giving a long weld pool, viz. at high travel speeds. High welding speeds also encourage equiaxed growth because of the overlap of the regions of solute accumulation ahead of the converging solidification fronts at the centre of the tear-shaped pools formed at rapid welding speeds (Fig.9). This provides a region of weld pool uniquely suited to the growth of fragments ahead of the melt as the weld pool progresses along the parent plate.

3.5 Growth Substructures in Weld Metals

One of the first investigations into the nature of growth substructures in weld metal was by Calvo, Bentley, and Baker[82] in which cellular, cellular–dendritic, and free dendritic growth modes were observed in stationary melt pools for a variety of materials. It was found that the higher the alloy content of the pool, or the flatter the thermal gradients, the greater the tendency for cellular–dendritic and ultimately free dendritic growth modes to form. These observations were originally explained using concepts of constitutional supercooling although they should now be considered in terms of the total cellular and dendritic undercooling[17–20] (*see* Section 1.2). Savage *et al.*[56] confirmed these findings and extended the work to include substructures observed in normal weld beads laid down over a range of welding conditions. This work and a later, more detailed study by Savage, Lundin, and Hrubec[83] showed that it was possible to generate a range of growth substructures in melt runs in a given material simply by varying the welding conditions. Working on TIG melt runs in low-alloy steel, they found that increasing welding current at a fixed welding speed, or decreasing speed at a fixed current level, caused the melt run substructure to change from a cellular to a cellular–dendritic growth mode. Although it was again proposed that the variation in welding conditions had promoted the observed growth transitions by flattening the thermal gradients in the pool, so increasing the undercooling ahead of the advancing interface it is feasible that a decrease in welding speed alone might have been expected to stabilize cellular growth through the associated reduction in the solidification rate of the pool (*see* Section 1.3).

While these extensions of the theories of undercooling to the study of weld-metal growth substructures are further indications of the basic similarity of fusion welding to other solidification processes, it is worth remarking at this point that structural transitions in weld metal of the type outlined above have been explained in detail by a number of investigators, notably Savage and his co-workers, on the basis of the solidification parameter $G/R^{\frac{1}{2}}$. This parameter was first introduced by Tiller and Rutter[11] in an attempt to quantify the boundary solidification conditions for particular growth modes. There is, however, no sound experimental evidence for the adoption of this *specific* form of thermal gradient–solidification rate relationship[84] and correspondingly its limited value in weld-pool solidification studies should be recognized.

The variation in both local solidification rate and thermal gradient in a single weld on moving around the fusion boundary from the side to the weld centre line causes a progressive change in solidification substructure across an individual weld bead. At the side of the pool steep thermal gradients together with comparatively low solidification rates favour cellular growth while at the weld centre line, high solidification rates promote a transition to dendritic growth modes. As a result, a range of growth substructures can be observed in melt pools[82] and in individual weld beads, particularly at relatively high welding speeds.[53, 79, 80] At speeds used in normal welding practice only a gradual increase in the dendritic nature of the substructure is observed on moving across the weld bead.

Although well defined, preferred <100> crystallographic growth directions have been confirmed in welds of both fcc and bcc materials,[53, 60, 69] Nakagawa *et al.*[67, 71] observed that the secondary dendrite arms could be misoriented from the main stem by as much as 10° in some instances. It was proposed that this was due to physical distortion by the high levels of turbulence characteristic of molten weld pools. This theory had been advanced previously by Weinberg and Chalmers[85] to explain misorientations of a similar nature observed in ingots. Cell orientations during welding show a more marked dependence upon welding conditions than do more dendritic growth modes[69] and, in particular, appear to be influenced markedly by welding speed. During a study of melt runs on aluminium single crystals,[60] the direction of cellular growth at slower welding speeds (225 mm/min) was observed to move away from <100> towards the direction of maximum thermal gradient. Increasing the welding speed, however, reduced this deviation and at higher welding speeds (1500 mm/min) the cellular growth direction was found to correspond closely to the characteristic easy-growth direction of <100> for fcc metals. In this context, it is worth noting that these results are in agreement with earlier fundamental work on the general effect of solidification rate upon cellular growth directions.[86]

As discussed earlier, solidification rates in fusion welds are normally much greater than those in conventional castings and this is reflected in the fine scale of the resultant solidification substructures. Brown and Adams[87] found that the only castings in Al–4·4Cu–0·9Si which had interdendritic spacings of the same order (9 μm) as welds made with heat inputs of around 1·18 kJ/mm, were droplets of 1–2 mm diameter quenched in a stream of nitrogen. The local solidification time[14] (*see* Section 1.2) in a weld will depend upon the rate of cooling of the weld through the solidification range at that locality. From these considerations, Brown and Adams[87] predicted theoretically that the dendrite arm spacing in partial penetration welds deposited under conditions of three-dimensional heat flow on relatively thick plate would be related directly to the square root of the heat input per unit length of weld. This calculation was based on a very much simplified analysis of one-dimensional dendritic growth,[88] which yields the expression for dendrite arm spacing L,

$$L^2 = \frac{8\,D\Delta T t_0}{m(1-k_0)C_0}$$

where D is the diffusivity of solute in the liquid, ΔT is the undercooling, t_0 is the local solidification time, m is the slope of the liquidus, k_0 is the distribution coefficient, and C_0 the alloy composition.

Substituting in this expression the cooling rate (local solidification time) at the centre of a partially penetrating arc deposit, assuming three-dimensional heat flow, i.e.

$$t_0 = \frac{L_m q}{2\pi K C_p V (T_m - T_0)^2}$$

where L_m is the latent heat of fusion, q is the arc power, K is the thermal conductivity, C_p is the specific heat of the solid alloy, V is the arc travel speed, T_m is the liquidus temperature of the alloy, and T_0 is the initial temperature of the plate, gives the relationship between dendrite spacing and arc energy or heat input per unit length of weld

$$L \propto \left(\frac{q}{V}\right)^1$$

Results of work on aluminium, copper, and nickel alloys confirmed their predictions, and subsequent work by Jordan and Coleman[89] and Lanzafame and Kattamis,[90] which is summarized graphically in Fig.14, has substantiated the existence of such a relationship.

Jarman and Jordan[91] extended this work to full penetration welds on Al–4·5Cu sheet, where the conditions of heat flow were essentially two-dimensional. Using the same approach as that of Brown and Adams, they showed both theoretically and practically that dendrite arm spacings under these conditions were directly proportional to heat input per unit length of weld. The results of work on the influence of local solidification time upon interdendritic spacing in castings would thus seem to be equally applicable to weld-pool solidification, again emphasizing the basic similarity of the two processes.

A progressive decrease in dendrite arm spacing between the fusion boundary and weld centre line can be observed in individual welds. It has been suggested[90] that this may be due to the increased solute segregation at the weld centre line (*see* below) reducing the rate of dendrite coarsening[16] during the local solidification process so promoting a finer final solidification substructure. The effect of solute content upon dendrite arm spacing is not yet clear, however, even in ingot solidification[11, 14, 92] and it is more likely that the variation in spacing within a given weld is simply the result of the changes in local solidification rate at different positions on the advancing solid/liquid interface necessary to maintain constant weld-pool geometry (*see* above). Most rapid weld-pool solidification occurs at the centre of the bead, which would thus be expected to have the finest solidification substructure.

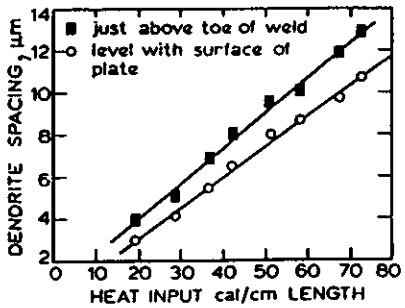

14 *Relationship of dendrite arm spacing and heat input in cal cm length for Al–Mg–Mn alloys (Jordan and Coleman[89])*

3.6 Solute Segregation During Weld-Pool Solidification

As will be seen in Section 4 segregation during weld-pool solidification may lead both to variations in mechanical properties throughout the deposit and to the occurrence of solidification cracking. Despite this influence upon in-service performance, however, comparatively little quantitative information is available on the form which solute segregation may take in a weld bead, probably because of the very fine nature of the solidification substructure which often precludes meaningful electron probe microanalysis. Nevertheless, Miller[81] has established the presence of a solute-rich layer ahead of the advancing solid/liquid interface in a weld pool and, using microprobe analysis on back-filled weld-metal cracks, has also shown that the values of the equilibrium distribution coefficients for a variety of solute elements are the same in both weld-pool solidification and ingot solidification. The basic mechanism of solute segregation thus appears to be the same in both cases and, just as in ingot solidification, microsegregation is more pronounced in a weld bead, the more dendritic is the solidification mode, e.g. interdendritic Mn levels of 6·9% have been recorded in welds on a Cu–Si–Mn alloy compared to 5·4% at cell boundaries, on changing the welding conditions.[93] Furthermore, it has been found[80] during the welding of a commercial aluminium alloy that increasing the weld cooling rate by decreasing the energy input from 3·31 kJ/mm to 1·65 kJ/mm reduces the amount of any non-equilibrium interdendritic second phase caused by solute segregation while at the same time increasing the solute content (Cu) at the centre of the dendritic arms. The reasons for this latter effect are not yet clear, but may be associated with solute entrapment in the primary phase at the very rapid solidification rates characteristic of welding.[90, 94]

Segregation at grain boundaries will be greater than that encountered within the substructure composing the grains and both Miller[81] and Bell[95] have identified the existence of such enhanced grain-boundary segregation during welding. This is particularly true where the outward growing grains from both sides of a weld impinge at the centre line and tend to trap the solute-rich liquid (cf Fig.7*b*). This is most marked for welding conditions which produce a tear-shaped weld pool and hence a steep angle of abutment between the columnar grains at the weld centre.[83]

A very characteristic segregation pattern observed frequently in both manual and automatic welding, made with or without the use of filler additions, is solute banding (*see* Section 1.3). This solute banding may be observed as periodic regions of solute enrichment or depletion and is revealed on etching a weld surface, as light or dark lines marking successive positions of the advancing interface (Fig.15). In extreme cases, lines of porosity may be located on subsequent sectioning of the weld bead outlining an instantaneous position of the trailing edge of the weld pool. It was realized quite early in the study of weld-pool solidification that such segregation patterns in weld metal could adversely affect the subsequent physical and mechanical behaviour of the weld metal and the possible mechanisms of formation of this solute banding have thus received considerable attention.

Since the mode and extent of solute redistribution is a function of the solidification conditions and partitioning characteristics of the system, solute banding must reflect some periodic change in these characteristics. The surface of a weld bead, even when deposited using an automatic process, exhibits

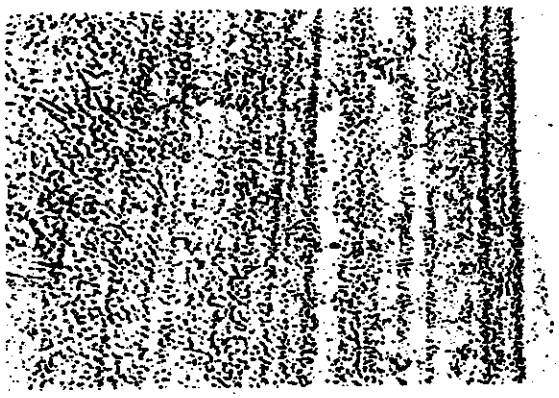

15 *Solute banding at fusion boundary of submerged arc weld; etched in a saturated solution of picric acid containing a wetting agent to reveal S and P segregation; material, mild steel* ·60

periodic undulations or ripples (Fig.16). These ripples represent a disturbance of the molten weld pool which is likely to be reflected in the solidification of the bead and some correlation thus might be expected between such surface ripples and the change in solidification behaviour of the weld pool necessary to cause solute banding. Direct experimental evidence for such a relationship was obtained on welds made with cyclic current characteristics by Cheever and Howden,[98] who found a similarity in the periodicity of the two effects. This was substantiated in a later, more detailed study by Garland and Davies.[21] In this investigation, weld-surface ripples in TIG ac melt runs were found to correspond not only with solute banding, but also with an associated periodicity in the solidification substructure (*see* Fig.4).

A number of explanations have been advanced to account for surface rippling and solute banding. Prior to the work outlined above most of these were based on an *assumed* correlation between the two disturbances in weld-pool solidification. The essentials of these various proposed mechanisms of formation are considered below:

(a) solidification halts are said to occur during welding due to the removal of supercooling at the interface by the rapid evolution of latent heat caused by the high rates of solidification[66, 96, 101]; during each halt, it is proposed that diffusion of solute takes place from the solid to the adjacent liquid which, when solidified on the recommencement of growth, generates the solute banding observed, e.g. as in Fig.15

(b) local periodic variations in the solidification rate of the weld bead take place due to a retardation in growth of the primary dendrite arms caused by heat evolution during branching to form secondary arms[102]; surface rippling of the weld bead is supposed to be formed concurrently by an interaction between the surface tension of the receding melt pool and the periodic growth of the advancing dendrite tips

(c) variations in the power supply to the welding head cause periodic changes in solidification rate through their effect on the arc force on the weld pool and the heat input to the weld[102, 103]

(d) fluctuations in weld-pool turbulence due to either "arc resonance",[83] or to the Lorentz forces acting on the pool[85, 88] disturb the surface of the pool and form both rippling and solute banding

(e) the confined weld pool under the influence of the downward stream of shielding gas, e.g. in TIG welding, assumes a mode of periodic oscillation with an associated effect on solidification characteristics due to the change in surface tension of the liquid metal with temperature as it moves either nearer or further from the welding heat source[100]; this effect would seem of marginal importance, however, since rippling is observed in electron beam welds in the absence of a gas shield and in melt pools after the extinction of the arc[21]; further, the variation in surface tension of liquid metal with temperature is very small.[105]

A number of these hypotheses would, however, have been expected to be equally applicable to solidification processes other than welding, e.g. (a) and (b), where solute banding and associated surface rippling are *not* normally observed, and all lacked conclusive supporting experimental evidence until comparatively recently, when it was found that surface rippling was only associated with solute banding and structural periodicity in the weld bead where the welding current had cyclic characteristics, e.g. ac or dc arcs with superimposed ripple.[24]

The frequency of this surface rippling is the same as that of

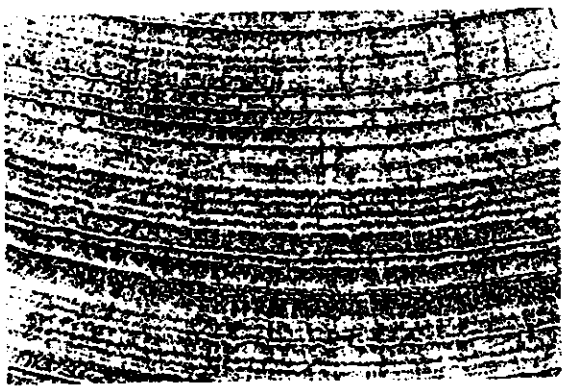

16 *Surface undulations in TIG melt run on an Al–2·5Mg alloy* 30

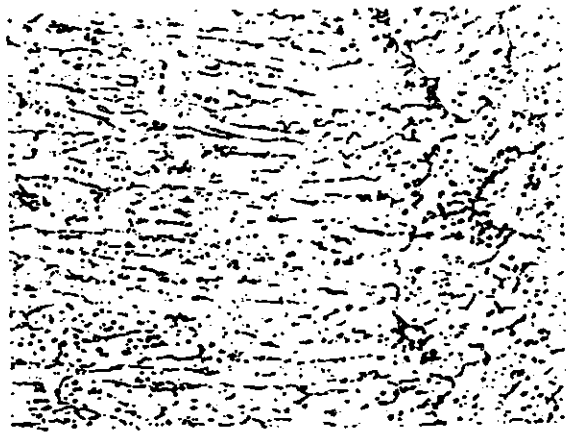

17 *Characteristic form of a growth perturbation in an Al–2·5Mg alloy* ·500

the power source and it now seems well established that specific regular changes in the arc characteristics once every complete current cycle[51] can cause an increase in temperature at the solid/liquid interface, and with this a periodic retardation in its rate of advance into the weld pool. Such a change in solidification rate will generate both the characteristic pattern of structural banding observed in the weld bead (Figs.4 and 17) and the line of solute enrichment marking the instantaneous position of the interface when the normal faster growth mode is reassumed for the majority of the current cycle.

Less regular surface rippling without any corresponding perturbation of the solidification substructure has also now been recognized in welds and melt pools made without any periodicity in the power source.[21, 106] While the former effect would seem to be due simply to uncontrollable variations in arc stability,[24] it has been demonstrated conclusively[106] that melt-pool rippling is caused by oscillation of the weld surface after the removal of the pressure of the arc plasma on the extinction of the arc.

For castings it has been proposed[19] that solute-rich or solute-poor bands can result from fluctuations in the position of the growing interface. These fluctuations were the result of periodic changes in heat flow and are analogous to those observed in arc welds when the arc energy is varying.

It will be evident from the preceding discussion that solute segregation in the weld bead can take a number of forms which could lead to variation in mechanical properties throughout the weldment and also to the occurrence of a range of weld-metal defects including porosity and solidification cracking. The influence of the nature of weld-pool solidification upon the subsequent in-service performance of the welded joint and the soundness of the deposit is outlined in the following section.

4. Relationship Between Solidification Structure and the Properties of Weldments

Since the mode of weld-pool solidification controls the size and pattern of solidified grain development as well as the nature and extent of the associated solute segregation in the weld bead, a significant correlation would be expected between solidification pattern and the properties of the weld deposit. While the existence of such a relationship has long been recognized, the absence until comparatively recently (*see* Section 5) of any systematic study of the effect of modifications in the mode of weld-pool solidification, independent of welding conditions, upon the properties of the weld bead has limited the direct experimental evidence available. Many of the experimental data, as outlined below, have been obtained with a variety of alloy systems, emphasis being placed on the particular property under consideration rather than on the nature of the parent material. No detailed investigations have been performed on the effect of the mode of weld-pool solidification upon the whole range of relevant weld-metal properties in a given alloy system. The remainder of this section must, of necessity, reflect the limited nature of the available data and it is intended, therefore, to concentrate in turn on individual weld-metal properties, identifying where appropriate the alloy systems which have provided the experimental data.

4.1 Solidification Cracking

Solidification cracking frequently occurs between the growing grains during the terminal stages of weld-pool solidification (Fig.18), when the thermal strains applied across adjacent grains exceed the ductility of the almost solidified system.[19, 107] The various theories[105, 110] are effectively identical and embody the idea of the formation of a coherent interlocking solid network separated by essentially continuous thin liquid films which are ruptured, without healing, by the contraction stresses. As the contacting dendrites pull apart, the liquid films solidify giving the fracture surface a rounded dendritic morphology (Fig.19). Solidification cracking is thus favoured by factors which decrease the solid solid contact area during the last stages of solidification. This concentrates

18 *Solidification cracking in two-pass submerged arc weld in a C-Mn steel* ×4

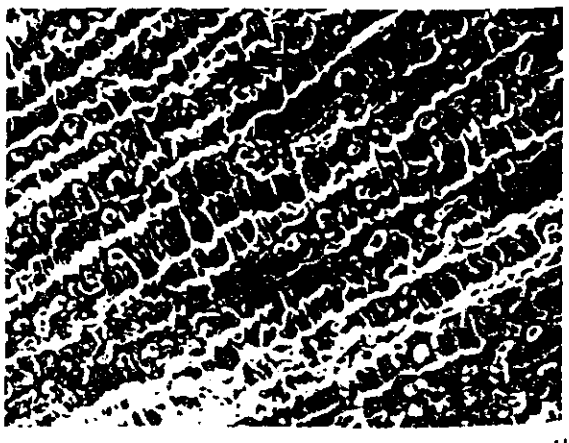

19 *Fracture surface of solidification crack in maraging steel weld metal viewed in scanning electron microscope* ×90
(Courtesy V. Bailey, Welding Institute)

the contraction stresses at a relatively small number of solid bridges in the weld pool. These factors include:

(i) low melting point segregates
(ii) the solidified grain size.

Low melting point segregates may persist as grain-boundary films to temperatures well below that of the effective alloy solidus. This allows the contraction stresses to rise to a high level in the pool while at the same time keeping the area of grain-boundary contact small.[111] The larger the solidifying grain size the smaller the area of grain-boundary contact is for a given liquid content.[112] This increases the solidification crack susceptibility. Thus coarse-grained weld metals are more prone to the formation of solidification cracks.

Both these factors are critically dependent on the nature of the solidification processes in the weld pool. The role of solidified grain size in determining crack susceptibility has only recently become clear with the advent of reproducible techniques for refining the solidification structure of the weld pool. This is discussed in Section 6 after techniques of refining the solidified grain structure have been considered.

A number of studies have been carried out, however, in which the important influence of segregation patterns in controlling solidification cracking susceptibility have been examined. Before discussing this work, it is appropriate to note that the importance of solute segregation in determining the likelihood of solidification cracking has stimulated interest in predicting the nature of the solidification processes in the weld pool and the form of the associated grain-boundary segregates in a given alloy system from a consideration of equilibrium phase diagrams.[110] The extent of the departure from equilibrium during weld-pool solidification due to the rapid solidification rates (*see* Section 2) is so great, however, and its variation with welding conditions so large, that such an approach has little real value. Information of this nature can only be obtained from an initial direct experimental study over the range of welding conditions likely to be encountered in practice. Accordingly, it is not proposed in this section to pursue further the application of equilibrium diagram data to weld-pool solidification. The work correlating segregation patterns with solidification crack susceptibility is presented on an essentially empirical basis.

The influence of the solidification macrostructure of a weld bead upon the extent of solute segregation, and hence the likelihood of solidification cracking, is most clearly evident at the weld centre line. Solidification cracking occurring at the point of impingement of the columnar grains growing from opposite sides of the weld pool is a very frequently observed weld-metal defect. As the columnar grains grow out into the weld metal and take part in the competitive growth process, the solute-rich liquid present at the solid/liquid interface moves toward the weld centre line. Where the outward growing grains impinge, the solute-rich liquid from both solidification fronts tends to be trapped, forming a boundary region at the weld-pool centre line. When the angle of abutment of columnar grains is steep a liquid film is retained between the impinging grains and fracture can occur under the influence of transverse contraction stresses. Working with a low-alloy steel, Savage *et al.*[43] have shown that welds made with a tear-shaped weld pool, where the angle of abutment between the columnar grains is steep (Fig.9), are inherently more susceptible to solidification cracking than welds made with elliptically shaped pools. In the latter case, the much shallower angle of abutment of the grains tends to sweep the solute-rich liquid out into the weld pool instead of trapping it at the weld centre line (Fig.10), and under these conditions the contraction stresses have a much less marked effect.

From a general consideration of the solute segregation associated with different solidification substructures a dendritic substructure would be expected to have a greater susceptibility to solidification cracking than a more cellular growth morphology. This has been investigated by Bray and Lozano[93] in the Cu–Si–Mn alloy system, where they tested the solidification cracking susceptibility of different substructures using a cruciform-type cracking test. The observation that crack propagation in these tests ceased when a structure transition from cellular-dendritic to cellular took place in the solidified bead led them to claim that the cellular growth mode was the least susceptible to cracking. The strain applied to the solidifying bead in this work, however, was thermally induced. A structure transition in the weld implies a change in the thermal field surrounding the bead and this will alter the strain applied to the solidifying pool. It is this strain which causes cracking. It was, therefore, impossible to determine unequivocally whether it was a change in structure, or simply a change in applied strain, which terminated the crack. Such problems are inherent to cracking tests of this type, where thermally generated strains developed in the testpiece during welding cause cracking. The influence of different solidification substructures upon solidification crack susceptibility thus remains to be established.

If low melting point segregates occur and are concentrated at the regions of grain impingement then there is a marked increase in cracking susceptibility. This is particularly the case with steels in which sulphur and phosphorus segregation can enhance weld cracking[113, 114] by prolonging the stage at which liquid films exist.

In cast metals it has been observed[107, 115, 116] that fine-grained materials are far more resistant to cracking than coarse-grained materials. This has been shown[117] to be due to the greater ability of fine-grained castings to deform to accommodate the contraction strain. Furthermore, it is clear that liquid feeding can proceed more effectively in fine-grained material. Thus incipient solidification cracks can more readily be healed. The evidence of the grain-size effect in welding is less well established.

4.2 Mechanical Properties

Apart from some anisotropy in weld-metal properties as a result of the preferred orientation developed in the fusion zone during competitive grain growth,[60] particularly under conditions favouring a tear-shaped weld pool, the effect of the mode of weld-pool solidification upon mechanical properties again stems directly from the pattern of segregation in the bead. This is evident on both a macroscopic and microscopic scale.

Probably one of the most significant results of the normal columnar growth mode of fusion welds is the formation of a plane of weakness at the centre of the bead where the two solidification fronts from opposite sides of the weld impinge. This is most pronounced in large, coarse-grained deposits such as those formed in the submerged arc or electroslag processes,[118] e.g. Fig.18.

The enhanced level of solute and impurity segregation at the centre of a bead need not cause solidification cracking but instead can, under certain circumstances, so impair the toughness of the weld deposit as to make it unsuitable for in-service application. Indeed, acceptance codes for particular high heat-input welding procedures now contain provisions to assess the extent of this effect by specifying Charpy V-notch impact test specimens from about the centre line of the weld. The causes of this low level of toughness at the weld centre line may include embrittlement due to grain-boundary precipitation and

non-metallic inclusion films[119] or, in the case of transformable alloys, a change in the nature of the weld microstructure in this region as compared with the rest of the bead (*see* below).

The nature and extent of interdendritic and cellular solute segregation can influence the strength and response of a non-transformable weld deposit to post-weld heat treatment, or where solid-phase transformation occurs after solidification, can alter the form of the final microstructure of the weld bead. It has been shown in a range of commercial aluminium alloys, for example, that the smaller the dendrite size, the higher the yield strength[90, 119] and ductility[119] of the weld, and the more rapid the attainment of optimum mechanical properties during heat treatment,[87, 90, 119] due to the finer distribution of interdendritic, second-phase precipitates associated with this solidification mode.

For example, Fig.20, from the work of Lanzafame and Kattamis,[90] shows how this is achieved by refining the dendrite arm spacing by decreasing the heat input (cf Fig.14).

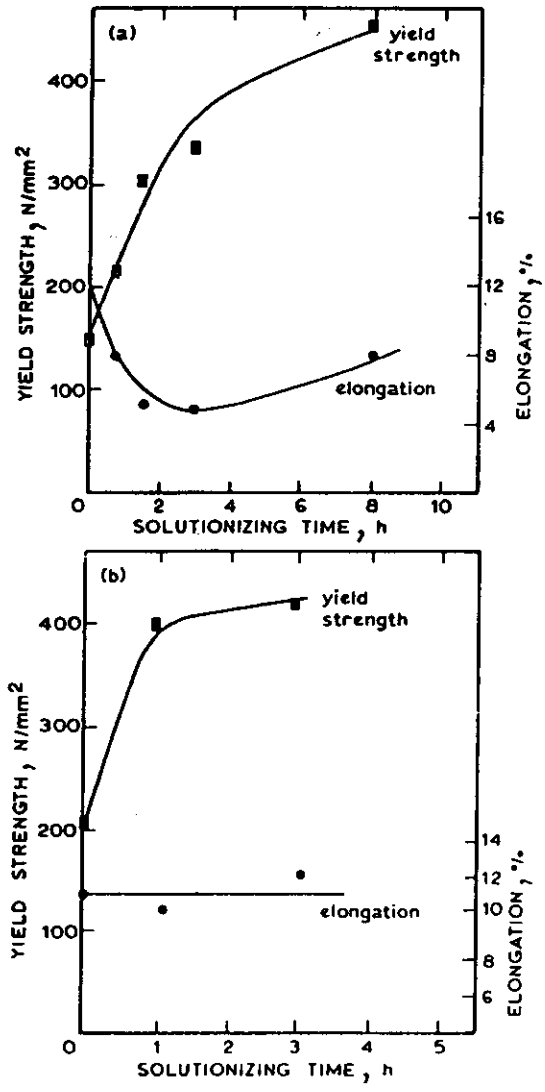

a coarse dendrite structure, 3·3 kJ mm weldments
b fine dendrite structure, 1·6 kJ mm weldments

20 *Variation of yield strength and elongation with solutionizing time at 500 C in 2014 aluminium alloy welds (Lanzafame and Kattamis[90])*

It is less easy to identify any correlation between mechanical properties and solidification substructure in a weld bead which has undergone solid-phase transformation since the original solidification mode tends to be obscured by the final microstructure. In mild and low-alloy steel weld metal, however, a relationship is clearly apparent between the segregation associated with the extended cellular-dendritic growth characteristic of these materials and the formation of low-temperature transformation products and, in particular, low- and high-carbon martensites.[120, 121]

Under particular welding conditions and with particular consumables, low- and high-carbon martensites and bainitic carbides form in groups of islands along the prior solidification boundaries (Fig.21). This produces a marked falling away in as-welded impact strength.[120] After a standard stress-relief heat treatment, e.g. 650 C for 2 h,[122] degeneration of these phases into ferrite–carbide aggregates occurs which gives an increment of toughness provided no other microstructural changes occur.

Some form of relationship must also exist between the segregation associated with the extended cellular–dendritic growth characteristic of alloy steels and thin veins of pro-eutectoid ferrite in the transformed microstructure (Fig.22). This relationship may be due essentially to the grain boundaries formed during the initial solidification of the bead acting as nucleating sites for the first transformation products, the nature of which is determined by the effect of the segregation of alloying elements upon the hardenability of the deposit.[34] Such elongated veins of pro-eutectoid ferrite, separated by lower-temperature transformation products, are known to reduce the toughness of the weld bead compared to more equiaxed microstructures.[123, 124] Similar correlations may also be established under certain circumstances between the distribution of delta ferrite in austenitic stainless steel weld metal and the initial solidification substructure.[125]

With the increasingly severe demands being placed on the properties of welded fabrications, the deleterious influence of normal weld-pool solidification upon certain properties of the weld deposit has stimulated research into techniques for controlling weld-pool solidification to produce welds with improved properties. The results of this work are discussed in the following section.

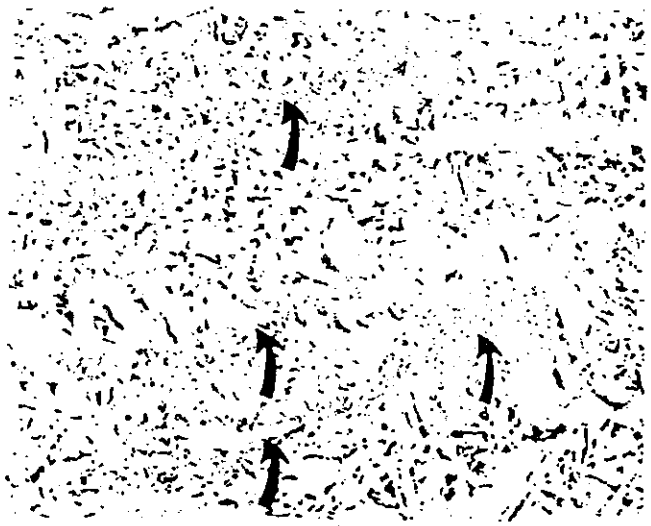

21 *Banding of martensitic microphases (arrowed) along solidification boundaries in a C–Mn–Si–Al–Nb steel weld metal* 500

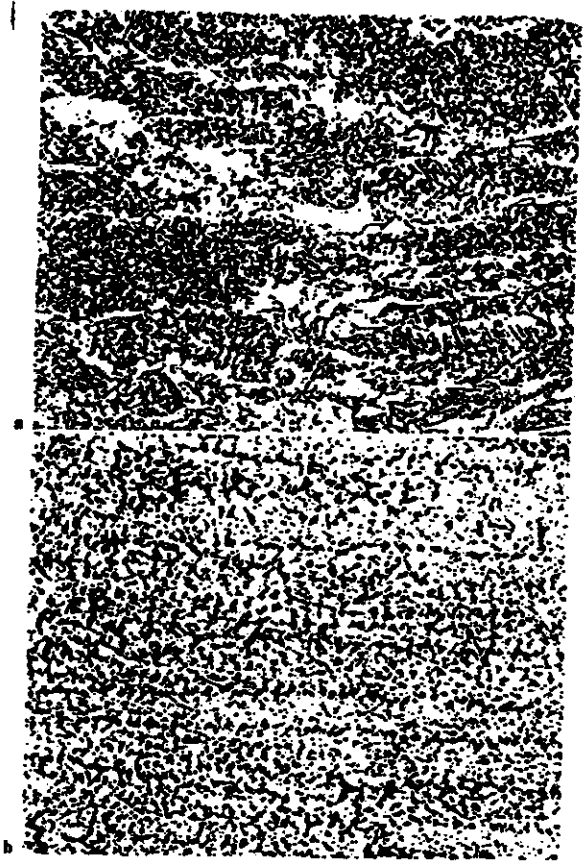

a general microstructure: etched in 2 % nital
b S and P segregation at the cellular-dendrite solidification boundaries in the same area of the weld: etched in a saturated solution of picric acid containing a wetting agent

22 *Mild steel submerged arc weld metal showing the general correlation between pro-eutectoid ferrite banding and segregation pattern in head* · 5*0*

5. Control of Weld-Pool Solidification

The need for the control of the structure of solidifying weld pools is clear from the results described in the previous section. As outlined there are three major requirements:

(i) control of the distribution of grain sizes and shapes
(ii) control of segregation
(iii) control of solidification cracking.

In normal casting practice[1-3] structure control can readily be obtained either by control of nucleation using heterogeneous inoculants, or by dynamic grain refinement utilizing (a) nucleation events at the free surface, and or (b) fragmentation of the growing dendrites by mechanical or thermal means. Because of scale effects (*see* Section 2) control of events occurring in the weld pool is more difficult than the control of structure in castings. In addition, the absence of a discrete nucleation event (*see* Fig.8) introduces further complications. In controlling the grain structure, and particularly when aiming to produce grain refinement, it is necessary both to produce nuclei for new grains *and* to ensure that they survive. In this section the different methods which have led to structure control will be described.

5.1 Control by Using Inoculants

This is, in principle, one of the simplest approaches to the control of grain structure in the weld pool. It involves the introduction into the pool of effective heterogeneous inoculants which will induce the nucleation of new grains and which will, in due course, be incorporated into the advancing interface. The main difficulty in applying this technique in fusion welding arises because of the high temperatures in the pool, particularly in the vicinity of the arc. The inoculating particles must be protected from these high temperatures if they are to survive. Attempts to inoculate the pool by introducing the inoculants as part of the wire which is actually supporting the arc thus have little chance of success. Early work on the grain refinement of mild steel submerged arc weld pools[124, 125] either used alloyed filler rods or tubular electrodes filled with the addition agents and iron powder. Some grain refinement and some reduction in the dendrite arm spacing were produced but these were probably as much the result of alloying effects and the introduction of melt supercooling as they were the result of inoculation action. In one study[126] which formed part of a more general examination of the inoculation of steel castings[129, 130] it was possible to identify ferro-titanium, ferro-niobium, and titanium carbide as effective grain refiners of steel. This last compound together with titanium nitride were also found to be most effective inoculants in a separate extensive study of the nucleation of liquid iron.[131]

Very few attempts have been made to introduce the inoculants near to where they are required to act, i.e. immediately

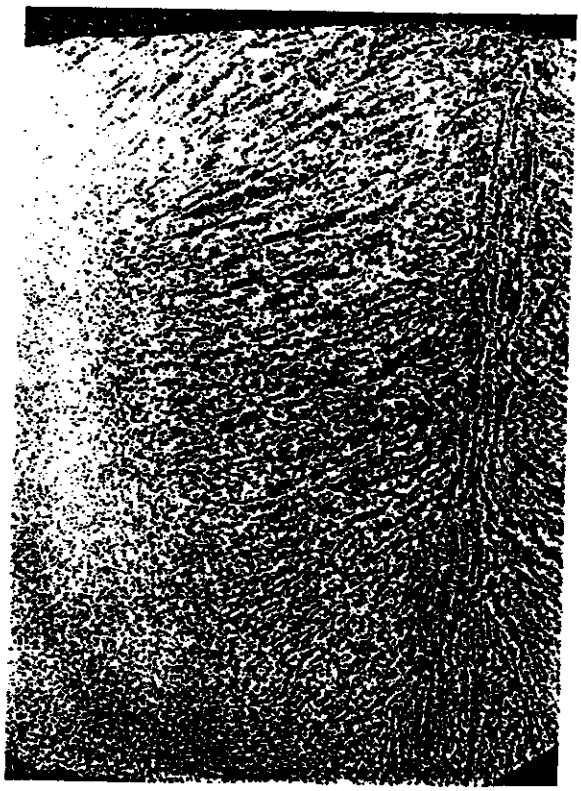

23*a* *Columnar solidification pattern of a mild steel submerged arc weld deposited without modification* · 6

23b *Submerged arc weld produced under conditions of optimal grain refinement by inoculation* · 6

ahead of the trailing edge of the weld pool. Alov and Bobrov[132] achieved considerable grain refinement of submerged arc welds in aluminium by introducing zirconium or titanium inoculants from the flux. Similar work on steel[127] using titanium in a ceramic flux reportedly led to complete suppression of columnar growth although no metallographic evidence was provided in support of the claim.

In the work already described and in work to be discussed below, attention has been concentrated on submerged arc welds. Only with the large weld pools obtained in submerged arc welding is it possible to make additions easily to the weld pool. This is particularly the case if substantial additions are to be made away from the arc near the trailing edge of the weld pool. Grain refinement in austenitic stainless steel submerged arc welds was achieved[133] by introducing the inoculant using an auxiliary feed wire situated some distance behind the arc. In a similar way it has been shown that additions of metal powder[134] or chopped wire[135] having the same composition as the weld metal can produce some grain refinement and some refinement of the dendrite arm spacing. None of this work investigated in any detail the effect of the position of introduction of the inoculant supply upon the grain refinement achieved. Furthermore, neither the influence of welding parameters on the efficiency of inoculation nor the subsequent properties of the inoculated weldment were satisfactorily studied.

In recent work by Garland[51] on the inoculation of mild steel submerged arc welds with titanium carbide and ferrotitanium titanium carbide mixtures a number of variables

24a *Microstructure of an unmodified weld bead; etched in nital* 50

were studied in detail. The inoculant was introduced by feeding it in inside a mild steel tube. This tube was led through the flux into the rear of the pool at various selected positions. The rate of inoculant supply, the position of introduction of the inoculant, the size of the inoculant powder, and the welding conditions were all examined as variables. The undisturbed weldment showed a well developed columnar structure (Fig. 23*a*). Equiaxed growth could be induced (Fig.23*b*) provided sufficiently high feed rates of inoculant were achieved. Conventional metallography reveals evidence of grain refinement (Figs.24*a* and 24*b*) but unequivocal evidence is only obtained by the use of a selective etchant (in this case picric acid together with a wetting agent SASPA–Nansa) which reveals the location of segregated sulphur and phosphorus. This is determined by the original as-solidified grain structure and is not affected by the subsequent γ to α transition. Typical results are given in Figs.25*a* and 25*b*.

This grain refinement involved the formation of heterogeneous solidification nuclei of titanium carbide in the weld pool, together with the generation of sufficient constitutional supercooling through titanium solution in the melt to provide

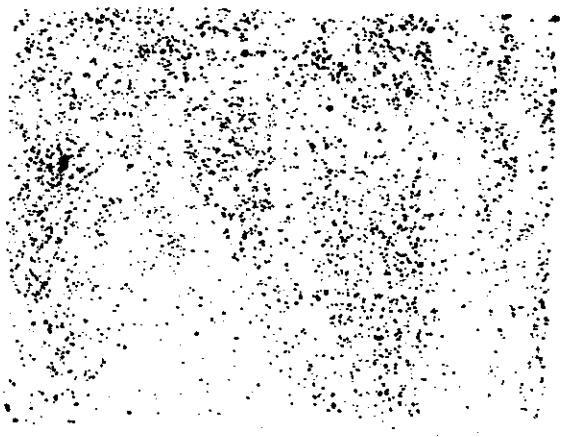

24b *Microstructure of a modified weld bead; etched in nital* · 50

25*a* *The section of Fig.24a etched to reveal columnar solidification structure* · 50

the necessary driving force for growth on these nuclei ahead of the advancing solid/liquid interface. Grain refinement only became possible when enough of the growing crystals were present in the melt to obstruct further extensive columnar development. The effective operation of this grain-refining technique was shown to depend critically upon:

(i) *the rate of inoculant supply*: fully equiaxed solidification only occurred at inoculant supply rates above a critical level, in this case corresponding to a total titanium content in the weld pool of 0·18%.

(ii) *the position of inoculation in the pool*: inoculation near the trailing edge of the weld pool was the most effective in promoting grain refinement

(iii) *the size of the inoculant powder*: the equiaxed grain size generated with ferro-titanium powder of 75–53 μm particle size was noticeably finer than that formed with a particle size of 500–390 μm

(iv) *welding conditions*: the higher the heat input during welding, the less effective was the TiC formation in the melt essential for grain refinement.

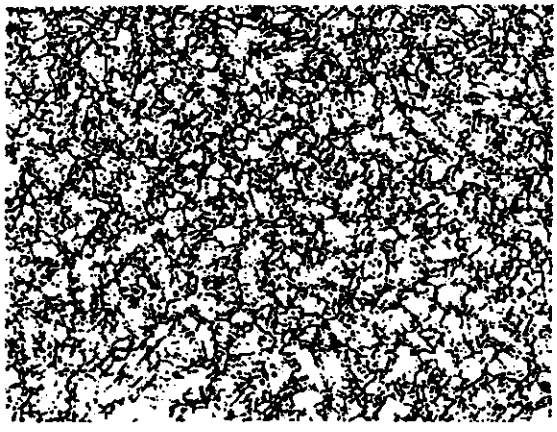

25*b* *The section of Fig.24b etched to reveal equiaxed solidification structure* · 50

If excessive amounts of titanium (> 0·3%) were retained in solution then undesirable low-temperature transformation products were formed on cooling. Control could be exerted to some extent by using an equally proportioned mixture of ferro-titanium and titanium carbide. With such a mixture the onset of effective grain refinement occurred at a reduced rate of inoculant supply.

The presence of titanium in solution in the weld pool also led to the formation of other products, e.g. titanium sulphide, which had a deleterious effect on the properties of the weldment (*see* Section 6).

This work thus clearly indicated the general feasibility of the grain refinement of large welds by inoculation without providing any indication that such an approach would yield any significant practical benefit.

5.2 Control by Stimulated Surface Nucleation

As established by Southin[36] a significant contribution to the formation of the equiaxed zone in ingots comes from crystal fragments generated by cooling and subsequent nucleation at the surface. This suggests that some degree of suppression of columnar growth in the weld pool might result if conditions were created which induced nucleation on the surface of the weld pool. This has been studied by Garland[34] who produced nuclei by directing streams of argon on to the weld pool surface through small nozzles. Various nozzle geometries were examined. The most effective was one in which three nozzles

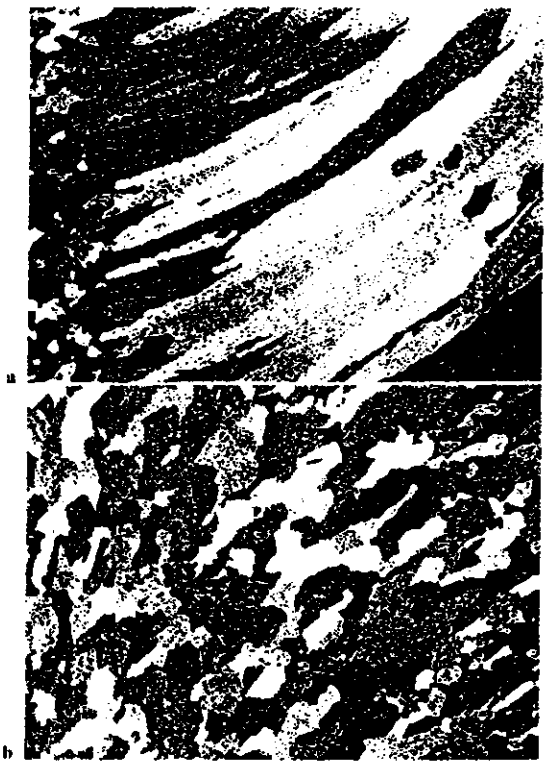

a without argon flow on to the surface
b with argon flow on to the surface

26 *Solidification structures of an Al–2·5Mg alloy weld, 3·2 mm thick, deposited* · 50

were used, one impinging on the pool surface ahead of the arc and two impinging on the plate at the trailing edge of the weld pool. These latter two nozzles were also instrumental in controlling the weld-pool shape and producing the most advantageous pool geometry (cf Figs.9 and 10). This technique was effectively used to produce the complete suppression of columnar growth in TIG welds of an Al–2·5Mg alloy (Fig. 26*a* and *b*) although it was found that refinement occurred only over a limited range of welding conditions (Fig.27).

The equiaxed grains formed have the same characteristic comet-shaped morphology as those found by Southin[38] in ingots. The head of each of these 'comet' grains exhibits a free dendritic type of substructure, while the tail develops in the same mode and direction as the body of the weld bead. The presence of two clearly distinguishable growth régimes in a single grain implies, under these conditions, two distinct periods in the life of the grain. For the first part of its life, the grain must presumably have existed as a discrete fragment of solid which was detached from the interface and able to grow in a free dendritic manner. Eventually it would appear that this solid fragment met the advancing interface and became incorporated into its growth pattern. Rapid growth could then take place along those dendrite arms in the fragment oriented nearly parallel to the direction of the maximum thermal gradient of the solid/liquid interface as it advanced past, thus generating the highly directional substructure composing the tail of the grain. Each grain could then take part in the normal competitive growth process in the weld pool until it was eliminated by ultimately more favourably oriented grains, so forming the comet-like morphology exhibited to varying degrees by all of these grains.

One possible effective source of the very many free dendritic solid fragments composing the heads of the comet grains was the surface nucleation and growth stimulated by the action of the argon jet on the surface of the pool ahead of the arc. Under the conditions of rapid cooling present at the pool surface at the point of impingement of the argon jet, free dendritic growth was promoted by the local high driving force for solidification and the characteristic substructure form of the comet heads was developed by the individual growing fragments. Although the solid fragments so formed were subjected almost immediately to the passage of the arc, some must have already been carried to the sides of the pool by the high levels of turbulence present in the melt, and were thus in a position to survive the passage of the arc without complete remelting. Once the arc had passed, these remaining fragments were carried to the advancing solidification front by the weld-pool turbulence, where sooner or later incorporation into the overall solidification pattern took place.

For complete grain refinement, enough solid fragments had to be supplied to physically block columnar development at all points on the advancing interface. Furthermore the nuclei supply needed to be continuous or else a reversion to the natural columnar growth occurred. The high level of weld-pool turbulence therefore must play a critical role in the achievement of weld-metal grain refinement through its action in continuously transporting the solid fragments from the surface of the pool, ahead of the arc, to the whole of the advancing solidification front.

This method of grain refinement was not, however, effective with material in excess of ~5 mm thickness. Here only the upper part of the fusion zone exhibited a refined grain structure, due to the failure of sufficient nuclei to survive during transport from the weld surface to the increased depths of the weld pool.

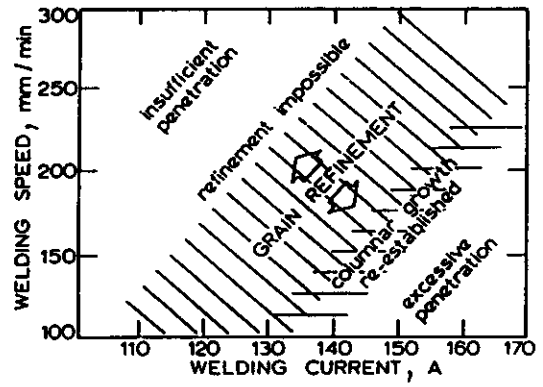

27 *Effect of variations in welding conditions on the effectiveness of grain refinement by stimulated surface nucleation of an Al–2·5Mg alloy, 3·2 mm thick*

5.3 Control by Dymanic Grain Refinement

As described in Section 1.5 crystal fragments generated by dendrite remelting are a prominent source of equiaxed crystals in ingots and castings. The formation of these fragments is enhanced by stirring arising either from free or forced convection. The primary requirement is that the growing interface becomes subjected to fluctuating thermal conditions.

There has been little attempt to apply this approach to the solidification of welds, even though the mechanics of weld solidification were long known to be basically identical to those of castings.

Arc Vibration and Weaving

In an effort to improve the external appearance of the weld bead and the stability of the arc in TIG and MIG welding, Alov and Vinogradov[136, 137] studied the effect of arc motion transverse to the direction of welding. Not only was a considerable improvement in weld appearance and arc stability achieved, but also the weld metal was found to possess enhanced properties. This effect was most noticeable at the lower level of the electrode vibration frequencies studied (15 Hz) and at vibration amplitudes of about 5 mm. Although the improvement in properties was ascribed to the refining effect of arc vibration on weld-pool solidification, no systematic investigation was undertaken. As the results of this work indicated that the optimum effect of transverse arc motion was at the lowest frequency and highest amplitude levels studied, Russian work tended to concentrate on frequencies and amplitudes of arc movement within the electrode weaving range, e.g. 5 Hz, 3–5 mm amplitude. Electrode weaving was found to improve bead shape considerably in TIG,[138] submerged arc,[139] and electroslag welding [140] as well as producing better weld-metal properties compared with those of welds made without electrode weaving.[141] Deminskii and Dyatlov[142] used an alternating magnetic field about the arc to generate electrode motion transverse to the welding direction in the MIG welding of Al–Mg alloys and they observed a reduction in weld porosity, together with some unspecified grain refinement. No further details were given, however, regarding the frequency and amplitudes of weaving studied.

Electrode weaving in submerged arc welding has been used on an industrial basis to achieve improved weld-metal appearance[143] and also to refine the solidification structure.[144] The arc weaving was generated by two severely kinked consumable

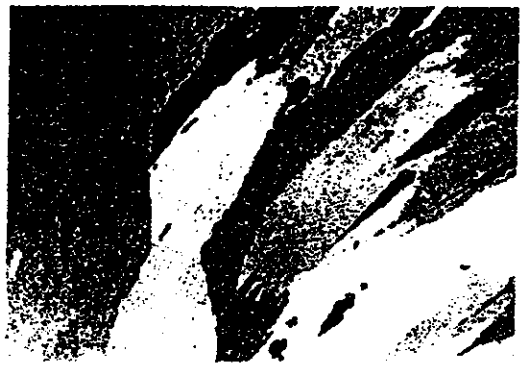

28a Normal columnar structure of a TIG weld in an Al-2·5Mg alloy · 25

electrodes in a twin arc assembly. The pool motion so formed was described, hardly surprisingly, as vigorous and some resultant grain refinement was claimed, although the photomicrographs published to illustrate this refinement show very little suppression of columnar growth. The mechanism proposed for this grain refinement was interface fragmentation caused by pressure pulses resulting from the motion of the kinked electrodes, but it is very doubtful that vibrations at 8 Hz and amplitudes of 8 mm could have generated this cavitation type of effect. Moreover, all of the photomicrographs, published in this and previous work on weaving, seem to indicate that geniune grain refinement was not in fact achieved. No repeated substantial nucleation and growth of the new grains needed to block columnar development is evident. Instead, the effect of weaving appears to have been to ensure the survival of many more columnar grains during competitive growth by producing continual distortion of the weld-pool shape. Although this would undoubtedly give some improvement in weld-metal properties it cannot be considered as a true grain-refining effect. Suppression of columnar growth does appear to have been achieved in the electron beam welding of aluminium bronze at relatively high welding speeds (500 mm/min).[115] Vibration of the electron beam was applied parallel to the welding direction at frequencies of up to 300 Hz and amplitudes of 2·5 mm. Some grain refinement was observed under these very favourable conditions of high solidification rates and alloy content, although once again the interpretation of the photomicrographs is not clear and no detailed investigation was attempted.

Transverse and longitudinal arc vibration has also been made use of by Tseng and Savage.[116] This failed to produce grain refinement but formed a refined substructure with enhanced properties (*see* Section 6). On the other hand very effective grain refinement was produced in Al-Mg by Garland[31] using vibration parallel to the weld direction. The resultant motion of the arc caused backwashing of the pool over the interface which fragmented and reoriented the solidification substructure at the trailing edge of the pool to yield the necessary supply of nuclei.

This work showed that this technique could be used to completely suppress columnar growth as shown in Figs.28*a* and 28*b*. The feasibility of achieving high levels of grain refinement using torch vibration was found to depend critically upon a number of factors:

(a) *the frequency of torch vibration*: an optimum frequency was observed which was determined by the welding conditions themselves

(b) *the amplitude of torch vibration*: this is illustrated in Fig.29

(c) *the rate of heat input during welding*: this was a function of the welding current and the welding speed and it was found that refinement was limited to a band of welding conditions for a sheet of given thickness (Fig.30)

(d) *sheet thickness*: overall grain refinement was only possible in sheet up to 3·2 mm thick; above this a considerable increase in grain size with depth in the weld bead occurred until, at a thickness of 6·3 mm, no significant suppression of columnar growth could be achieved anywhere in the bead

(e) *arc length*: for a maximum refinement at given conditions of welding and torch vibration, the arc length needed to be as short as was compatible with process stability.

The general restrictions to grain refinement, discussed above, do not detract from the fact that practically meaningful refinement can be achieved in TIG welds in thin aluminium alloy sheet using the simple physical technique of arc vibration parallel to the welding direction.

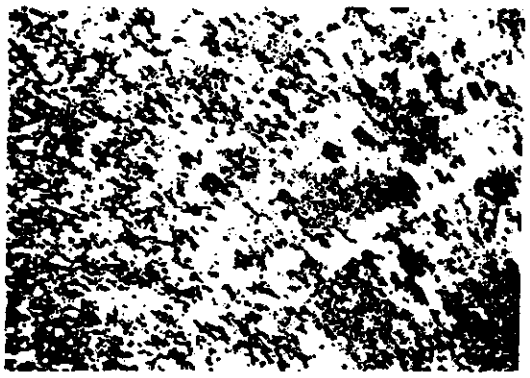

28b Equiaxed grain structure produced by longitudinal vibration of the arc, vibration frequency 20 Hz, vibration amplitude 1·2 mm; in an Al-2·5Mg alloy · 25

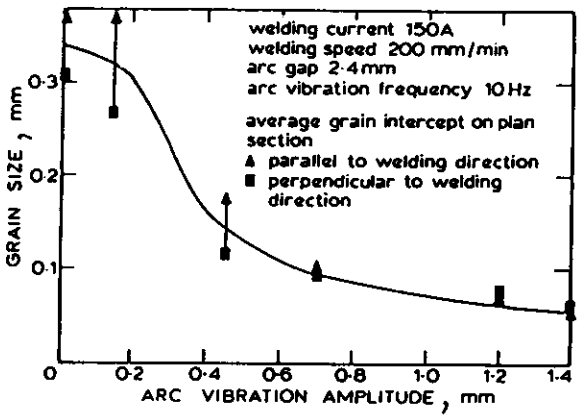

29 Effect of arc vibration amplitude on the as-solidified grain size of the fusion zone of Al-2·5Mg

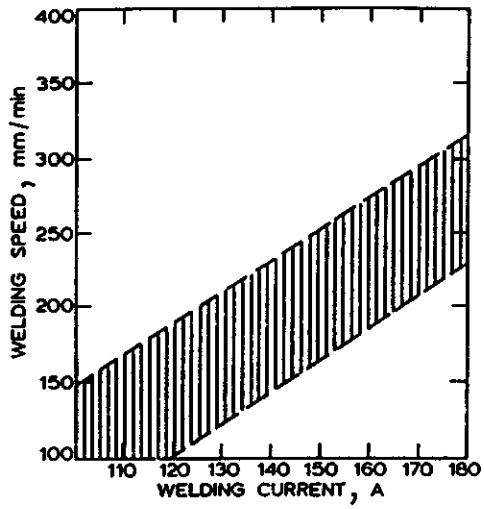

30 *Grain refinement is possible with longitudinal arc vibration at 10–30 Hz and 1·2 mm amplitude only at welding conditions falling within the cross-hatched band; limits of grain refinement in 3·2 mm Al–2·5Mg sheet*

The direct application of torch vibration parallel to the welding direction to achieve grain refinement in melt runs on stainless steel sheet (AISI 321) was not successful.[54] Extensive grain refinement was only attainable in 2·0 mm thick plate at electrode vibration amplitudes as large as 1·8 mm, with an associated loss in process stability over long weld lengths. The reduced effectiveness of torch vibration as a grain-refining technique in this material was believed to be due to the extensive natural stirring present in a stainless steel weld pool.[54] The action of high amplitude vibration does demonstrate, however, that provided some means of delivering a significant disturbance to the advancing solidification front can be developed, grain refinement in stainless steel welds is perfectly feasible.

In the work carried out by Garland[54] it was found that transverse arc vibration had a less significant grain-refining effect.

Ultrasonic Vibrations

Despite the fact that grain refinement in castings using ultrasonic vibrations applied to the melt has been studied in some detail, it is only in the USSR, with the exception of early work by Welty,[147] that any serious attempt has been made to apply these techniques to the control of weld-pool solidification. Methods of introducing ultrasonics into the weld pool were developed for a range of processes[148–150] and it was found that the most efficient and practical method was through a vibrating filler wire. Where this was not possible, however, or where the pool size permitted, e.g. electroslag welding, water-cooled copper probes were designed to transmit the ultrasonics by insertion in the melt. Lebiga[151] and Erokhin, Balaudin, and Kodolov[152] studied the effect of introducing ultrasonics into the pool during submerged arc and electroslag welding. They observed that the welds formed were much less prone to solidification cracking (*see* Section 6) and proposed that this was associated with the quite considerable grain refinement generated. It must be stressed, however, that is apparent from some of the work[149, 153] that very great care must be taken in the choice of the manner in which the ultrasonic vibrations are applied to the solidifying weld if acceptable properties are to be achieved. This is discussed in further detail in the following section.

None the less, it seems that a significant improvement in the resistance of the weld metal to solidification cracking may be achieved in both submerged arc and electroslag welding by the careful use of ultrasonics. Industrial application in these fields[153] would seem to substantiate the usefulness of this technique.

Weld-Pool Stirring

As discussed above controlled stirring of solidifying melts is an important grain-refining technique in casting. Before discussing how this has been applied to weld-pool solidification, it is necessary to consider the natural motion of metal in the pool during welding. When a current flows through a conductor, a magnetic field is set up around the conductor which leads to a self-compressive effect on the conductor due to the resultant Lorentz forces. In a fluid medium, this leads to a pressure build-up on the axis of the conducting column of the fluid. Any asymmetry in the conducting column produces a pressure gradient in the column as the compressive effect of the Lorentz forces is greatest where the current density is greatest. This causes fluid flow. Such an imbalance in the Lorentz forces is operable in welding, where under most circumstances an asymmetrical current path, determined by the position of the earth connection, exists outside the pool. This imbalance generates rotational motion of the metal in the weld pool. Woods and Milner[154] have studied the mechanism of self-induced stirring in the weld pool using shorted arcs on pools of mercury and extended this work to include simulated welds on thin copper sheet, where direct observation of the fluid motion in the pool was possible. Further work by Telford[155] using the same technique showed that the effect of an applied magnetic field perpendicular to the plane of the pool was to produce stirring in a particular direction in the weld pool, independent of the asymmetry of the current flow, but dependent solely upon the polarity of the applied field. This effect had been used some years previously by Brown, Crossley, Rudy, and Schwartzbart[156] to induce stirring in a periodically reversed direction in the weld pool by applying an alternating vertical magnetic field parallel to the arc. As in casting, they found that the application of controlled, periodically reversed stirring generated grain refinement, the extent of which depended upon the frequency of reversal and extent of the stirring, i.e. the strength and frequency of the alternating magnetic field. Maximum effect was recorded at 4–7 Hz. Refinement lines were observed in the weld bead corresponding to the field periodicity indicating that the renewal of motion in the pool was apparently generating interface fragmentation, and hence grain refinement.

It must be emphasized that Brown *et al*,[156] only observed significant grain refinement at such severe field reversal frequencies and strengths that the MIG welding process studied became extremely unstable due to arc blow and occasional ejection of the pool. These conditions made any meaningful solidification study difficult and would prohibit any commercial application. The problem of process stability during the electromagnetic stirring of weld pools does not, however, appear to be anything like so prohibitive in electroslag welding. Russian work[157, 158] has shown that it is possible to achieve almost complete suppression of columnar growth in electroslag welding, using an alternating magnetic field parallel to the direction of welding. No deterioration in the process was observed in this work, and some improvement in deposition rate was recorded. The frequency of field reversal and the

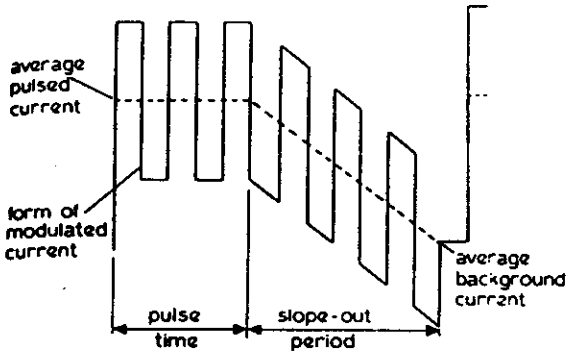

31 *Schematic current waveform for low amplitude modulation of a pulsed TIG arc welding process*

field strength were so adjusted as to give an effective vibratory motion of the pool which was found to generate optimum grain refinement. Indeed, the results of Russian work appear to have been so encouraging that the study of the grain-size control in welding using electromagnetic stirring has become a major research field and equipment has been developed for industrial use applying this technique to ac or dc welding.[159] Since this stage was approached, however, few papers on the topic have appeared in journals made available outside the USSR. It is thus difficult to judge to what extent the industrial application of electromagnetic stirring to achieve grain refinement has been successful.

5.4 Grain Refinement by Arc Modulation

It is clear from the work described in Section 5.3 that whereas mechanical or physical disturbance of the weld pool, e.g. by arc vibration or electromagnetic stirring, is effective in inducing grain refinement the method has limitations. The essence of the technique is the generation of dendrite fragmentation at the growing solid/liquid interface by forced thermal fluctuations. An alternative approach is to generate these fluctuations by varying the energy input into the weld pool. This can be achieved by using either a pulsed arc or modulation of the arc current, or even a combination of the two.

32*a* *Columnar solidification structure in a modulated pulsed arc without slope-out; banding associated with the pulse fronts is clearly evident; material, stainless steel, 3·2 mm thick* · 9

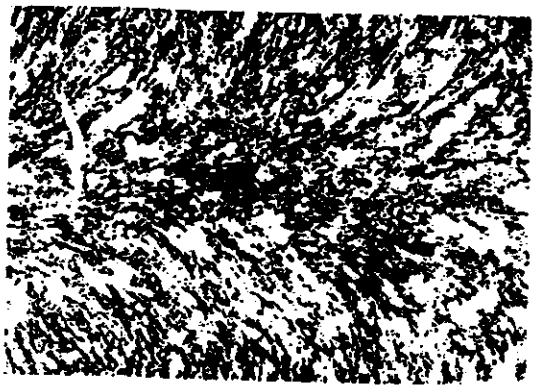

32*b* *Equiaxed solidification structure in a modulated pulsed arc with slope-out; material, stainless steel, 3·2 mm thick* · 9

It has been reported[140, 141] that high-frequency arc modulation can have beneficial effects on the structure and properties of TIG welds but the results are far from conclusive.

Pulsed arc welding is an established process which is well documented.[142, 143] The basic waveform consists of a background welding current which has superimposed upon it a pulse with a square front and a linear trailing section. This can be seen as the average line in Fig.31. In practice the relative size of the pulse, the duration of the pulse and the 'slope-out' of the trailing edge are independently variable. Pulsing of the arc alone does not seem to generate effective grain or substructure refinement. If, however, current modulation is superimposed upon the pulse to give a waveform as shown in Fig.31 quite significant effects can result[31] provided a slope-out period is used (Figs.32*a* and 32*b*).

Work on arc modulation is still very exploratory but this technique has considerable promise.

6. Effect of Control of the Solidification Structure on Weldment Properties

The nature of the solidification process in a weld pool has been shown to exert a considerable influence upon the occurrence of defects, e.g. undercutting, porosity, solidification cracking in the solidified bead.[48, 161] Only a few results are available which present a quantitative assessment of the relative properties of unmodified and modified weldments.

Alov and Vinogradov,[136, 137] Mandelberg and Gordonnyi,[138, 139] Markara,[110, 111] Deminskii and Dyatlov,[142] Autonets *et al.*[113, 131] have all reported improved bead shape, improved weld-metal properties, and lower defect densities as a result of arc vibration or weaving. In addition Lebiga[151] and Erokhin *et al.*[152] have reported a reduction in solidification cracking after introducing ultrasonic vibrations into the weld pool.

Using the Varestraint test, Tseng and Savage[116] made a comparison of hot-cracking sensitivity in welds of an alloy steel (HY 80) with and without transverse or longitudinal arc vibration. Typical results are given in Table I. These results showed that modification of the structure reduced both the total amount of cracking and the size of the largest crack. Similar results were reported by Garland[31] in his study on the effects of arc vibration on TIG welds in an Al–2·5Mg alloy. In this case a modified Houldcroft test[165] was used. Results are shown in Table II.

In contrast it was found[31] that although inoculation with titanium carbide could be used to produce grain refinement in

TABLE I

Effect of Arc Vibration on Hot-Cracking in an Alloy Steel (HY 80)*

Vibration frequency, Hz	Vibration amplitude, mm	Mean total crack length, mm	Mean maximum crack length, mm
No oscillation	No oscillation	6·0	0·71
0·42	1·65	5·7	0·57
1·19	1·65	1·9	0·42

* Tseng and Savage [140]

submerged arc welds in mild steel (*see* Figs.23*a* and 23*b*) there was an effective embrittlement of the steel. This was contrary to the expected behaviour[165] and was shown to be the result of grain-boundary films of Ti_2S. Presumably desulphurizing procedures, e.g. rare-earth additions, could be used to eliminate film formation of this type and thus allow the realization of acceptable toughness levels.

There is clearly a need for considerable research effort in this area.

7. Future Developments

The demands of industry for a welding process capable of consistently depositing weld metal with enhanced mechanical properties and low defect concentrations have directed attention away from detailed studies of normal weld-pool solidification towards the development of practical grain-refinement techniques based on the recently established fundamental principles for the suppression of columnar growth in the weld pool.

Future developments in lower heat-input automatic welding processes such as pulsed TIG and MIG are likely to be derived from the arc modulation technique first described by Garland[54] (*see* Section 5.4), since this does not require periodic deflection of the welding arc, but may be achieved simply by modification of the characteristics of the welding power source. Considerable progress has already been made in this area and the first practical applications of the technique in special high-quality welded assemblies are now under serious consideration.[167] Arc vibration has also been employed in practical welding situations to generate grain refinement. In this technique, practical limitations of mechanically induced arc vibration can be overcome by deflecting the arc magnetically, but the results achieved to date with this approach have not been fully satisfactory. The whole area of the magnetic control of weld-pool solidification, however, is one which requires further attention in view of its potential rich rewards. In particular, further fundamental study is required into the feasibility of using the interaction between an externally applied, alternating magnetic field and the Lorentz forces created by the passage of current through a weld pool to induce periodically reversed stirring at the advancing solid liquid interface,[154] and hence grain refinement, while at the same time maintaining the stability of the welding process. The successful development of such a technique could have a wide range of practical applications as it involves only the attachment of a suitable probe to the welding head[156] and, more important, it may be effective up to a much higher range of heat inputs than the other physical grain-refining processes outlined previously.

TABLE II

Solidification Crack Lengths in Modified Houldcroft Tests on 3·2 mm thick Al–(1·7–2·8)Mg (NS 4) Sheet

Test condition	Mean crack length, mm
Normal TIG weld	196 · 6
TIG weld with longitudinal arc vibration of amplitude 1·2 mm at 20 Hz	147 · 5

Welding conditions:	current	160 A
	travel speed	275 mm min
	arc gap	2·4 mm
	shielding gas supply	9 l/min argon

The welding conditions selected for study were chosen to give cracking of maximum severity

The physical grain refinement of high heat-input welds such as those formed in the submerged arc process is much more difficult since, as discussed above, the size of the weld pool is normally so large that any disturbance applied to the welding arc is damped out before it can reach the solidification front and modify the grain size. Under these circumstances, a possible solution could be the application of a modulated or vibrated trailing arc to the weld pool, where the proximity of the solid/liquid interface would ensure the maximum perturbation to the growth process from any disturbance of the form of the trailing arc, irrespective of weld-pool size and the distance of the actual welding arc. Although this could lead to a versatile grain-refining technique, it is not a practically attractive approach due to the problems involved in introducing a second trailing arc in many applications. Periodically reversed weld-pool stirring induced magnetically, as described above, could be a much more viable development, as its effectiveness is less dependent on pool size and this has been a surprisingly neglected area. In this context, it is worth noting that the grain refinement of electroslag welds using controlled electromagnetic stirring appears to be widely practised in the USSR.[159]

The problems involved in applying physical grain-refinement techniques to large weld pools, and the limitation of these techniques to automatic welding processes, have stimulated research into methods of chemically controlling weld-pool solidification by inoculation of the melt via, where appropriate, the welding flux, the electrode coating, or flux-cored wire additions to the rear of the pool (*see* Section 5.1). Much of this work has concentrated initially on the submerged arc welding of mild and low-alloy steel,[51, 168] where probably the greatest benefits would accrue from the suppression of columnar growth both in terms of improved toughness and a reduced incidence of solidification cracking. While very fine weld-metal grain sizes have been achieved in this process using TiC/Fe–Ti mixtures fed into the rear of the weld pool, the deleterious side effects of this type of inoculation practice upon toughness due to grain-boundary embrittlement have precluded any further advances in this technique. It now seems possible, however, that changes in the nature of the inoculant used might eliminate these problems and research at present is being directed at the development of welding consumables capable of introducing TiB_2, rather than TiC, into the pool.[169] This approach offers more promise than the earlier choice of inoculant mix as TiB_2 appears able to survive for a longer period than TiC in the severe thermal conditions of the weld pool. Encouraging results have already been achieved by a number of workers[169, 170] using consumables specifically designed to add Ti and B into the pool by a variety of techniques. Further work is required, however, to identify the most effective method of introducing these additions into the pool so as to maximize their influence upon weld-pool solidification while at the same time minimizing any deleterious side-effects. Success in this field could have important implications

for future developments in the formulation of welding fluxes and electrode coatings.

It has not been possible in this section to draw more than a very brief outline of future developments in weld-pool solidification research. Current trends indicate that this will be concentrated primarily on techniques to control weld-pool solidification and, as discussed previously, some of these are already finding commercial application. It is likely, however, that as knowledge increases, more sophisticated methods of suppressing columnar growth in a weld pool will become available, especially since the interest of fabricators in improved weld-metal performance should ensure that research continues to be pursued actively in this field.

Acknowledgments

The authors wish to express their appreciation of the encouragement and assistance provided by members of the staff of the Welding Institute during the course of preparation of this review. In addition, one of us (J. G. G.) would like to thank the British Steel Corporation for permission to publish this review.

References

1. G. J. DAVIES: 'Solidification and casting'; 1973, London, Applied Science Publishers.
2. 'Solidification', (ed. T. J. Hughel and G. F. Bolling); 1971, Cleveland, Ohio, American Society for Metals.
3. M. C. FLEMINGS: 'Solidification processing'; 1974, New York, McGraw-Hill.
4. D. TURNBULL: *J. Chem. Phys.*, 1950, 18, 198.
5. G. A. CHADWICK: *Metals and Materials*, 1969, 3, 77.
6. I. C. H. HUGHES: 'Progress in cast metals', 1.1; 1971, London, Institution of Metallurgists.
7. K. A. JACKSON and B. CHALMERS: *Can. J. Phys.*, 1956, 34, 473.
8. J. H. HOLLOMAN and D. TURNBULL: *Progress Met. Phys.*, 1953, 4, 333.
9. F. C. FRANK: *Disc. Faraday Soc.*, 1949, 5, 48.
10. W. A. TILLER *et al.*: *Acta Met.*, 1953, 1, 428.
11. W. A. TILLER and J. W. RUTTER: *Can. J. Phys.*, 1956, 34, 96.
12. F. WEINBERG and B. CHALMERS: *ibid.*, 1951, 29, 382.
13. A. HELLAWELL and P. M. HERBERT: *Proc. Roy. Soc.*, 1962, A269, 560.
14. T. F. BOWERS *et al.*: *Trans. AIME*, 1966, 236, 624.
15. T. Z. KATTAMIS and M. C. FLEMINGS: *ibid.*, 1967, 239, 992.
16. T. Z. KATTAMIS *et al.*: *ibid.*, 1967, 239, 1504.
17. R. M. SHARP and A. HELLAWELL: *J. Crystal Growth*, 1970, 16, 253.
18. R. TRIVEDI: *Acta Met.*, 1970, 18, 287.
19. M. H. BURDEN and J. D. HUNT: *J. Crystal Growth*, 1974, 22, 99.
20. M. H. BURDEN and J. D. HUNT: *ibid.*, 1974, 22, 109.
21. W. G. PFANN: *Trans. AIME*, 1952, 194, 747.
22. J. A. BURTON *et al.*: *J. Chem. Phys.*, 1953, 21, 1987.
23. F. WEINBERG: *Trans. AIME*, 1961, 221, 844.
24. J. G. GARLAND and G. J. DAVIES: *Metal Construction*, 1970, 2, 171.
25. D. E. ADAMS: *J. Inst. Metals*, 1948, 75, 809.
26. J. S. KIRKALDY and W. V. YOUDELIS: *Trans. AIME*, 1960, 218, 628.
27. D. R. UHLMANN and G. A. CHADWICK: *Acta Met.*, 1961, 9, 835.
28. J. A. SARTELL and D. J. MACK: *J. Inst. Metals*, 1964–65, 93, 19.
29. D. R. UHLMANN *et al.*: *J. Appl. Phys.*, 1964, 35, 2986.
30. C. E. RANSLEY and H. NEUFELD: *J. Inst. Metals*, 1948, 74, 599.
31. B. CHALMERS: 'Principles of solidification', 189; 1964, New York, Wiley.
32. F. R. HEUZEU: *Trans AIME*, 1937, 124, 300.
33. J. L. WALKER: 'Liquid metals and solidification', 319; 1958, Cleveland, Ohio, American Society for Metals.
34. B. CHALMERS: *J. Australian Inst. Metals*, 1963, 8, 255.
35. K. A. JACKSON *et al.*: *Trans. AIME*, 1966, 236, 149.
36. R. T. SOUTHIN: *ibid.*, 1967, 239, 220.
37. L. BACKERUD and L.-M. LILJENVALL: *J. Inst. Metals*, 1972, 100, 357.
38. R. D. DOHERTY *et al.*: *Metall. Trans.*, 1973, 4, 115.
39. H. FREDRIKSSON and M. HILLERT: *ibid.*, 1972, 3, 565.
40. L. BACKERUD and L.-M. LILJENVALL: *J. Inst. Metals*, 1972, 100, 366.
41. S. WOJCIECHOWSKI and B. CHALMERS: *Trans. AIME*, 1968, 242, 690.
42. D. B. SPENCER *et al.*: *Metall. Trans.*, 1972, 3, 1925.
43. A. H. FREEDMAN and J. F. WALLACE: *Trans. AFS*, 1957, 65, 578.
44. H. BILONI *et al.*: *Trans. AIME*, 1965, 233, 1296.
45. E. A. FEEST and R. D. DOHERTY: *Metall. Trans.*, 1973, 4, 125.
46. B. THRESH *et al.*: *Trans. AIME*, 1968, 242, 853.
47. F. WEINBERG: *ibid.*, 1961, 221, 844.
48. M. C. FLEMINGS and G. NEREO: *ibid.*, 1967, 239, 1449.
49. M. C. FLEMINGS *et al.*: *ibid.*, 1968, 242, 41.
50. M. C. FLEMINGS and G. NEREO: *ibid.*, 1968, 242, 50.
51. D. J. HEBDITCH and J. D. HUNT: *Metall. Trans.*, 1974, 5, 1557.
52. 'Atlas of defects in castings'; 1961, London, Institute of British Foundrymen.
53. F. MATSUDA *et al.*: *Trans. Nat. Research Inst. Metals (Japan)*, 1969, 11, 43.
54. J. G. GARLAND: Ph.D. thesis, 1972, University of Cambridge; *see also* J. G. GARLAND: *Metal Construction*, 1974, 6, 121.
55. R. A. WOODS and D. R. MILNER: *Weld. J.*, 1971, 50, 164s.
56. W. F. SAVAGE *et al.*: *ibid.*, 1965, 44, 175.
57. W. F. SAVAGE and A. H. ARONSON: *ibid.*, 1966, 45, 85.
58. S. S. BRENNER: 'The art and science of growing crystals', (ed. J. J. Gilman), 30; 1963, London, Wiley.
59. A. G. WALTON: 'Nucleation', (ed. A. C. Zettlemeyer), 225; 1969, New York, Marcel Dekker.
60. H. NAKAGAWA *et al.*: *J. Japan Weld. Soc.*, 1970, 39, 94.
61. T. F. CHASE, JR: M.S. thesis, 1967, Rensselaer Polytechnic Institute, Troy, N.Y.
62. R. S. BRAY *et al.*: *Weld. J.*, 1969, 48, 181.
63. C. R. LOPER *et al.*: *ibid.*, 1969, 48, 171.
64. W. F. SAVAGE and E. S. SZEKERES: *ibid.*, 1967, 46, 94.
65. D. S. DUVALL and W. A. OWCZARSKI: *ibid.*, 1968, 47, 115.
66. A. M. MAKARA and A. A. ROSSOSHINSKII: *Automat. Weld. (USSR)*, 1956, 9, 65.
67. H. NAKAGAWA *et al.*: *Trans. Japan Weld. Soc.*, 1971, 2, 10.
68. J. WARING: *Australian Weld. J.*, 1967, 11, 15.
69. M. KATO *et al.*: *Trans. Japan Weld. Soc.*, 1972, 3, 59.
70. C. F. LOPER and J. T. GREGORY: Proc. Spring Meeting, 166; 1973, American Welding Society.
71. H. NAKAGAWA *et al.*: *Trans. Japan Weld. Soc.*, 1971, 2, 1.
72. N. N. PROKOROV and A. S. MASTRYUKOVA: *Weld. Prod. (USSR)*, 1961, 8, 7.
73. A. S. MASTRYUKOVA and N. N. PROKOROV: *Automat. Weld. (USSR)*, 1963, 16, 6.
74. N. N. PROKOROV and A. S. MASTRYUKOVA: *ibid.*, 1965, 18, 15.
75. G. L. PETROV and M. U. SHAMANIN: *Weld. Prod. (USSR)*, 1968, 15, 1.
76. R. L. APPS and D. R. MILNER: *Brit. Weld. J.*, 1955, 2, 475.
77. N. CHRISTENSEN *et al.*: *ibid.*, 1965, 12, 1965.
78. M. M. PERLE: Proc. Spring Meeting, 52; 1973, American Welding Society.
79. P. J. ZANNER: Ph.D. thesis, 1967, Rensselaer Polytechnic Institute, Troy, N.Y.
80. M. KATO *et al.*: *Trans. Japan Weld. Soc.*, 1972, 3, 69.
81. T. W. MILLER: M.S. thesis, 1967, Rensselaer Polytechnic Institute, Troy, N.Y.
82. F. A. CALVO *et al.*: *Acta Met.*, 1960, 8, 898.
83. W. F. SAVAGE *et al.*: *Weld. J.*, 1968, 47, 420s.
84. G. J. DAVIES: 'The solidification of metals', 66; 1968, London, The Iron and Steel Institute.
85. F. WEINBERG and B. CHALMERS: *Can. J. Phys.*, 1952, 30, 488.
86. H. ATWATER and B. CHALMERS: *ibid.*, 1957, 35, 208.
87. P. E. BROWN and C. M. ADAMS, JR: *Weld. J.*, 1960, 39, 520.
88. P. E. BROWN and C. M. ADAMS: *Trans. AFS*, 1961, 69, 879.
89. M. F. JORDAN and M. C. COLEMAN: *Brit. Weld. J.*, 1968, 15, 552.
90. J. N. LANZAFAME and T. Z. KATTAMIS: *Weld. J.*, 1973, 52, 226s.
91. R. A. JARMAN and M. F. JORDAN: *J. Inst. Metals*, 1970, 98, 55.
92. L. R. MORRIS and W. C. WINEGARD: *J. Crystal Growth*, 1967, 1, 245.
93. R. S. BRAY and L. J. LOZANO: *Weld. J.*, 1965, 44, 424.
94. J. B. RADZIMENSKI *et al.*: Structural Research Series No. 361; 1970, University of Illinois.
95. J. R. BELL: M.S. thesis, 1966, Renssalaer Polytechnic Institute, Troy, N.Y.
96. D. L. CHEEVER and D. G. HOWDEN: *Weld. J.*, 1969, 48, 179.
97. S. V. AUKYAN and N. F. LASHKO: *Avtog. Delo*, 1952, 23, 25.
98. N. F. BRUK: *Weld. Prod.*, 1955, 2, 8.
99. H. S. GUREV and R. D. STOUT: *Weld. J.*, 1963, 42, 298.
100. B. A. MORCHAN and A. ABITDNAR: *Automat. Weld. (USSR)*, 1968, 21, 4.
101. Y. A. STEVENBOGEN *et al.*: *ibid.*, 1969, 22, 5.
102. A. T. D'ANNESSA: *Weld. J.*, 1970, 49, 41.

103. A. T. D'ANNESSA: *ibid.*, 1966, 45, 569.
104. K. ISHIZAKI: *J. Japan Weld. Soc.*, 1963, 32, 38.
105. E. PELZEL: *Berg- u. Hüttenmänn. Monatsh.*, 1948, 93, 248.
106. D. J. KOTECKI *et al.*: *Weld. J.*, 1972, 52, 386s.
107. D. C. G. LEES: *J. Inst. Metals*, 1946, 72, 343.
108. A. R. E. SINGER and P. H. JENNINGS: *ibid.*, 1947, 73, 273.
109. H. F. BISHOP *et al.*: *Trans. AFS*, 1960, 68, 518.
110. J. C. BORLAND: *Brit. Weld. J.*, 1960, 7, 508.
111. C. S. SMITH: *Trans. AIME*, 1948, 175, 175.
112. C. S. SMITH and L. GUTMAN: *ibid.*, 1953, 197, 81.
113. E. C. ROLLASON and D. F. T. ROBERTS: *Trans. Inst. Weld.*, 1950, 13, 129.
114. A. J. D. WILLIAMS *et al.*: WADC Tech. Rep. 52-143, 1952.
115. M. D. TWITTY: *BCIRA J.*, 1960, 8, 144.
116. J. VAN EEGHEM and A. DE SY: *Mod. Cast.* 1965, 48, 100.
117. D. B. SPENCER *et al.*: *Metall. Trans.*, 1972, 3, 1925.
118. P. COLVIN and A. F. BUSH: *Welding Met. Fabr.*, 1971, 39, 40.
119. T. FUKUI and K. NAMBA: *Trans. Japan Weld. Soc.*, 1973, 4, 49.
120. J. G. GARLAND and P. R. KIRKWOOD: Internat. Inst. Welding, Document IX-92-74, 1974.
121. J. G. GARLAND: BSC Rep. PROD/500/1/73/A, 1973.
122. BS 1515, Appendix C, 1968.
123. W. COLE and P. COLVIN: *Metal Construction*, 1971, 3, 131.
124. D. WIDGERY: Welding Institute Members Rep. M/76/73, 1973.
125. J. HONEYCOMBE: Welding Institute, personal communication, 1973.
126. C. R. SIBLEY: *Weld. J.*, 1956, 35, 361.
127. K. K. KHRENOV *et al.*: *Weld. Prod. (USSR)*, 1959, 6, 12.
128. G. K. TURNBULL *et al.*: *Trans. AFS*, 1961, 69, 792.
129. P. WEISER *et al.*: *J. Metals*, 1967, 19, (6), 44.
130. N. CHURCH *et al.*: *Trans. AFS*, 1967, 75, 113.
131. B. L. BRAMFITT: *Metall. Trans.*, 1970, 1, 1087.
132. A. A. ALOV and G. V. BOBROV: *Weld. Prod. (USSR)*, 1959, 6, 1.
133. B. A. MORCHAN and B. N. KUSHNIRENKO: *Automat. Weld. (USSR)*, 1960, 13, 89.
134. I. I. IVOCHKEN: *Weld. Prod. (USSR)*, 1965, 12, 1.
135. K. OKADA *et al.*: *J. Japan Weld. Soc.*, 1965, 34, 1.
136. A. A. ALOV and V. S. VINOGRADOV: *Weld. Prod. (USSR)*, 1957, 4, 38.
137. A. A. ALOV and V. S. VINOGRADOV: *ibid.*, 1959, 6, 19.
138. S. L. MANDELBERG and V. G. GORDONNYI: *Automat. Weld. (USSR)*, 1962, 15, 4.
139. S. L. MANDELBURG: *ibid.*, 1965, 18, 8.
140. A. M. MAKARA: *ibid.*, 1965, 18, 12.
141. A. N. MAKARA and B. N. KUSHNIRENKO: *ibid.*, 1967, 20, 31.
142. Y. A. DEMINSKII and V. I. DYATLOV: *ibid.*, 1963, 16, 82.
143. O. P. AUTONETS and F. I. BUKIN: *ibid.*, 1964, 17, 47.
144. O. P. AUTONETS and G. G. PSARAS: *ibid.*, 1966, 19, 54.
145. F. N. RYZHKOV and V. S. POSTNIKOV: *ibid.*, 1969, 22, 43.
146. C. F. TSENG and W. F. SAVAGE: *Weld. J.*, 1971, 50, 777.
147. J. W. WELTY: *ibid.*, 1952, 31, 361.
148. L. L. SILIN: *Russ. Met. Fuels*, 1960, 3, 117.
149. A. A. EROKHIN and L. L. SILIN: *Weld. Prod. (USSR)*, 1960, 7, 4.
150. V. D. KODOLAV: *ibid.*, 1961, 8, 35.
151. V. A. LEBIGA: *Automat. Weld. (USSR)*, 1960, 13, 21.
152. A. A. EROKHIN *et al.*: *ibid.*, 1960, 13, 15.
153. Y. M. MATVEEV: *Weld. Prod. (USSR)*, 1968, 15, 30.
154. R. A. WOODS and D. R. MILNER: *Weld. J.*, 1971, 50, 164s.
155. D. G. TELFORD: Ph.D. thesis, 1969, University of Birmingham.
156. D. C. BROWN *et al.*: *Weld. J.*, 1962, 41, 241.
157. D. A. DUDKO and I. N. RUBLEUSKII: *Automat. Weld. (USSR)*, 1960, 13, 14.
158. I. P. TROCHUN and V. P. CHERNYSH: *Weld. Prod. (USSR)*, 1965, 12, 3.
159. M. N. GAPCHENKO: *Automat. Weld. (USSR)*, 1970, 23, 36.
160. S. E. GOODELL *et al.*: *Weld. J.*, 1970, 49, 372; *see also* G. R. STOECKINGER, AWS Spring Meeting, 1973.
161. F. RIENKO and R. C. ASHAUER: *Weld. J.*, 1971, 50, 222s.
162. J. A. LUCEY and P. BOUGHTON: *Brit. Weld. J.*, 1965, 12, 159.
163. J. C. NEEDHAM and A. W. CARTER: *ibid.*, 1965, 12, 229.
164. H. BAACH: *Oerlikon Schweissmitt.*, 1965, 23, 16.
165. J. G. GARLAND and G. J. DAVIES: *Metal Construction*, 1969, 1, 565.
166. N. J. PETCH: *J. Iron and Steel Inst.*, 1953, 173, 25.
167. P. BOUGHTON: CEGB, personal communication, 1973.
168. D. C. WILLINGHAM: Welding Institute, personal communication, 1973.
169. H. SUZUKI *et al.*: Internat. Inst. Welding, Document IX, 750, 1971.
170. M. POEBER: National Physical Laboratory, personal communication, 1973.

Microstructure and Impact Toughness of C-Mn Weld Metals

The formation of acicular ferrite in over half of the weld appears to be the key to improving impact toughness

BY L-E. SVENSSON AND B. GRETOFT

ABSTRACT. The effect of variation in carbon and manganese contents on the microstructure and impact properties of all weld metal samples has been studied. The welds were made using the shielded metal arc welding technique. Four different carbon levels, ranging from 0.03–0.12 wt-% and four different manganese contents (0.8–2.1 wt-%) were used.

It was found that significant improvements in impact toughness at low temperatures were achieved with increasing amounts of acicular ferrite. High levels of acicular ferrite could be achieved with several different combinations of carbon and manganese. At excessive amounts of alloying additions, the impact toughness decreased. This is attributed to the presence of bands of microphases being aligned with the notch in the fracture surface. For the lowest carbon content, unexpectedly low toughness was observed. This may be due to the fact that these metals contained a somewhat higher nitrogen content.

Introduction

The effect of carbon and manganese on the microstructure and mechanical properties of mild steel arc welds has been the subject of many investigations. Vuik (Ref. 1) has recently summarized the investigations made concerning the effect of carbon. Evans has published a number of papers dealing with the effect of carbon (Ref. 2), manganese (Ref. 3), silicon (Ref. 4), interpass temperature (Ref. 5), impurity elements (Ref. 6), molybdenum (Ref. 7), heat input (Ref. 8) and heat treatment (Ref. 9) on the microstructure and mechanical properties of mild steel welds. The welds that Evans examined were of the all-weld-metal type, deposited with a shielded metal arc multipass technique. In the work most comparable to the present one, Evans found that the optimum impact toughness properties were achieved with an alloying combination of 0.07 wt-% C-1.4 wt-% Mn, and attributed this to the competitive action between the progressively finer ferrite grain sizes obtained by increasing alloying additions and by the simultaneously increasing yield strengths.

In this paper, an investigation of the microstructure and impact toughness of 16 different welds, with varying carbon and manganese contents, is described. The experiment to a large extent mirrors the one of Evans (Refs. 2, 3), but the results differ somewhat. The intention of this paper is to clarify the reason for the discrepancy between the different investigations and to point out some additional microstructural effects that might be of importance for the impact toughness. However, first a short description of the role of carbon and manganese in controlling the microstructure and how this may influence the impact properties will be given.

L-E. Svensson and B. Gretoft are with the Esab Group, Central Laboratories, Göteborg, Sweden.

Background

With the help of experimental (Refs. 1–9) and theoretical (Refs. 10–12) work, the effects of various elements on the microstructure of the as-deposited area in a weld is now relatively well understood.

The as-deposited microstructure of C-Mn weld metals is commonly described with three major microstructural components: grain boundary ferrite, ferrite with aligned M-A-C (martensite-austenite-cementite) and acicular ferrite. The classification of the various microstructures is based on the visual impression in the optical microscope. However, in the theoretical work based on thermodynamics, the microstructural components are described from the mechanism of formation point of view. The components are then called allotriomorphic ferrite (same as grain boundary ferrite, but a more correct name), Widmannstätten ferrite side plates (according to Dubé classification) and acicular ferrite. It should be noted that the mechanism of formation of acicular ferrite is not yet known. In the following text, the last mentioned denotation will be used.

KEY WORDS

Microstructure
Impact Toughness
C-Mn Weld Metal
Acicular Ferrite
Mechanical Properties
Mild Steel
Arc Welding
Alloying Content
Microphases

The effect of carbon is mainly to limit the width of the coarse-grained allotriomorphic ferrite, formed at the prior austenite grain boundaries, and in influencing the rate of Widmannstätten ferrite formation. During the transformation from austenite to ferrite, the carbon atoms diffuse into the remaining austenite and the growth (or thickening) rate of the allotriomorphic ferrite is controlled by the diffusion rate of carbon in austenite. A higher carbon content gives a slower growth rate of the ferrite and, thus, a thinner layer of ferrite at the prior austenite grain boundaries.

Increasing carbon content leads to lower contents of both allotriomorphic and Widmannstätten ferrite, giving room for increasing contents of the fine-grained acicular ferrite. However, it is not known whether the actual growth rate of acicular ferrite is influenced by the carbon content.

The manganese atoms, on the other hand, are not redistributed during the transformation, but an increased manganese content reduces the driving force for the transformation. Thus, increasing manganese also leads to a thinner layer of allotriomorphic ferrite. In a way, manganese and carbon can be considered as complementary elements, and in principle, the same microstructure should be attainable

with several combinations of these elements.

However, there is at least one point where this way of reasoning fails. During solidification, manganese segregates to the remaining melt and is, thus, enriched at the cell boundaries at the solid/liquid interface. This segregation pattern (although much less pronounced than for nickel) persists during the whole cooling sequence of the weld since manganese is not redistributed during the transformations. Especially when the weld is heavily alloyed with manganese, extensive formation of microphases (retained austenite, martensite, degenerate pearlite, bainite or carbides) takes place in areas where the manganese content is high. The term microphases indicates that the volume fraction of these phases is low and this is true also for welds with high manganese content, but the difference is that the microphases appear in bands, reflecting the solidification pattern, while in the lower manganese welds, the microphases are more evenly distributed. This will be illustrated more clearly later in this paper.

It should be noted, that in practice there are many other alloying elements used to control the microstructure. Apart from carbon and manganese, the most frequently used ones are Ni, Mo and B. The influence of inclusions on the amount of acicular ferrite has been debated for several years. It has been argued that certain types of inclusions are better nucleants for acicular ferrite than others, due to lattice matching between ferrite and the inclusions. Thus, another route for controlling the microstructure would be to choose the slag system in such a way as to obtain the most favorable type of inclusions.

Turning to the mechanical properties and the relationship between microstructure and properties, it should first of all be noted that the mechanical properties of weld metals are usually not just determined by the as-deposited microstructure, since commonly many beads have been deposited to complete the weld. Thus, a range of microstructures exists in the weld. The reheated area under a bead can be divided into a coarse-grained zone, a fine-grained zone and a recrystallized zone. The relative amounts of these zones will vary with, among other things, chemical composition, and this will, of course, influence the mechanical properties. However, it can be assumed that there is a relationship between the as-deposited microstructure and the microstructure in the other zones and, therefore, it is possible to discuss the mechanical properties with reference to the microstructure in the as-deposited region.

When designing weld metals, the most difficult thing is to meet requirements on impact properties while maintaining operational properties as good as possible. Tensile properties are, at least for mild steels, a smaller problem since usually the strength of the weld metal is higher than the strength of the steel.

Specifications on impact toughness vary substantially, but in many cases the requirement is 27 J (20 ft-lb) at a certain temperature. For more advanced applications, higher toughness values are required, *e.g.*, 34 or 40 J (25 or 30 ft-lb). These levels of toughness values are achieved with only a relatively small fraction of the fracture surface of an impact toughness test bar having a ductile, fibrous fracture, while the remaining part is a brittle, cleavage type. To achieve acceptable impact toughness at lower temperatures (which in many cases is the trend in development work today) it is necessary to avoid cleavage fracture starting too near the notch in the impact bar. This can be achieved by control of the microstructure.

To improve impact toughness, some well-known physical metallurgy principles are used. First, increasing the amount of acicular ferrite by the control of alloying elements gives a reduced grain size. Secondly, use of basic-type consumables gives a low amount of oxygen, which leads to a low volume fraction of inclusions. Finally, strict control of impurity elements like S, P, Sn, As, Sb and N helps to prevent embrittlement of the structure.

The application of the first of these principles leads us back to the main question of this paper: how can the microstructure be optimized by changing carbon and manganese contents?

As a contrast to this, Dolby (Ref. 13) suggested that weld metals with a very lean alloying content, having mainly a coarse-grained structure and a low yield strength, could have good impact toughness.

Although there have been major improvements in the toughness levels that can be achieved in weld metals during the last few decades, by application of the principles mentioned above, there is still room for further improvement. A more fundamental understanding of the mechanisms controlling the onset of cleavage fracture and the complex interrelationship between microstructure and fracture needs to be developed. Major advances have indeed already been made in this field by Knott and coworkers (Refs. 14-16) who have studied the fracture behavior of C-Mn welds in detail and combined that with their earlier experience of fracture in steels. They concluded that cleavage fracture in welds often originated from cracking of oxide inclusions, in particular those situated in the coarse-grained allotriomorphic ferrite, and that the size distribution of these inclusions had a significant effect on the fracture toughness results. In steels, where the volume fraction of oxide inclusions is much less, fracture toughness is linked more to the carbides precipitated along grain boundaries nucleating cleavage cracks (Ref. 17). However, it should be noted that in testing fracture toughness of weld metals, Knott and coworkers used small size notched bars and tested them in slow strain-rate four-point bending, in a manner similar to CTOD testing. The observation of cleavage cracks nucleating from inclusions were numerous in these tests but similar observations on impact specimens are, in fact, fairly rare.

Experimental

Laboratory-made shielded metal arc electrodes, 4 mm (0.16 in.) in diameter, of E7018 type with basic coatings were used for the investigation. The electrode coatings were varied to a systematic series of four different manganese contents (0.8, 1.1, 1.2 and 2.1 wt-%) at each carbon level (0.03, 0.06, 0.09 and 0.12 wt-%). All welding was made in accordance with ISO 2560, with a current of 180 A, voltage 23 V and a maximum interpass temperature of 250°C (484°F). A stringer bead technique was used giving a welding speed of about 4 mm/s (9 in./min). The heat input then was around 1 kJ/mm (25 kJ/in.).

The chemical composition of the weld deposits was measured using an optical emission spectrometer (OES), except for oxygen and nitrogen, which were determined using combustion furnaces. The OES analyses were made on the head of the tensile specimen.

Two longitudinal all-weld-metal tensile specimens (10 mm/0.4 in. in diameter) and 25 Charpy V-notch impact specimens were taken from each weld. The specimens were taken from the middle of the plate. The impact toughness was tested at five different temperatures, with five specimens tested at each temperature.

The microstructures of the weld metals were examined by conventional metallography, using light optical microscopy. The etching was made using first a solution of 4% picric acid in alcohol, followed by 2.5% nitric acid in alcohol.

The quantitative assessment of the microstructure was made using a Swift point counter. At least 500 points were measured on each specimen. The microstructure constituents were identified according to the classification of the IIW (Ref. 18). The austenite grain size was measured normal to the length axis of the grains (*i.e.*, the results are equal to L_{tn} as denoted by Bhadeshia, *et al.* – Ref. 19).

To further study the microphases, transmission electron microscopy (TEM) was used. Thin foils were prepared by polishing in a Struers Tenupol in a 5% solution of perchloric acid in methanol.

Table 1—Chemical Compositions of the Weld Metals[a]

Sample No.	C	Si	Mn	P	S	Al	Ti	Sn	As	Sb	N	O
1	0.030	0.45	0.78	0.010	0.013	0.009	0.014	0.006	0.001	0.002	95	336
2	0.032	0.45	1.27	0.010	0.008	0.009	0.013	0.006	0.001	0.003	94	321
3	0.031	0.42	1.71	0.010	0.004	0.008	0.011	0.006	0.001	0.003	109	297
4	0.032	0.45	2.05	0.010	0.002	0.009	0.012	0.006	0.001	0.005	119	320
5	0.059	0.34	0.77	0.010	0.010	0.007	0.011	0.003	0.001	0.001	66	306
6	0.059	0.33	1.09	0.010	0.008	0.007	0.010	0.005	0.001	0.005	64	310
7	0.059	0.30	1.44	0.010	0.006	0.007	0.009	0.004	0.001	0.005	65	305
8	0.065	0.33	1.83	0.010	0.003	0.007	0.009	0.004	0.001	0.005	76	291
9	0.090	0.41	0.78	0.010	0.013	0.003	0.014	0.005	0.004	0.004	36	421
10	0.089	0.35	1.18	0.010	0.011	0.008	0.012	0.005	0.003	0.003	73	404
11	0.088	0.37	1.59	0.010	0.011	0.003	0.012	0.005	0.005	0.004	77	491
12	0.098	0.39	2.25	0.014	0.008	0.003	0.013	0.006	0.005	0.005	88	330
13	0.12	0.43	0.86	0.014	0.011	0.005	0.015	0.005	0.003	0.003	54	329
14	0.12	0.44	1.35	0.014	0.010	0.003	0.015	0.006	0.005	0.006	55	326
15	0.13	0.37	1.83	0.011	0.010	0.003	0.013	0.006	0.005	0.005	63	318
16	0.11	0.36	2.18	0.011	0.008	0.003	0.012	0.006	0.007	0.008	74	342

(a) All concentrations are in wt-%, except for oxygen and nitrogen, which are given in weight ppm.

Results

Chemical Composition

The chemical compositions of the weld metals are given in Table 1. The carbon contents have successfully been kept close to the nominal values. The manganese content scattered somewhat around the nominal values, the maximum deviation being around 0.15%.

The phosphorus content was relatively constant throughout the investigation, typically 0.010%. The sulfur content decreased with increasing manganese content. This decrease was especially pronounced at the lower carbon contents. The other impurity elements (Sn, As and Sb) were all on a low level, and their sum did not exceed what is considered a safe level (Ref. 20).

The nitrogen content increased somewhat with increasing manganese content, being especially pronounced for the low-carbon electrodes, while the oxygen content on the whole was constant. It should, however, be noted that the three lower manganese contents in the 0.09%C specimens had an oxygen content approximately 100 ppm higher than in the other specimens.

Mechanical Properties

The yield strength measured is shown as a function of Mn-content in Fig. 1. As expected, the yield strength increased with increasing carbon and Mn-content. The influence of Mn is relatively strong, while the influence of carbon is quite small, except for the highest carbon content.

The Charpy V-notch impact toughness curves are plotted in Figs. 2 A-D. First, it can be noted that increasing manganese content decreased the upper shelf energies, probably simply due to an increased yield strength of the matrix. The impact properties at lower temperatures showed mixed behavior, depending on the combination of C and Mn. For the lower manganese contents, increasing carbon content led to significant improvement in impact toughness at lower temperatures. At the higher manganese contents, the intermediate carbon contents gave the best impact values at the lower temperatures.

In Fig. 3, impact toughness at −60°C (−76°F) is plotted as a function of Mn content, for constant carbon levels. For two of the carbon levels (0.09 and 0.12%), optimum contents of Mn were found, while for the two lower carbon contents, the optimum Mn content seemed to be higher than the maximum contents used in this investigation.

The best impact toughness at −60°C was found for the combination 0.12C-1.35Mn, but also the intermediate carbon levels, combined with a relatively high manganese level, showed good results. At −40°C (−40°F) almost the same pattern was followed. The best impact toughness was achieved with the combination 0.12%C-1.2%Mn. Also, the combinations 0.09%C-1.2%Mn and 0.06%C-1.4-1.8% Mn gave satisfactory toughness. Increasing the manganese content above 1.4% gave a reduction in toughness for the two

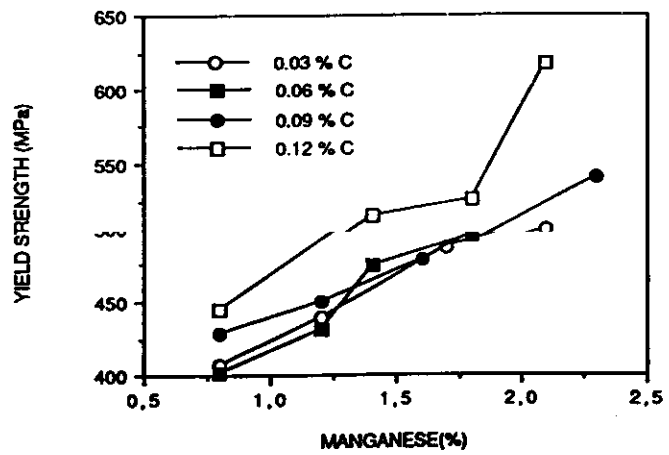

Fig. 1—Yield strength as a function of carbon and manganese content.

Microstructure

The austenite grain size, measured in the last deposited bead, decreased with increasing carbon and manganese content, except for the 0.06% carbon welds, which all had a slightly larger austenite grain size. The austenite grain sizes are given in Table 2.

There is no systematic variation in austenite grain size with oxygen content. However, it should of course be noted that the oxygen content varies within a fairly narrow range.

The results of the quantitative assessment of the microstructure are given in Figs. 4 A-D. For a given carbon content, the amount of acicular ferrite increased at the expense of both allotriomorphic ferrite and ferrite side plates with increasing manganese content. The maximum

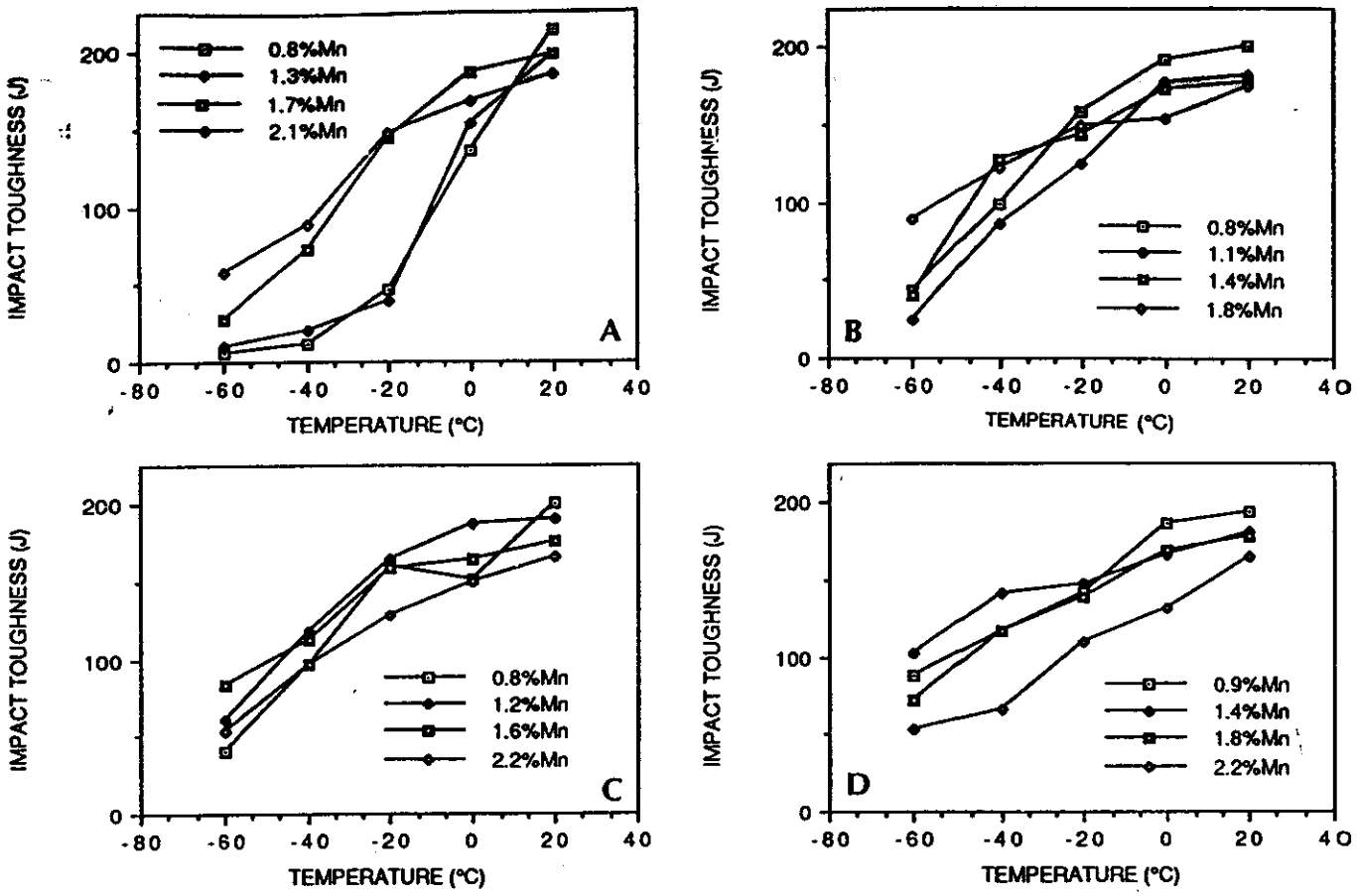

Fig. 2—Charpy V-notch impact toughness curves. A—0.03%C; B—0.06%C; C—0.09%C; D—0.12%C.

amount of acicular ferrite achievable with only carbon and manganese additions seems to be around 65–70% for this particular set of welding conditions. Keeping Mn constant and looking at increasing carbon content, the same trends are found. However, it should be noted that for a manganese content of 0.8, a maximum acicular ferrite content of only about 50% is achieved, and for both 1.1 and 1.5% Mn, 0.12% carbon is necessary to maximize the amount of acicular ferrite. Representative micrographs of the weld metals with "extreme" compositions are shown in Figs. 5–8.

The number of microphases naturally increased with increasing carbon and manganese content. For the lower alloy contents, the microphases were evenly distributed in the microstructure. With increasing manganese content, the microphases became more segregated. This can be seen by comparing Figs. 9 A and B.

The nature of the microphases can lead to ambiguous identification by light optical microscopy. Therefore, the last bead in some of the specimens was examined by TEM to establish the nature of the microphases. For the low-carbon/low-manganese weld metal, a few regions with grain boundary carbides were found. With high carbon content, but still low manganese content, isolated grains of retained austenite were found, as well as grain boundary carbides (Fig. 10). With both high carbon and high manganese content, continuous layers of retained austenite were found—Fig. 11.

The impact specimens were extracted from the middle of the plate, and therefore, it cannot be directly assumed that the microphases present in these specimens are of the same kind as those in the

Table 2—Austenite Grain Size of the Weld Metals[a]

Specimen No.	Austenite Grain Size (μm)
1	65
2	55
3	42
4	42
5	71
6	65
7	60
8	48
9	45
10	45
11	45
12	45
13	36
14	36
15	40
16	45

(a) Measured perpendicular to the length axis of the grains.

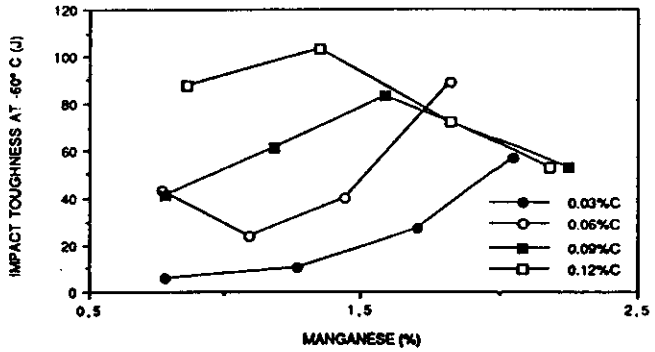

Fig. 3—Impact toughness at −60°C as a function of manganese content.

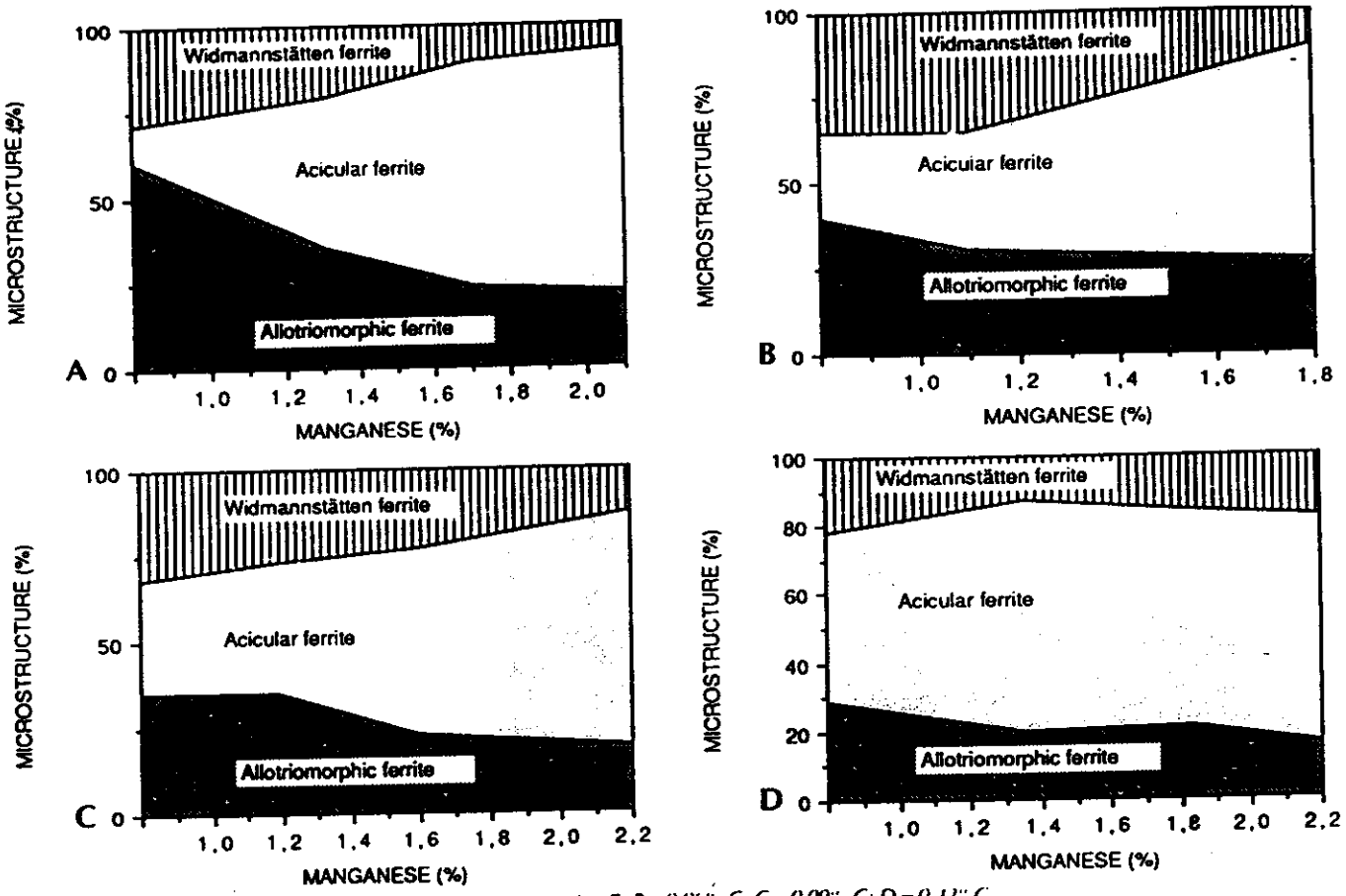

Fig. 4 – Quantitative description of the microstructure. A – 0.03% C; B – 0.06% C; C – 0.09% C; D – 0.12% C.

Fig. 5 – Optical micrograph of the weld metal with 0.03% C – 0.8% Mn. The microstructure consists mainly of a coarse allotriomorphic ferrite, ferrite side plates and coarse acicular ferrite.

last bead. However, since the microphases appear as retained austenite in the as-deposited microstructure, they will be either ferrite + carbide aggregates, untempered martensite or still retained austenite in the reheated material, depending on reheating temperature. All these phases could induce brittleness. Examination of cross-sections of impact specimens containing segregated bands of microphases shows that in areas where the segregation bands are parallel with the notch, the fracture surface has a brittle appearance – Fig. 12. In other cases, in adjacent beads, where the segregation bands are inclined to the notch, the fracture surface has a more ductile appearance – Fig. 13.

These observations cannot be taken as strict evidence for microphase-induced cleavage cracking, but combined with many observations made earlier, we certainly feel confident that the segregated microphases are responsible for the drop in toughness at higher manganese contents.

Discussion

It is commonly assumed that a high amount of acicular ferrite should be present in the microstructure to obtain good impact toughness through the effect of the fine grain size. The increase in acicular ferrite is usually, but not always, accompanied by a decrease in the amount of coarse-grained allotriomorphic ferrite and, thus, as discussed previously, connected to the amounts of carbon and manganese.

In Fig. 14, the impact toughness values at −60°C is plotted as a function of the amount of acicular ferrite. Figure 15 shows similar information extracted from the data of Evans (Ref. 2).

In both investigations, the same general trend is found, that increasing amounts of acicular ferrite improves toughness. Indeed, there is large scatter in the relation between acicular ferrite and toughness, but as a rule of thumb, it can be said that more than 50% acicular ferrite gives acceptable impact toughness. However, in Fig. 14 it can be noted that the weld metals with the lowest C contents give much lower impact toughness values than expected from the acicular ferrite content. This behavior is in contradiction to the results of Evans (Ref. 2), who found a much faster improvement in impact toughness with increasing the amount of acicular ferrite.

The only element which clearly is different between the low-carbon welds and the other welds in this study is nitrogen; being much higher in the low-carbon welds. Nitrogen is well known to embrit-

Fig. 6 – Optical micrograph of the weld metal with 0.03 – 2.1% Mn. Mainly acicular ferrite and thin rims of allotriomorphic ferrite.

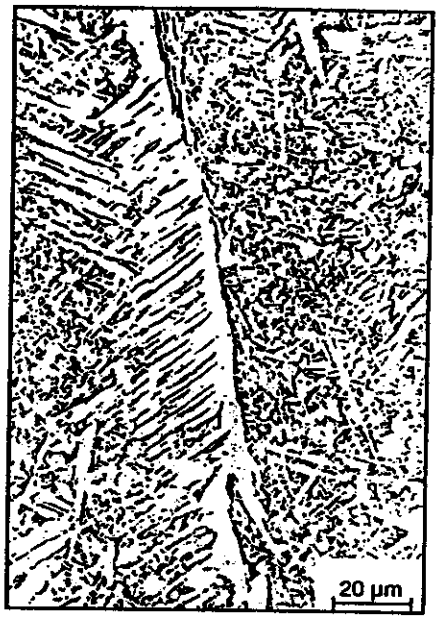

Fig. 7 – Optical micrograph of the weld metal with 0.12%C – 0.8%Mn. The rim of allotriomorphic ferrite is quite thin. The amount of ferrite side plates is quite high.

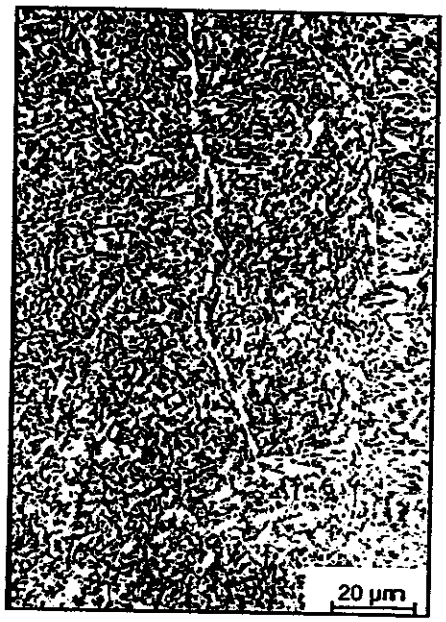

Fig. 8 – Optical micrograph of the weld metal with 0.12%C – 2.2%Mn. Shown is the extremely fine microstructure with a high amount of acicular ferrite.

tle weld metals, although the values found here would not be considered as dangerous. Unfortunately, Evans did not give values of nitrogen content in his report. The agreement for low values of acicular ferrite is not surprising, since this is determined by the overall brittle microstructure. The deviation at the high amounts of acicular ferrite is, for lack of a better explanation, assumed to be due to nitrogen. However, this is purely speculative and needs more investigation.

Another observation that can be made from both Figs. 14 and 15 is that the impact toughness shows a slight decrease for the highest amounts of acicular ferrite. This decrease in toughness seems to occur for acicular ferrite contents in excess of about 70%. Comparison with Fig. 12 shows that the lower toughness is due to increased amounts of brittle cleavage fracture.

Evans (Ref. 2) argued that the decreasing toughness of high alloying content welds was due to increasing yield strength without a corresponding decrease in grain size. As explained in the background section, the mechanical properties are a function of a mixture of microstructures. To assess the influence of each type of microstructure on the properties is a complex task. Even if it is a great oversimplification to relate the mechanical properties to the as-deposited microstructures, this approach should give guidance to the operating mechanisms.

However, as noted above, the highest alloyed welds contained higher amounts of acicular ferrite than the lower alloyed welds. The yield strength of these alloys also was higher than the lower alloyed metals. If the above way of reasoning is accepted, then a higher amount of acicular ferrite is equivalent to a decreasing grain size in the whole weld metal. The higher yield strength is, thus, partly a grain size effect. Finer grains should also lead to better toughness, contrary to what is observed.

The classical model of cleavage fracture is that this occurs at a temperature where the yield strength exceeds the fracture stress. However, both the yield strength and the fracture stress are grain-size dependent in such a way that finer grains lead to both higher yield and fracture strength. Thus, the amount of cleavage fracture is not expected to increase in the highest alloyed weld metals, but this is obviously what happens when the toughness falls. Obviously, something in the microstructure offsets the beneficial effect of finer grains. The most likely factor responsible for this is the segregated microphases, which is in line with the observations in Figs. 12 and 13.

Fig. 9 – A – Optical micrograph showing how the microphases (white small grains) are randomly dispersed; B – with higher alloying content, the microphases are becoming more segregated. Etching was made, using Klemms reagent (Ref. 21), to more easily distinguish the microphases.

Fig. 10 – TEM micrograph showing isolated islands of retained austenite (arrowed) and some grain boundary carbides.

Fig. 11 – Centered dark field TEM micrograph of weld metal 0.12%C – 2.2%Mn, showing an almost continuous layer of retained austenite.

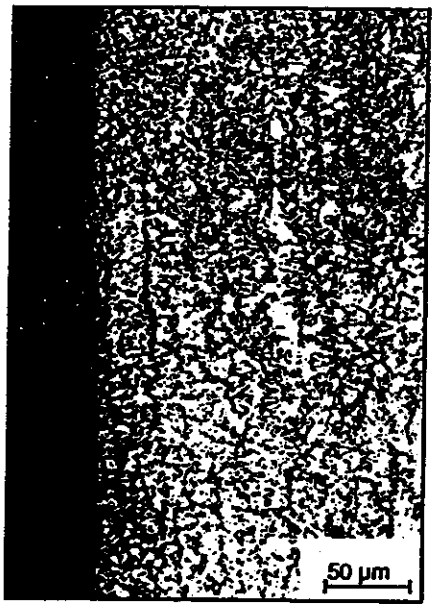

Fig. 12 – Optical micrograph of a polished cross-section through an impact specimen, showing that the brittle appearance of the fracture surface is parallel with the segregation band of microphases.

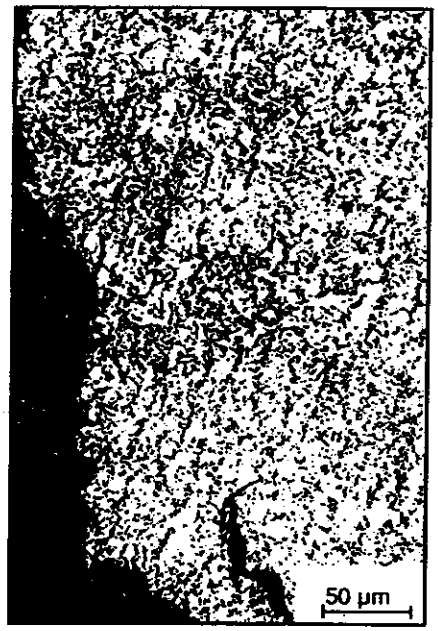

Fig. 13 – Optical micrograph showing a ductile appearance of the fracture surface in an area where the bands of microphases appear at an angle to the fracture surface.

Garland and Kirkwood (Ref. 22) have pointed out the detrimental effect to toughness of segregated microphases in the form of martensite. On the other hand, if the microphases appear as grain boundary carbides, they may facilitate propagation of cleavage cracks across grain boundaries, as suggested by Knott (Ref. 17). Also, if they appear as small, randomly dispersed regions of martensite or retained austenite, they may act as starting points of cleavage cracks, in a manner similar as suggested for oxide inclusions. Thus, the microphase generally has a negative effect on toughness, by facilitating the nucleation of cleavage cracks.

If the microphases are martensitic or retained austenite, they will have a high carbon content, since carbon is diffusing into these areas, away from the ferrite during the austenite to ferrite transformation. Martensitic regions would be very brittle, if they are not tempered. However, most of the martensite appearing under the notch in an impact specimen from a multipass weld metal would have been tempered and, thus, should not be detrimental to toughness. The work of Garland and Kirkwood (Ref. 21) is related to a two-pass welding procedure, and the impact testing was made on solely as-deposited microstructure, where no tempering of the martensitic regions could occur. Retained austenite microphases in multipass weld metal must, on the other hand, be considered as a more unreliable component in terms of toughness, since it is likely to be unstable and transform to brittle martensite during the impact testing. If the microphases appear as segregated bands, as in the high-carbon, high-manganese welds, the situation is even worse, since cleavage cracks should then be able to both nucleate and propagate easily.

The observation of the microphases in the high-carbon, high-manganese specimen being only retained austenite and not martensite can be understood by consid-

Fig. 14 – Impact toughness at −60°C as a function of acicular ferrite content, from this investigation.

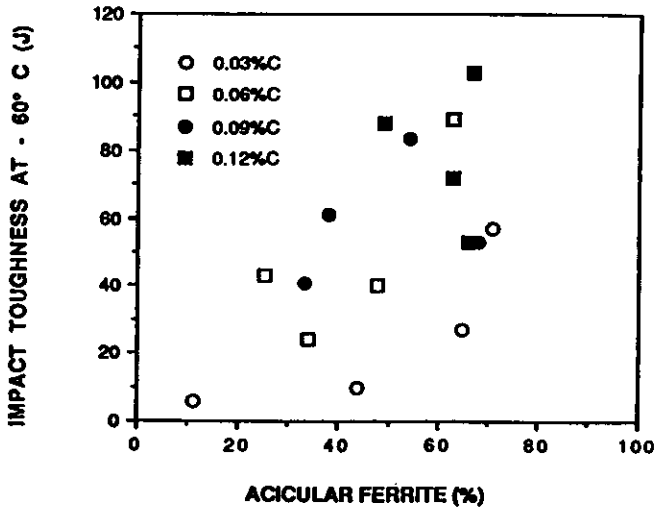

ering the enrichment of carbon in the remaining austenite. From average composition data, the M_s temperature is so high that no retained austenite is expected. However, with increasing carbon content, the M_s temperature falls below room temperature and, consequently, the austenite is retained.

As noted previously, the highest impact toughness in the present work was obtained with the combination 0.12 C - 1.35 Mn, but several other combinations had almost the same toughness. This shows that a proper microstructure, and hence good toughness, can be obtained balancing carbon and manganese in several combinations. What is obviously essential is to achieve high enough proportion of acicular ferrite, but then not alloy the welds further, since this causes segregated bands of microphases. This observation is somewhat at variance with the work of Evans (Refs. 2-9), where mainly the combination 1.4 Mn-0.07 C gave optimum toughness.

Thus, to summarize, the impact toughness values found can mainly be understood by considering the general microstructure and, for high manganese contents, the detrimental effect of microphases. Nitrogen may have caused low impact toughness values in some specimens.

We would further like to point out, that:

1) The positive effect of only 50% acicular ferrite is something seldom noticed, in fact it is more common to believe that 80-90% acicular ferrite is necessary to obtain satisfactory impact toughness at −60°C.

2) An increasing yield strength of the alloys did not negatively influence the impact toughness. The increase in yield strength was mainly achieved by a decreasing grain size and naturally, this improves the impact toughness.

3) The positive effects of decreasing grain size by increasing alloying content can be offset by the formation of segregated bands of brittle microphases.

We believe that these points are important to note for future developments in this field.

Conclusions

1) Several combinations of carbon and manganese produced impact toughness of the level of 100 J (74 ft-lb) at −60°C (−76°F).
2) The most important factor seemed to be an acicular ferrite content of more than 50%.
3) With excessive alloying, the segregation pattern of microphases caused decreasing toughness.
4) Although only a limited variation in oxygen content was studied, no influence of oxygen could be found on impact toughness.
5) With low carbon content, surprisingly low impact toughness was found. The nitrogen content of these specimens was higher than in the other specimens and this may lead to embrittlement.
6) The nature of the microphases varied from grain boundary carbides at low alloying content to more or less continuous layers of retained austenite at the higher alloying contents.

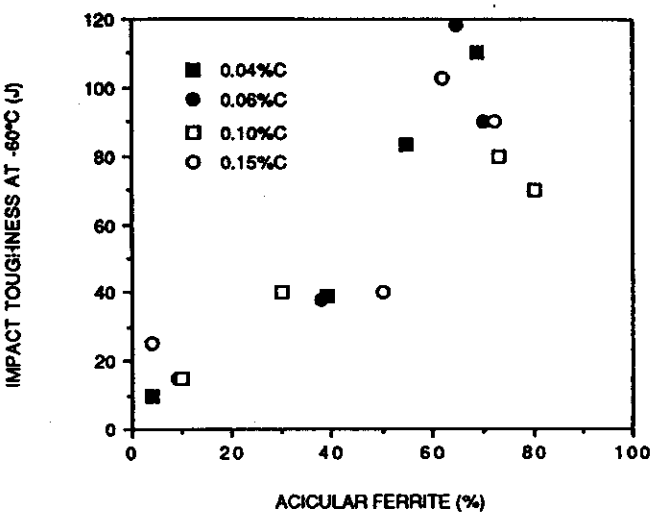

Fig. 15 — Impact toughness at −60°C as a function of acicular ferrite content, from the work of Evans (Ref. 2).

References

1. Vuik, J. 1985. Effects of carbon on the properties and microstructure of weld metal. IIW-doc. IX-1375-85.

2. Evans, G.M., 1981. The effect of carbon on the microstructure and properties of C-Mn all-weld-metal deposits. IIW-doc II-A-546-81.

3. Evans, G.M., 1977. Effect of manganese on the microstructure and properties of all-weld-metal deposits. IIW-doc. II-A-432-77.

4. Evans, G. M., 1986. Effects of silicon on the microstructure and properties of C-Mn all-weld-metal deposits. *Met. Constr.* 18(7):438R-444R.

5. Evans, G.M. 1978. Effect of interpass temperature on the microstructure and properties of C-Mn all-weld-metal deposits. IIW-doc. II-A-460-78.

6. Evans, G.M. 1986. Effects of sulfur and phosphorus on microstructure and properties of C-Mn all-weld-metal deposits. *Met. Constr.* 18(10):631R-636R.

7. Evans, G.M. 1986. The effect of molybdenum on the microstructure and properties of C-Mn all-weld-metal deposits. IIW-doc II-A-666-86.

8. Evans, G.M. 1980. Effect of heat input on the microstructure and properties of C-Mn all-weld-metal deposits. *Oerlikon-Schweissmitteilungen* 38,92:20-35.

9. Evans, G.M. 1985. The effect of heat treatment on the microstructure and properties of C-Mn all-weld-metal deposits. *Met Constr.* 17(10):676R-682R.

10. Bhadeshia, H.K.D.H., Svensson, L-E., and Gretoft, B. 1985. A model for the development of microstructure in low-alloy steel (Fe-Mn-Si-C) weld deposits. *Acta Met.* 33(7):1271-1282.

11. Gretoft, B., Bhadeshia, H.K.D.H., and Svensson, L-E. 1986. Development of microstructure in the fusion zone of steel weld deposits. *Acta Stereol* 5/2 pp. 365-371.

12. Bhadeshia, H.K.D.H., Svensson, L-E., and Gretoft, B., 1986. Prediction of microstructure of the fusion zone of multicomponent steel weld deposits. *Advances in Welding Science and Technology, — Proc. Int. Conf. Trends in Welding Research,* Gatlinburg, Tenn., ed. S.A. David.

13. Dolby, R. 1976. Factors controlling weld toughness — the present position. Part 2, weld metals. Weld. Inst. Res. Rep. 14/1976/M.

14. Tweed, J.H., and Knott, J.F., 1987. The effect of preheat temperature on the microstructure and toughness of a C-Mn weld metal. *Met. Constr.* 19(3):153R-158R.

15. McRobie, D.E., and Knott, J.F., 1985. Effects of strain aging on fracture toughness of C-Mn weld metal. *Mater. Sci and Tech.* 1(5):357-365.

16. Tweed, J.H., and Knott, J.F. 1987. Micromechanisms of failure in C-Mn weld metals. *Acta Met.* 35(7):1401-1414.

17. Curry, D.C., and Knott, J.F. 1978. Effects of microstructure on cleavage fracture stress in steel. *Metal Sci* 12 p. 511.

18. Duncan, A. 1987. Guide to the examination of ferritic steel weld metals. IIW-doc IX)-123-87.

19. Bhadeshia, H.K.D.H., Svensson, L-E., and Gretoft, B. 1986. The austenite grain structure of low-alloy steel weld depostis. *J. Mater. Sci* 21, pp. 3947-3951.

20. Almqvist, G., Gretoft, B., Svensson, L-E., and Wittung, L. 1983. The influence of impurity elements on the embrittlement of ferritic weld metals. Proc. Int. Conf. *The Effect of Residual, Impurity and Microalloying Elements on Weldability and Weld Properties.* London, England, ed. P. Hart.

21. Weck, E., and Leistner, E. 1983. Metallographic instructions for color etching by immersion, Part II. *Deutscher Verlag für Schweisstechnik.*

22. Garland, J.G., and Kirkwood, P.R. 1975. Towards improved submerged arc weld metal. *Met. Constr.* 7 pp. 275-283 (Part 1) and pp. 320-330 (Part 2).

Research & Development

This special section is devoted to technological progress reports and accounts of new experiment work in welding and also metal forming and cutting. Contributions of direct practical significanc from authors working on these aspects of fabrication both in Britain and overseas will be publishe

WELD HEAT-AFFECTED ZONE STRUCTURE AND PROPERTIES OF TWO MILD STEELS

E. SMITH, Ph.D., B.Sc., A.I.M., M. D. COWARD, M.Phil., B.Sc., A.R.S.M., and R. L. APPS, Ph.D., B.Sc., F.I.M., M.Weld.I.

SYNOPSIS: An examination has been made of the structures formed in the heat-affected zone (HAZ) of two mild steels by a submerged-arc bead-on-plate weld in 1½ in. thick plate using a heat input of 108 kJ/in. A simulation technique has been used to reproduce the structures of the HAZ in sufficient bulk for mechanical testing. An attempt is made to correlate the metallurgical microstructures with the mechanical properties, with special emphasis on notch-toughness. Finally, the effect of an applied restraint during thermal simulation on the notch-toughness properties has been assessed.

MILD steel is the most widely used metal in welded fabrications. It undergoes only minor hardening in the HAZ and tests carried out on welded joints show that, in general, weldments in mild steel are acceptable without having recourse to post-weld heat-treatment.

However, with the trend towards larger welded structures employing thicker material and operating under higher stresses, brittle fracture becomes a serious hazard, particularly where service temperatures are low. In addition, higher residual tensile stresses occur in the immediate vicinity of a weld in thicker material and this, coupled with the continuous nature of a welded structure and the strain rate sensitivity of steel increases the likelihood of catastrophic failure occurring. Thus, it becomes increasingly important to avoid conditions under which cracks may be initiated and grow to a critical size. At the same time, it is impossible to avoid completely potential sources of stress concentration which may arise, for example, from weld defects, because even carefully executed inspection methods cannot guarantee freedom from defects. However, stress concentrations can be rendered less harmful if they occur in a microstructure which is less sensitive to crack initiation and growth.

It is not surprising that the potential dangers of the weld HAZ were ignored for many years while considerable efforts were devoted to improving weld metal quality, since it is only in recent years that weld metal quality has equalled or surpassed that of wrought steel. However, in a minority of failures in welded structures, fractures have initiated and/or propagated in the weld HAZ. These structures have failed, usually with expensive results, because of regions of low ductility and fracture toughness produced in the HAZ by the complex thermal and strain cycles accompanying welding. Techniques for evaluating mechanical properties of the HAZ structures have been of limited value owing to the difficulty of isolating individual structures in a specimen of sufficient size for mechanical testing. In recent years, this problem has been overcome by the development of simulation techniques for reproducing the microstructures found in the HAZ[1–3]. These require rather costly pieces of equipment but can accurately simulate the heat effect of welding and produce weld HAZ structures of reasonable size.

The aim of the present work was t examine the relationship between th mechanical properties and the micro structures in synthetically produced wel HAZ structures of two commercial mil steels. These structures were produced b thermal cycles identical to those occurrin in submerged-arc welds made with a hea input of 108 kJ/in. in 1½ in. thick plate Previous work has established that ther are three main regions in the HAZ namely, the grain coarsened, grain refined and partial transformation regions[4–8]. Representative structures from each of these regions were examined.

Materials

One steel was a silicon-killed mild steel to BS1501-161 Grade B and was supplied as 2 in. thick hot rolled plate. The other was a mild steel to BS15 and was supplied as 1½ in. thick hot rolled plate. This steel was intermediate between a rimming and a semi-killed steel. The chemical analyses and mechanical properties of both materials are shown in Table 1.

Experimental Procedure

The thermal cycles used for simulating the HAZ structures are shown in Fig. 1 and

Table 1. Chemical Analyses and Mechanical Properties of BS 1501 and BS 15.

	C	Si	Mn	S	P	Ni	Cr	σy ton/in.²	UTS ton/in.²	Elong. %	Reduction of Area %
BS 1501	0·19	0·23	0·64	0·046	0·032	0·14	0·12	18·1	29·2	29	55
BS 15	0·21	0·065	0·89	0·050	0·040	n.d.*	n.d.*	n.d.*	n.d.*	n.d.*	n.d.*

*n.d.—not determined.

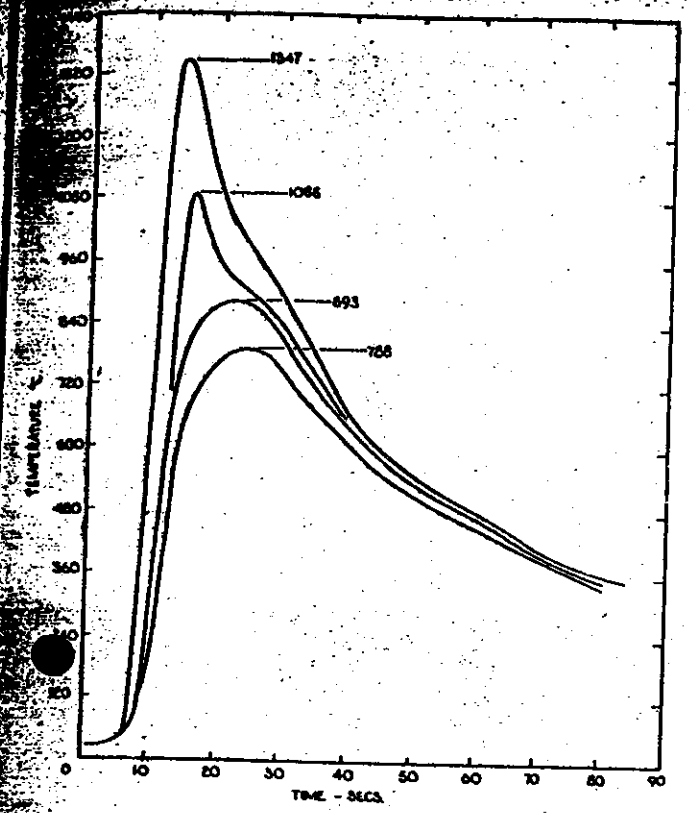

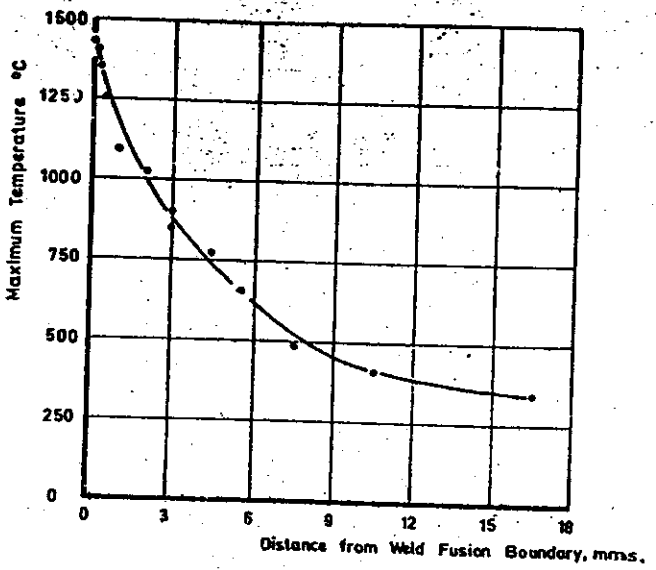

Fig. 1. (Left) Thermal cycles measured in the weld HAZ and used for specimen simulation.

Fig. 2. (Above) Variation of thermal cycle peak temperature with distance from the fusion boundary.

Table 2. Bead-on-Plate Welding Conditions.

Plate thickness	1½ in.
Filler wire	$\frac{3}{16}$ in. mild steel
Arc voltage	30±2 V
Arc current	390±10 A
Welding speed	6½±½ in./min
Heat input	108±2 kJ/in.

the variation of peak temperature across the HAZ in Fig. 2. These results were determined on a submerged-arc bead-on-plate weld using the conditions listed in Table 2. Embedded thermocouples were used to record the thermal cycles at various distances from the fusion boundary. Details of the procedure can be found elsewhere[9].

Specimen welds were prepared in both materials using the conditions shown in Table 2. Sections from each were ground, polished, and etched in 2% Nital and the range of microstructures across the HAZ examined by optical microscopy. The variation in hardness across the HAZ was determined using a Zwick hardness testing machine and a load of 5 kg.

Simulation of the HAZ structures was achieved using equipment designed and constructed at the Cranfield Institute of Technology. Details of this equipment can be found in another report[10]. Briefly, the equipment uses a.c. resistance heating and water cooling to impose the desired thermal cycle on specimens 2·5 in. by 0·4 in. by 0·4 in., the thermal cycle being chosen by adjustment of a bank of variable resistors to construct a voltage analogue. Control of specimen temperature is achieved using a thyristor and two ignitrons to control the input at 440 V to a welding transformer. Feedback is applied from a thermocouple welded to the specimen hot zone. The equipment has been shown to produce the desired thermal cycles in a reproducible manner.

Four thermal cycles were chosen for simulation in each material as representing the grain coarsened, grain refined and partial transformation regions of the HAZ. In the main part of the work the specimens were held in a pair of movable jaws so that they could expand and contract freely during heat-treatment. Another series of tests was carried out on the BS15 material in which the specimens were held rigidly in the jaws to prevent expansion and contraction and so determine the effect of restraint on the resulting microstructure and properties.

After simulation, one specimen from each category was sectioned and examined optically and the structures compared with the equivalent ones formed in the specimen weld HAZ. In addition, carbon extraction replicas were prepared and examined using the electron microscope.

Mechanical testing of the simulated structures consisted of hardness tests using the Zwick hardness machine and a load of 5 kg, standard Charpy V-notch impact tests, and tensile tests. The latter were performed on a 10,000 lb Instron universal testing machine at room temperature and a cross-head speed of 0·05 in./min. Hounsfield number 13 test-pieces with a modified gauge length of 0·3 in. were used to ensure a uniform structure throughout the gauge length. A series of preliminary tests indicated that these modified test-pieces yielded the same tensile property results as the standard ones[11].

Results

The ranges of microstructure produced in the HAZ of both materials are shown in Figs. 3. and 4. The HAZ could be divided into three distinct regions as follows:

1. The region of grain coarsening, immediately adjacent to the fusion boundary, where peak temperatures exceeded about 1,100°C. Marked austenite grain growth took place and the relatively rapid cooling rates through the critical range produced a Widmanstätten structure.

2. The region of grain refinement which experienced peak temperatures in the approximate range 1,100—900°C. Complete austenitization took place but the temperature and time were insufficient to cause grain growth so that a totally refined equiaxial grain structure was produced.

3. The region of partial transformation which experienced peak temperatures in the approximate range 900—750°C. This region was heated between the temperature limits of Ac_1 and Ac_3 which produced partial austenitization of the original structure. The regions richest in carbon where partial dissolution of the pearlite occurred, exhibited extremely fine grained structures, while the ferritic regions became less affected as the peak temperature diminished. No trace of martensite formation was observed.

In addition there was a very narrow region, about 0·1 mm wide, in which spheroidization of the pearlite had occurred. This region experienced peak temperatures just below the Ac_1. The lamellar carbides have partially dissolved and reformed as

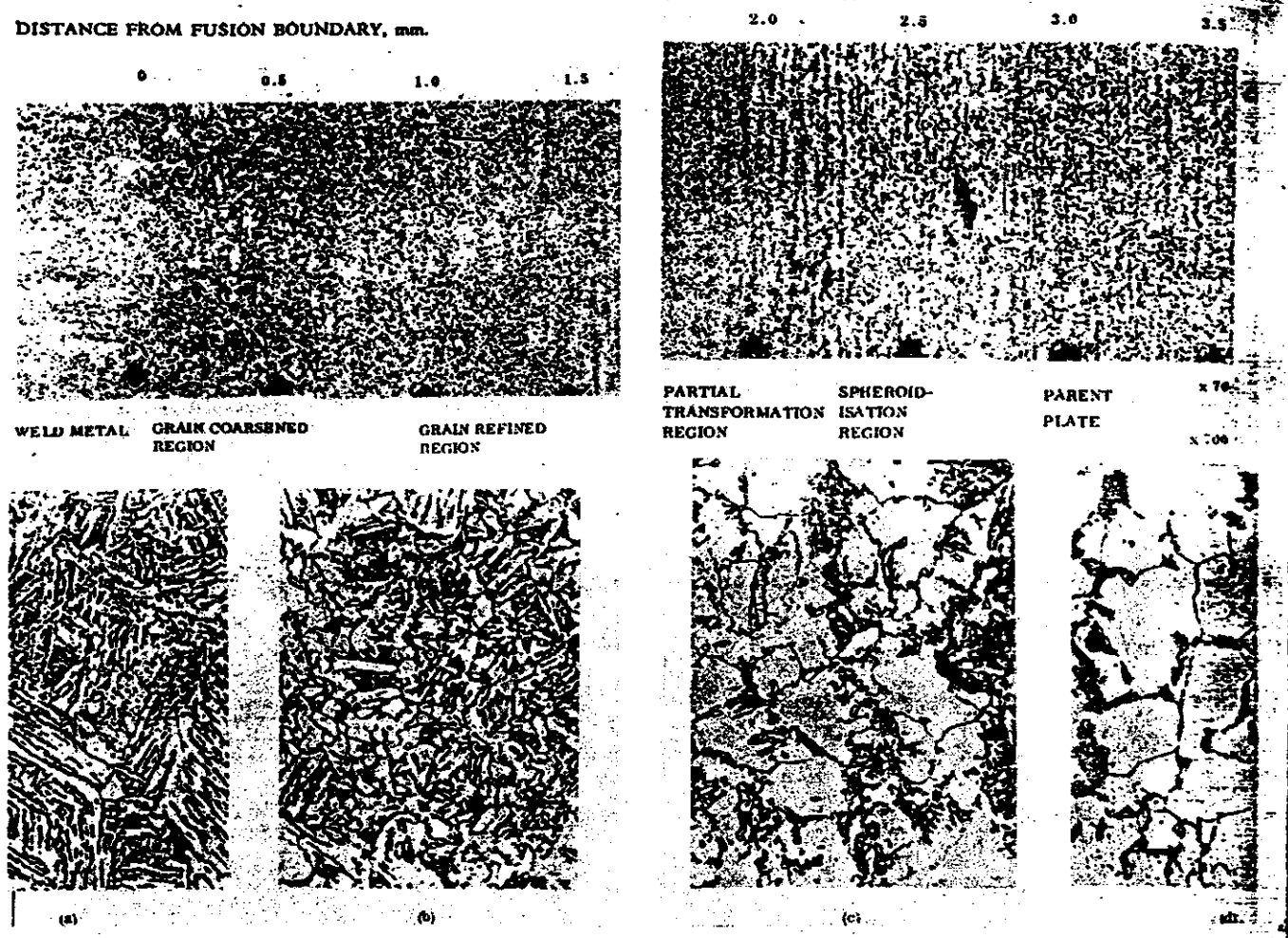

Fig. 3. (Above) The heat-affected zone microstructures associated with a bead-on-plate weld in BS 1501 mild steel.

Fig. 4. (Below) The heat-affected zone microstructures associated with a bead-on-plate weld in BS 15 mild steel.

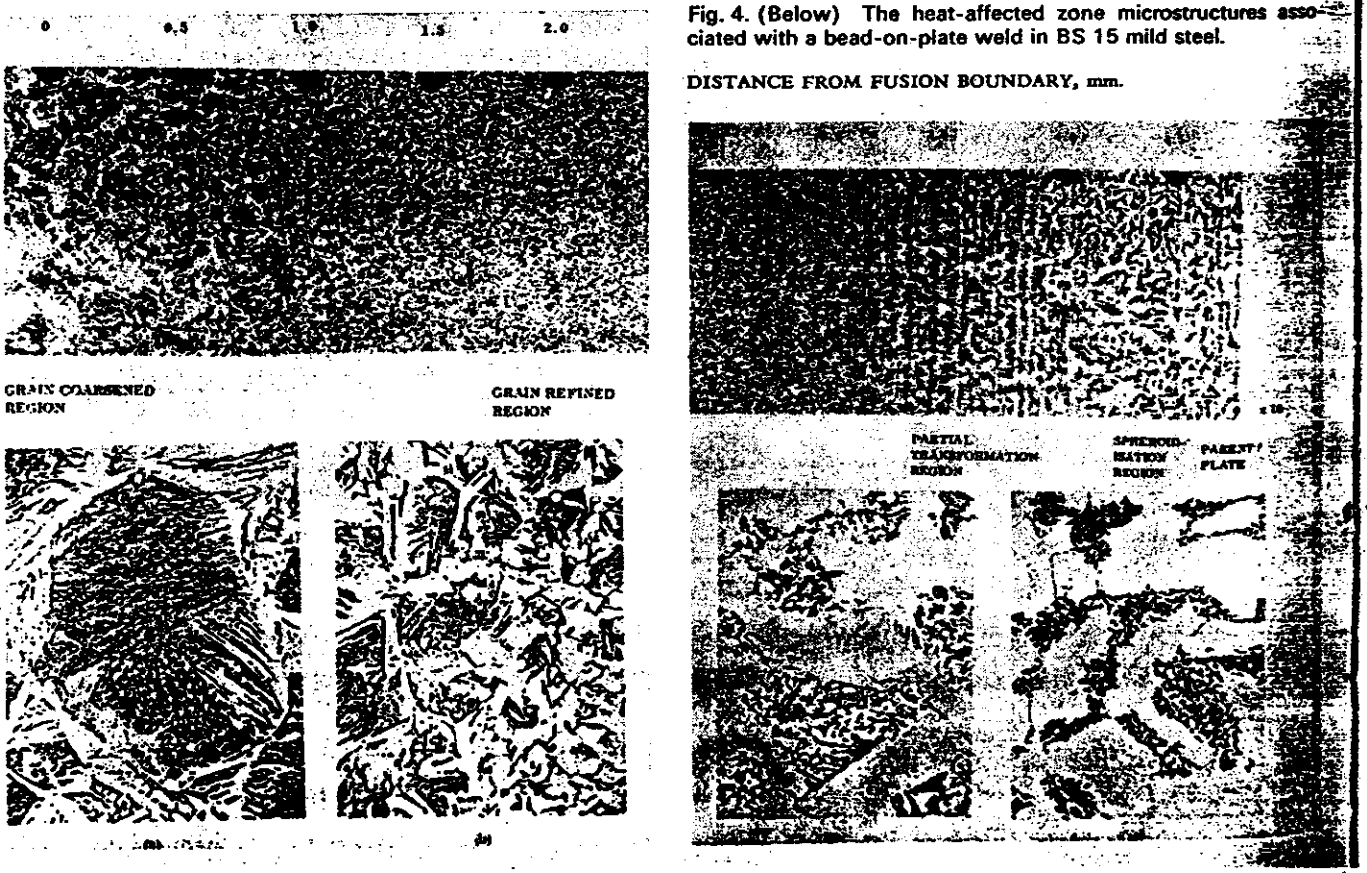

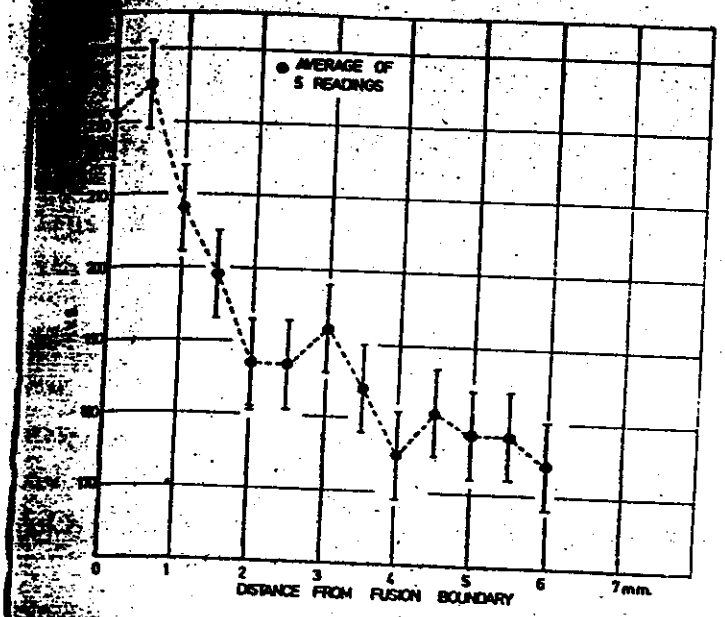

Fig. 5. BS 1501 heat-affected zone hardness survey.

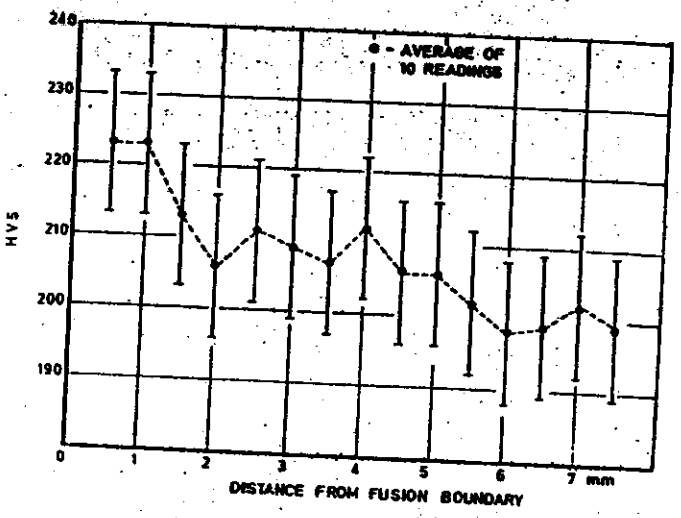

Fig. 6. BS 15 heat-affected zone hardness survey.

Fig. 7. (Right) BS 1501 mild steel parent material. (A) ferrite, (B) pearlite.

Fig. 8. (Below) BS 1501 mild steel simulated to a peak temperature of 788°C. (A) ferrite, (B) upper bainite.

Fig. 9. (Below right) BS 1501 mild steel simulated to a peak temperature of 893°C. (A) ferrite, (B) upper bainite.

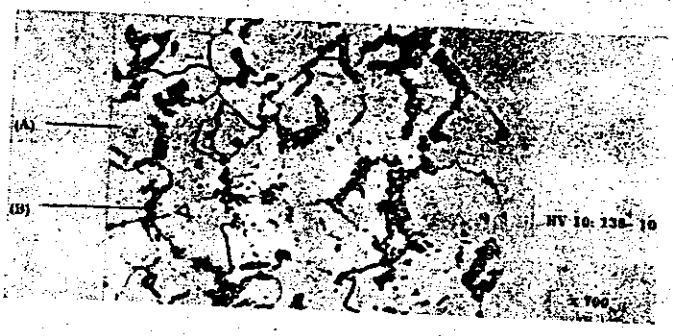

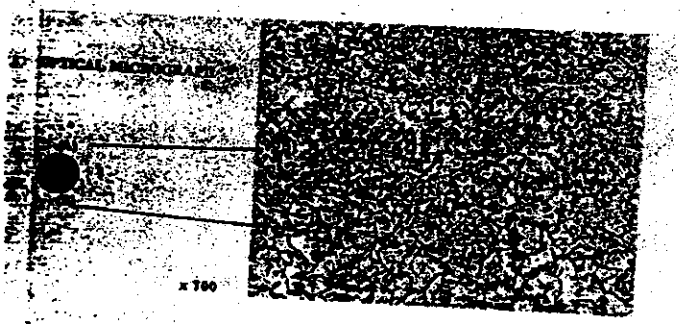

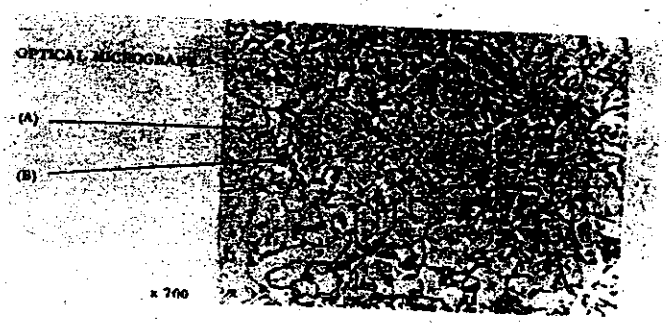

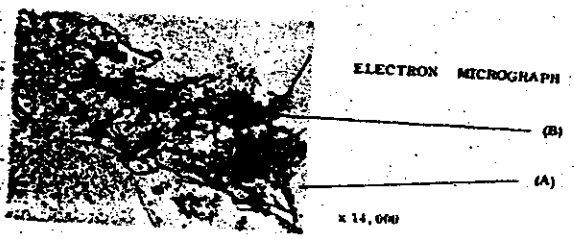

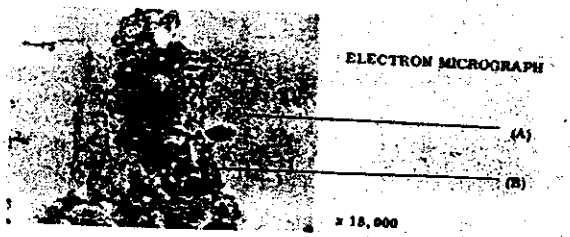

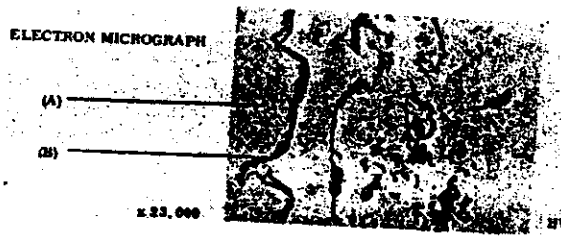

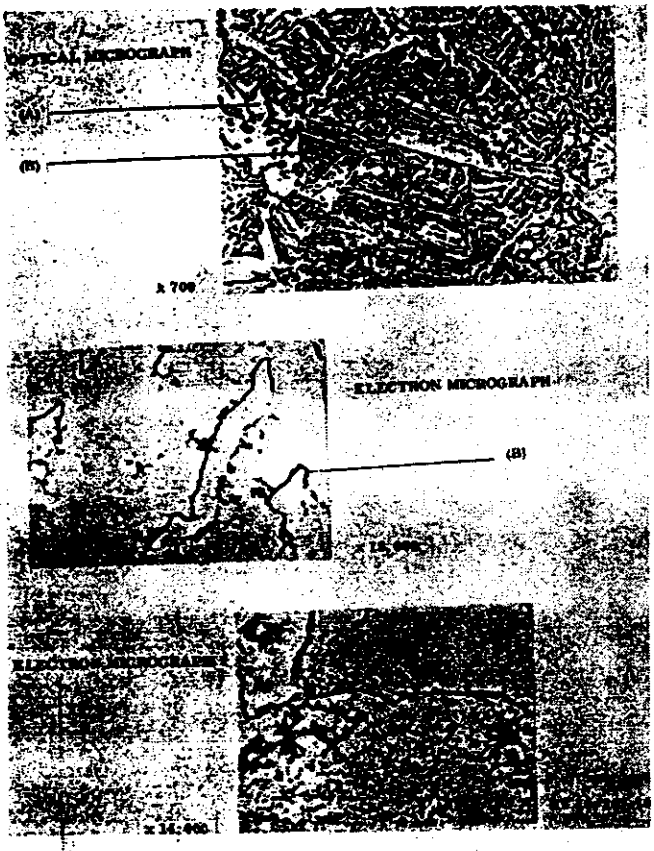

Fig. 10. BS 1501 mild steel simulated to a peak temperature of 1,088°C. (A) proeutectoid ferrite, (B) upper bainite.

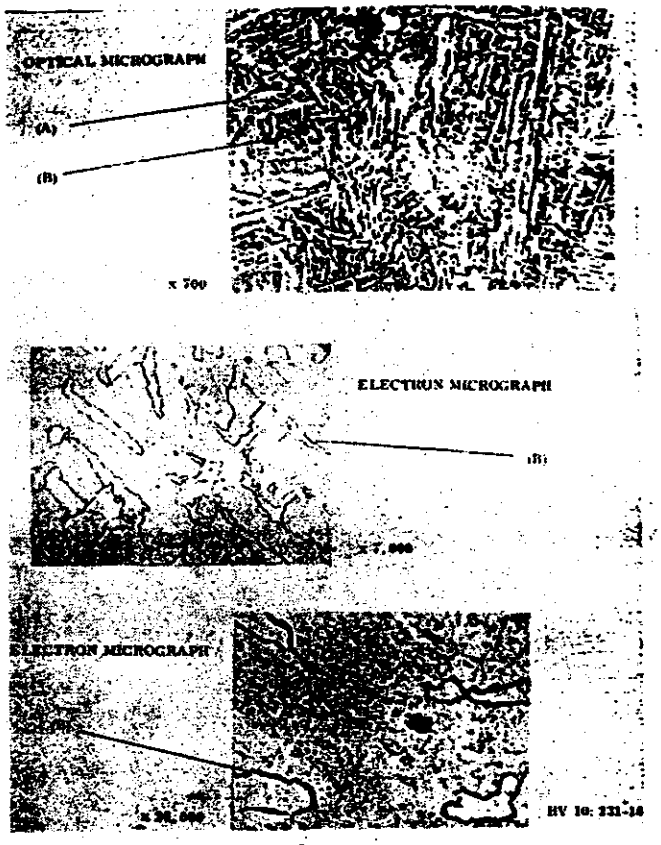

Fig. 11. BS 1501 mild steel simulated to a peak temperature of 1,347°C. (A) proeutectoid ferrite, (B) upper bainite.

spherical particles on cooling. The ferrite matrix was unaffected by these low temperatures. Beyond this region structural changes were not observed by optical microscopy and, therefore, this was defined as the boundary of the visible weld HAZ.

The variations in hardness across the HAZ are shown in Figs. 5 and 6. In general the hardness increased on approaching the fusion boundary, with maximum hardness in the grain coarsened region.

The Simulated HAZ Structures

The parent plate microstructures and those produced by simulation are shown in

Fig. 12. (Below) BS 15 mild steel parent material. (A) ferrite, (B) pearlite.

Fig. 13. (Right) BS 15 mild steel simulated to a peak temperature of 788°C. (A) transformed pearlite, (B) untransformed pearlite, (C) newly formed ferrite, (D) untransformed ferrite.

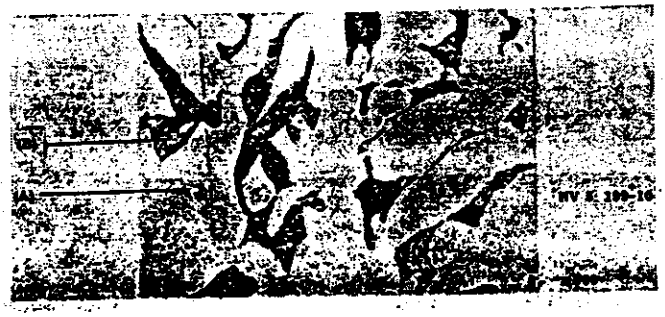

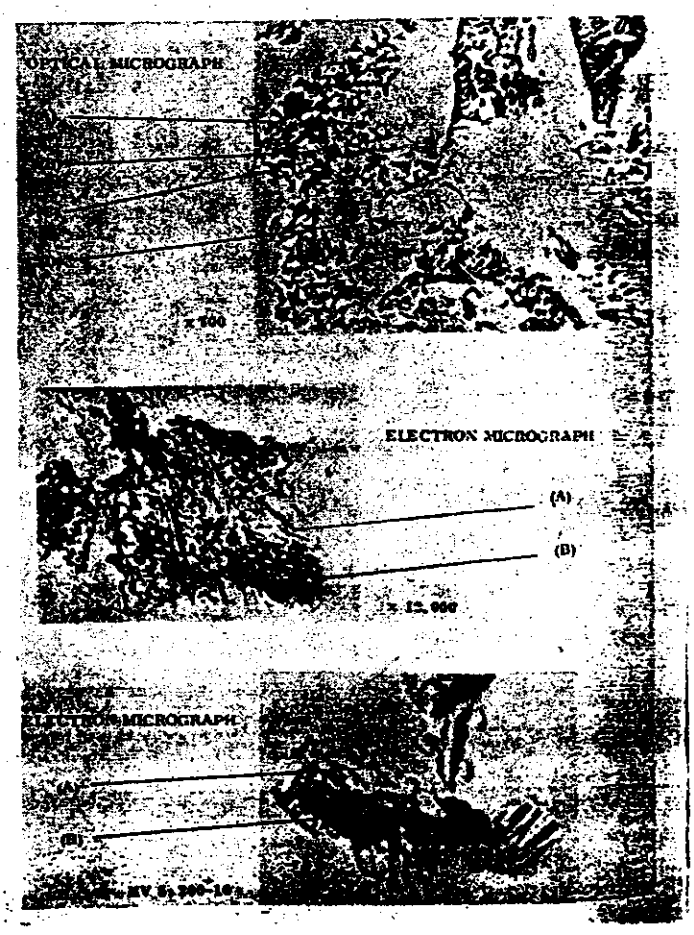

Fig. 14. BS 15 mild steel simulated to a peak temperature of 893°C. (A) ferrite, (B) upper bainite.

Fig. 15. BS 15 mild steel simulated to a peak temperature of 1,070°C. (A) Proeutectoid ferrite, (B) fine carbide and ferrite.

Fig. 16. BS 15 mild steel simulated to a peak temperature of 1,305°C. (A) proeutectoid ferrite, (B) fine carbon and ferrite.

Figs. 7—16. The parent plate microstructures (Figs. 7 and 12) were typical of hot rolled structures and consisted of banded pearlite in a ferrite matrix. Simulation to a peak temperature of 788°C produced structures typical of the partial transformation region (Figs. 8 and 13). Feathery upper bainite was observed in the electron micrographs. Simulation to a peak temperature of 893°C produced a refinement of the ferrite and acicular upper bainite formed in the former pearlite areas (Figs. 9 and 14). These structures simulated the grain refined region. Simulation to peak temperatures of 1,088°C and 1,070°C produced a fine Widmanstätten structure representing the start of the grain coarsening region (Figs. 10 and 15). Simulation to peak temperatures of 1,347°C and 1,305°C produced very coarse Widmanstätten structures typical of the grain coarsened region immediately adjacent to the fusion boundary (Figs. 11 and 16).

The hardnesses of each structure are recorded with the micrographs in Figs. 7—16. They compare directly with the equivalent structures formed in the actual weld HAZ (Figs. 5 and 6).

The results of the Charpy V-notch impact tests are shown in Figs. 17—20 and the variations of transition temperature with peak temperature of simulation in Figs. 21 and 22. The tensile test results on BS 1501 are shown in Fig. 23.

BS 1501 showed a continuous increase in hardness, proof stress and U.T.S. with increasing peak temperature of simulation. All the simulated structures had higher transition temperatures than the parent material, the highest transition temperature being associated with the grain-coarsened and partially transformed structures.

BS 15 also showed a continuous increase in hardness with increasing peak temperature of simulation. Most of the simulated HAZ structures had transition temperatures lower than the parent material which is most probably due to the refinement of the relatively coarse grain size of the parent material. However, an increase in transition temperature was observed in the grain coarsened region.

The restraining mechanism used in one series of tests on BS 15 was calculated to produce plastic deformations of 2% for a peak temperature of 788°C, 3% for 893°C and 4% for 1,070°C. There was no apparent difference in notch-impact properties between the specimens simulated with and without restraint.

Discussion

One of the main difficulties in attempting to explain the structural changes occurring during fusion welding is that, due to the marked departure from equilibrium conditions caused by the rapid heating and cooling rates and the short times at peak temperatures, conventional equilibrium data are not applicable.

The correlation of the temperature measurements made in the HAZ of the BS 15 bead-on-plate weld with the changes in microstructure showed that, owing to the rapid heating, the Ac_1 point was raised by approximately 35°C to 750°C and the Ac_3 point by approximately 75°C to 900°C. These results agree with those of Feuerstein and Smith[12]. The dependence of the Ac_1 and Ac_3 temperatures on heating rate is understandable in the light of the inability of carbon and other alloying elements to diffuse uniformly. Albutt and Garber[13] showed that for a given carbon content the distribution and shape of the carbide influenced the degree to which the Ac_3 was increased, whereas the Ac_1 was insensitive to this. However, it is possible that other factors, such as initial inhomogeneity and grain size may affect the values of the Ac_1 and Ac_3 temperatures.

Simulation of Thermal Cycles. Metallographic structure and hardness of the simulated regions of the weld HAZ compared directly with the equivalent regions of the actual weld HAZ in both materials. A comparison between the thermal cycles measured during welding and those reproduced by the simulation equipment is shown in Fig. 24. The two examples represent the extremes of the thermal cycles used in this work. In all instances, good agreement was obtained in heating and cooling rates and peak temperatures.

The measured difference of 30°C between the surface and the centre of the specimen during simulation was neglected[9]. In most cases the volume of simulated structure produced was approximately 0·4 in.³ and

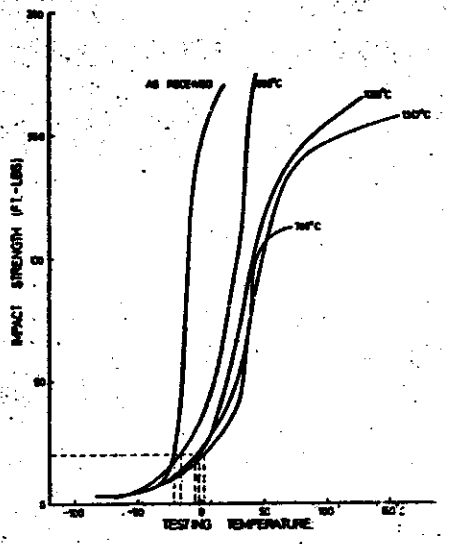

Fig. 17. Comparison of Charpy V-notch impact (ft lb)—temperature curves for BS 1501 mild steel.

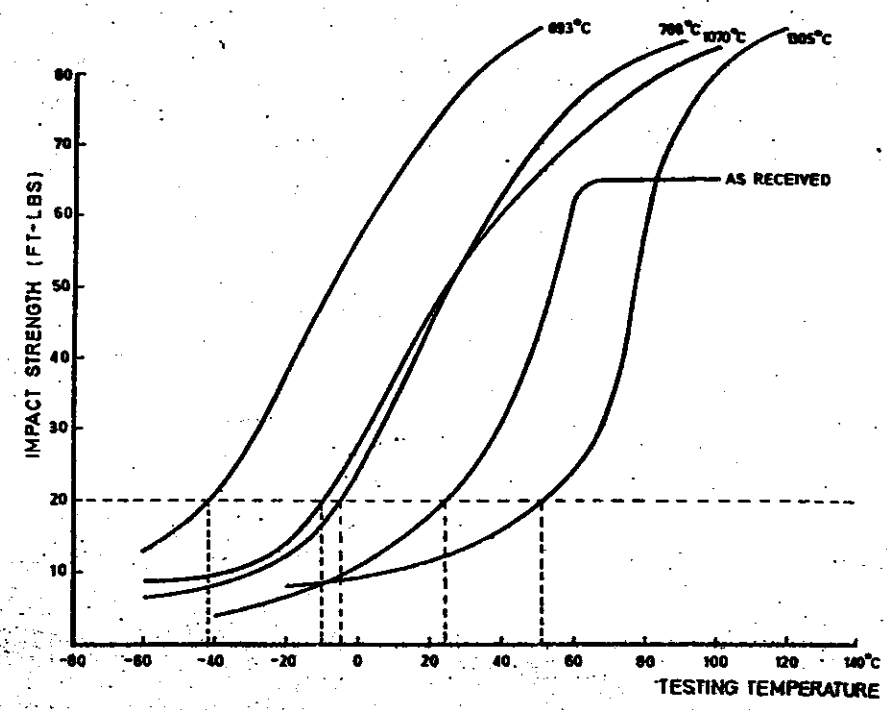

Fig. 19. (Above) Comparison of Charpy V-notch impact (ft lb)—temperature curves for BS 15 mild steel specimens.

in this volume the microstructure and hardness were found to be uniform.

The thermal cycles occurring in the weld HAZ are influenced by a number of factors:

1. Thickness of material.
2. The welding process.
3. The welding conditions, current, voltage and welding speed which control the heat input for unit length of weld.
4. Application of preheat.

The results reported here are concerned with one set of welding conditions; namely the submerged-arc welding of thick plate (i.e. > 1½ in. thickness), with a heat input of 106 kJ/in.

Mechanical Properties and Microstructures in BS 1501

The parent material had a low transition temperature due, probably, to its fine grain size and the degree of deoxidation used in its manufacture. The effect of thermal simulation to all temperatures above the Ac_1 point was to raise the transition temperature. These increases varied between 7 and 50°C depending upon the resulting microstructure and the criterion used for assessment. The poorest notch-toughness properties were associated with the region of grain coarsening experiencing a peak temperature of 1,347°C and the partially transformed region experiencing a peak temperature of 788°C. A similar increase in Charpy V-notch impact transition

Fig. 18. Comparison of Charpy V-notch impact (percentage crystallinity) — temperature curves for BS 1501 mild steel.

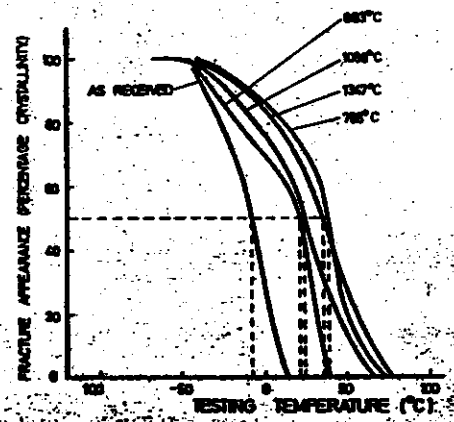

Fig. 20. (Below) Comparison of Charpy V-notch impact (percentage crystallinity) —temperature curves for BS 15 mild steel specimens.

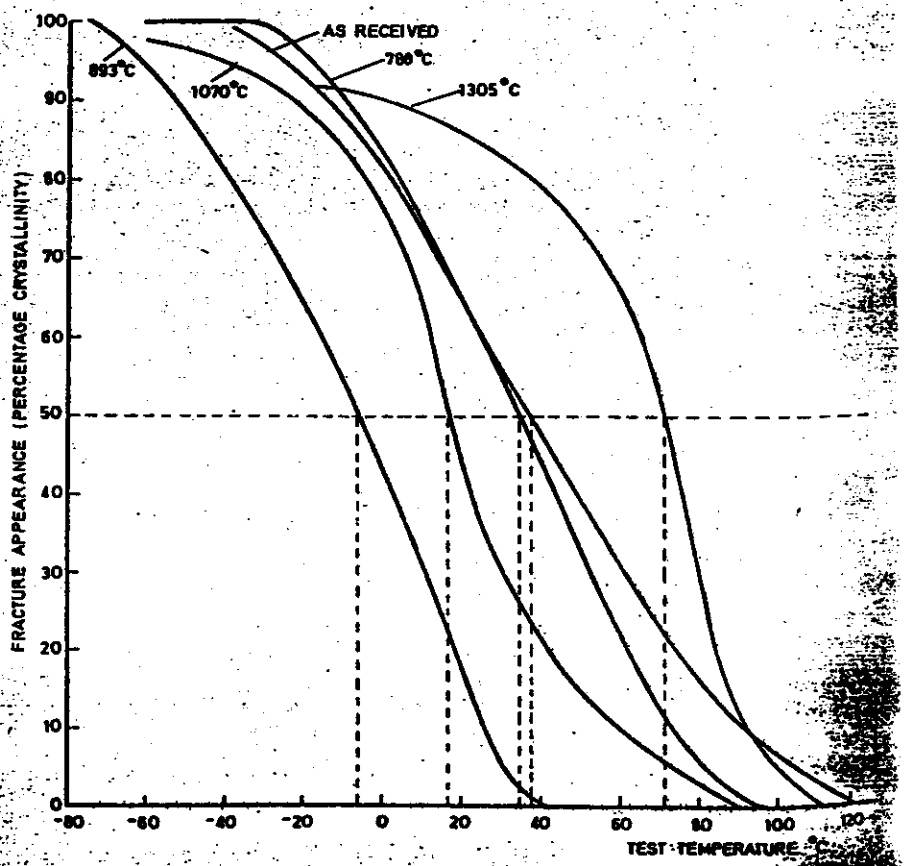

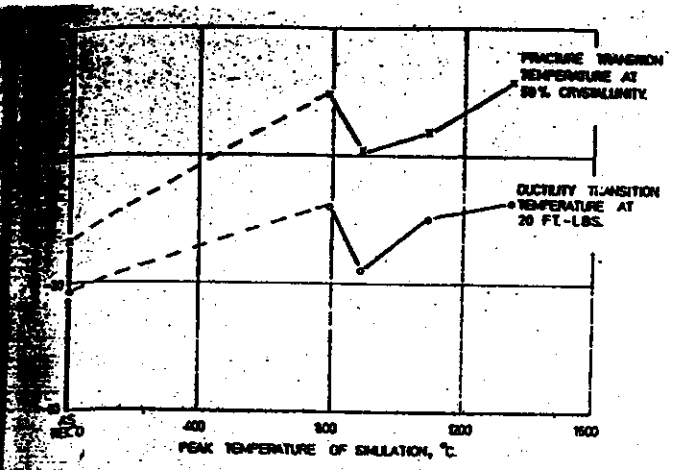

Fig. 21. (Above) Variation in transition temperature with peak temperature of simulation for BS 1501 mild steel.

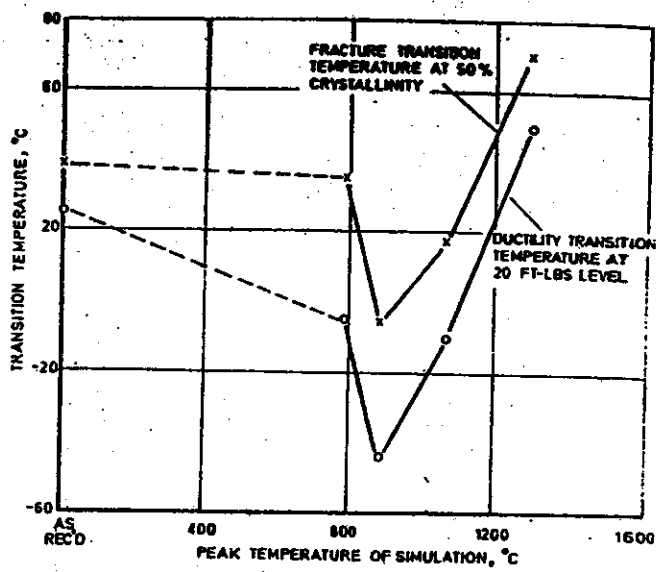

Fig. 22. (Right) Variation in transition temperature with peak temperature of simulation for BS 15 mild steel specimens.

temperature in the grain coarsened region was reported by Inagaki *et al*[3] for a steel of identical composition. This deterioration in notch impact properties was reflected in the tensile test results. All the simulated weld HAZ structures showed an increase in proof stress and U.T.S., and a decrease in ductility compared with the parent material. These changes were greatest in regions closest to the fusion boundary and in this respect, agreed with the hardness measurements. These changes in mechanical properties could be related to the observed microstructures.

(*a*) *Simulation to a Peak Temperature of* 788°C. Austenitization of the pearlite was well developed in this specimen (Fig. 8) and the resulting high carbon austenite transformed to a feathery upper bainitic structure on cooling. No trace of martensite formation was observed. The reduction in ductility and the deterioration in impact properties were probably due to the effect of this upper bainite which was partly compensated for by a slight reduction in the ferrite grain size. The hardness, on the other hand, was comparatively little affected owing to the small proportion of upper bainite in the structure.

(*b*) *Simulation to a Peak Temperature of* 893°C. Austenitization was more fully developed than in the previous sample and the structure had a coarser ferrite and bainite grain size (Fig. 9). The notch-toughness properties improved slightly probably because of some homogenization of the carbon content by dilution into the surrounding ferrite during the time the temperature was above the Ac_1. There was a slight increase in hardness due to the increased proportion of transformation product.

(*c*) *Simulation to a Peak Temperature of* 1,088°C. Austenitization was fully developed in this sample and the high rate of cooling through the critical range resulted in the formation of a Widmanstätten structure (Fig. 10). However, the total time at which the temperature was above the Ac_3 was too short (approximately 5 s) for homogenization and grain growth to occur so that the resulting structure was fine grained. Acicular upper bainite was resolved at higher magnifications. The transition temperature was slightly higher than in the previous sample but still lower than that of the specimen cycled to 788°C. The hardness, proof stress, and U.T.S. were higher than in the previous sample probably because of the greater proportion of transformation product.

(*d*) *Simulation to a Peak Temperature of* 1,347°C. This temperature was greatly in excess of the Ac_3. Consequently, the thermal conditions were sufficient for complete or near-complete homogenization of the austenite and for marked grain growth to occur. Subsequent cooling rates were fast enough to produce a very coarse Widmanstätten structure (Fig. 11) consisting of a network of proeutectoid ferrite outlining the prior austenite grain boundaries and enclosing large areas of carbide and ferrite in a fine distribution. More acicular upper bainite was present than in the previous sample resulting in a marked increase in transition temperature, proof stress, U.T.S. and hardness and a decrease in ductility. These results indicate that the grain-coarsened region experiencing peak temperatures in the vicinity of the melting point has the worst combination of mechanical properties from the viewpoint of susceptibility to brittle fracture. The properties of the partial transformation region are only slightly better. Some precautions would be advisable if the steel is to be used at low temperatures in welded construction.

Mechanical Properties and Microstructures in BS 15

The parent material had a higher transition temperature than the BS 1501 steel, which is probably due to its coarser grain size and the smaller degree of deoxidation used during manufacture. Thermal simulation to peak temperatures of 788°C, 893°C and 1,070°C produced an improvement in notch-impact properties, whilst simulation to a peak temperature of 1,305°C produced a severe deterioration. Once again these changes in mechanical properties were related to microstructural changes.

(*a*) *Simulation to a Peak Temperature of* 788°C. The microstructural changes observed were similar to the equivalent specimen of BS 1501. The slight improvement in notch-toughness properties over those of the parent plate was attributed to a breakdown of the coarse pearlite into a mixture of fine ferrite and pearlite (Fig. 13).

(*b*) *Simulation to a Peak Temperature of* 893°C. The microstructure produced by this treatment (Fig. 14), was quite different from the equivalent specimen in BS 1501, in that a considerable refinement of the ferrite grain size was apparent, leading to much superior notch-toughness properties.

(*c*) *Simulation to a Peak Temperature of* 1,070°C. The microstructure produced by this treatment (Fig. 15), was similar to the equivalent specimen in BS 1501. The notch-toughness properties had deteriorated slightly from those of the specimen cycled to 893°C, but were still better than the parent material properties.

(*d*) *Simulation to a Peak Temperature of* 1,305°C. A coarse Widmanstätten structure was produced by this treatment (Fig 16) similar to the equivalent specimen in BS 1501. The notch-toughness properties were considerably reduced, and the transition temperature was about 25°C higher than that of the parent plate.

The Effect of Restraint on Mechanical Properties

During welding, the HAZ undergoes an extremely complex strain cycle and the effects of this on the structure and proper-

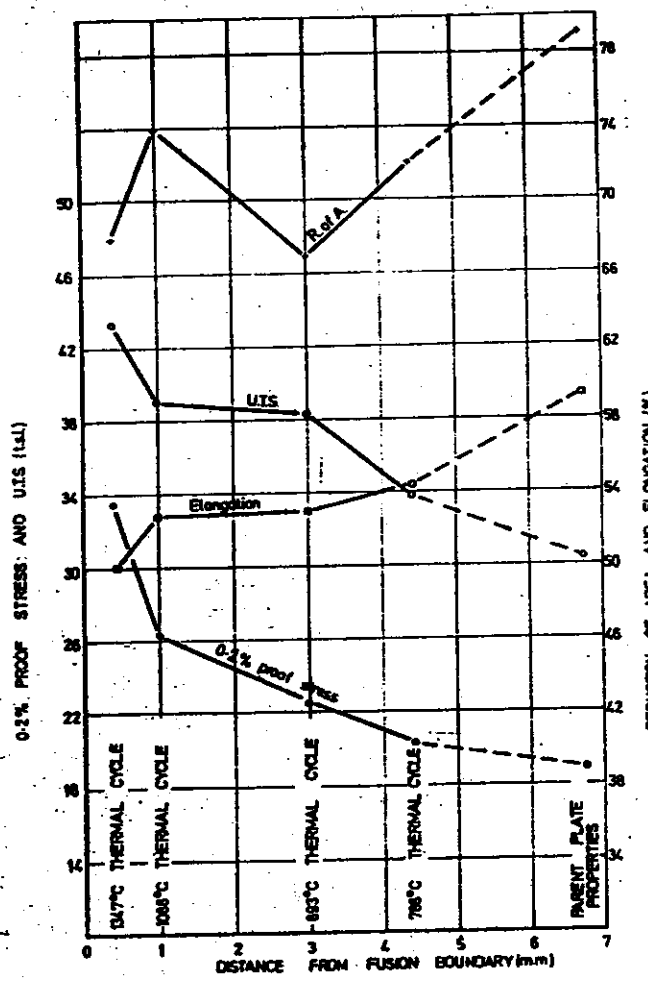

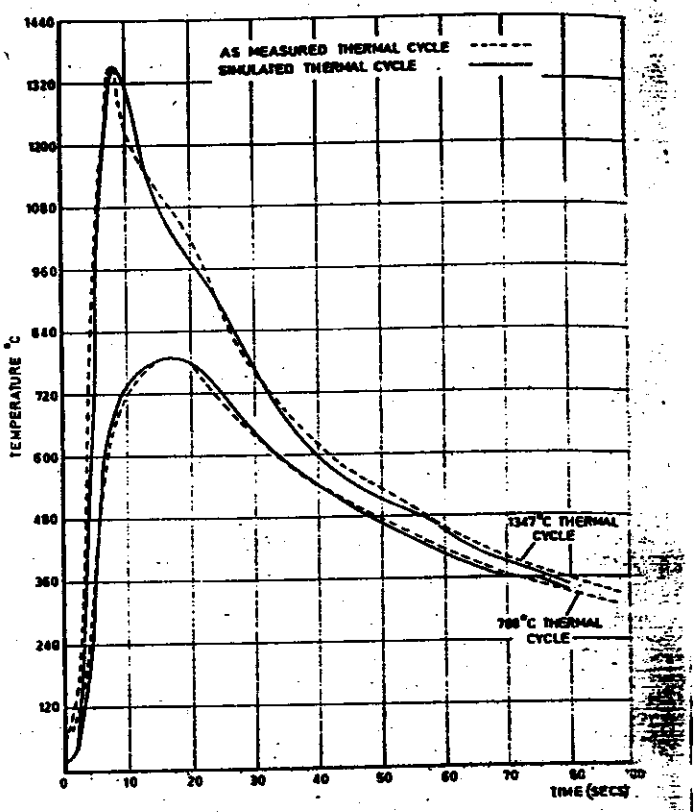

Fig. 23. (Left) Tensile properties of BS 1501 mild steel simulated specimens.

Fig. 24. (Above) Comparison of real and simulated thermal cycles.

ties are uncertain. Several workers [14–19] have observed the influence of an externally applied tensile stress and consequent plastic deformation on the isothermal transformation of austenite to ferrite and pearlite, bainite, and martensite. They found that the applied stress shortened the beginning and ending periods of transformation and accelerated the rate of transformation. Smallman[20] claimed that even elastic stresses, when applied above the M_s temperature and maintained during cooling, can affect the transformation behaviour. Uniaxial compression or tensile stresses raise the M_s temperature, while hydrostatic stresses lower the M_s temperature.

Hence it is possible that the temporary dynamic thermal stresses and strains produced in the HAZ during welding could affect significantly the resultant microstructure and its mechanical properties. This is particularly so in the neighbourhood of a defect where the stresses may be raised considerably. However, techniques to simulate HAZ structures containing defects were not employed in this work.

Because of the absence of reliable data on the strain cycles occurring in the HAZ, this problem has been tackled in a qualitative manner by applying a restraint during thermal simulation. No detectable changes in microstructure or mechanical properties were observed. This evidence is not conclusive since the nature and magnitude of the strains imposed in this approach are lower than those occurring during welding and much lower than those that could occur at the root of a stress concentrator.

Practical Significance of Results

This work has shown clearly the different effects of the weld thermal cycle on the HAZ properties of two mild steels manufactured to different levels of deoxidation. The fully-killed steel had markedly superior notch-toughness properties to the partially-killed steel in the unwelded condition. After welding, however, a marked deterioration in notch-toughness properties occurred in all regions of the HAZ in the fully-killed steel and in most cases these properties were inferior to the equivalent region in the partially-killed steel. By contrast, the partially-killed steel had better notch-toughness properties throughout most of the HAZ owing to the beneficial effects of grain refinement. However, in both steels very low notch-toughness occurred in the grain coarsened region owing to the coarse Widmanstätten structure and in this respect the partially-killed steel was distinctly inferior.

Conclusions

1. The non-equilibrium conditions attending a submerged-arc bead-on-plate weld in 1½ in. thick mild steel plate at a heat input of 108 kJ/in. resulted in an increase of approximately 35°C in the Ac_1 temperature and of approximately 75°C in the Ac_3 temperature.

2. The weld HAZ of mild steel could be divided into three distinct regions. These were: (a) the region of grain coarsening, (b) the region of grain refinement, and (c) the region of partial transformation. In addition there was a very narrow region at the low temperature boundary of the HAZ in which spheroidization of the carbides had taken place.

3. The peak hardness occurred in the region of grain coarsening and decreased on moving away from the fusion boundary.

4. Metallographic examination and hardness measurements indicated that the simulated structures were directly comparable to the equivalent ones in the actual weld HAZ.

5. In the BS 1501 material a decrease in notch-toughness occurred in all regions of the HAZ. The poorest properties were associated with the coarse-grained region and the partial transformation region. Embrittlement in the partial transformation region was due to the formation of feathery upper bainite, and in the grain coarsened region to the formation of a very coarse Widmanstätten structure containing proeutectoid ferrite and acicular upper bainite.

6. In the BS 1501 material, the proof stress, tensile strength and hardness increased continuously with increasing peak temperature of simulation, also with a decrease in ductility.

7. In the BS 15 material an improvement

notch-toughness properties occurred on simulation to peak temperatures of 788°C, 895°C and 1,070°C, and this was associated with a refinement of the ferrite grain size. Simulation to a peak temperature of 1,305°C reduced the notch-toughness properties owing to the formation of a very coarse Widmanstätten structure.

References

1. Nippes, E. F., and Savage, W. F., *Weld. Jnl.*, 1949, 28, 534-s.
2. Inagaki, M. *et al. Trans. Nat. Res. Inst. Met.* (Japan), 1964, 6, 39.
3. Watkins, B. *et al. Brit. Weld. Jnl.*, 1966, 6, 350.
4. Nippes, E. F., *Weld. Jnl.*, 1959, 38, 1-s.
5. Wilson, J. E. B., D.A.E. Thesis, College of Aeronautics, Cranfield, 1964.
6. Apblett, W. R., *et al. Weld. Jnl.*, 1952, 31, 421-s.
7. Severin, D., "The Metallurgy of Welding", Chapman and Hall, 1962.
8. Lancaster, J. F., "The Metallurgy of Welding, Brazing and Soldering", George Allen & Unwin Ltd., 1965.
9. Coward, M. D., and Apps, R. L., CoA Note, Met. No. 13, College of Aeronautics, Cranfield, 1967.
10. Clifton, T. E., and George, M. J., CoA Note, Met. No. 18, College of Aeronautics, Cranfield, 1968.
11. Smith, E., unpublished work, Cranfield, 1967.
12. Feuerstein, W. J. and Smith, W. K., *Trans. A.S.M.*, 1954, 46, 1270.
13. Altuzt, K. J., and Garber, S., *J.I.S.I.*, 1966, 204, 1,217.
14. Birla, L. B., *Trans. A.I.M.E.*, 1955, 179.
15. Bhattacharyya, S. and Kehl, C. L., *Trans. A.S.M.*, 1955, 47, 351.
16. Kehl, C. L. and Bhattacharyya, S., *Trans. A.S.M.*, 1958, 48, 234.
17. Porter, L. F., and Rosenthal, P. C., *Acta. Met.*, 1959, 7, 504.
18. Kanazawa, S., *Trans. Jap.I.M.*, 1963, 4, 195.
19. Wells, M. G. H. and West, D. R. F., *J.I.S.I.*, 1962, 200, 710.
20. Smallman, R. E., "Modern Physical Metallurgy" Butterworths, 1965.

FABRICATING EQUIPMENT NEWS

Arc Welding

Motor Generator Set—1

WELDING Industries Ltd. have introduced a new 375 A motor generator welding set. By eliminating shrouds, skirts and covers and by providing a leg in place of the wheel beneath the tow-bar it has been possible to provide the unit at a reduced cost. This set, the Armourweld DA324E diesel welding set, is powered by a Ruston 2YWA 27 hp air-cooled engine to provide an output of 35—375 A, 50—85 V. It will give continuous welding current of 300 A. The generator is of the "Brush Shift" type, controlled by a single hand wheel to give infinitely variable control over the current range. All rotating parts are statically and dynamically balanced. A central lifting point is provided for site work and the unit is mounted on a frame for towing. High speed Flexitor undergear and overrun brakes are incorporated. The unit can also be supplied as a static set. Overall dimensions are 7 ft 8 in. long, with tow bar, 4 ft 3 in. high and 3 ft 6 in. wide. Other engine versions can be supplied and electric starting is a further option.

Circle 167

Motorized Probe Slide—2

THE model SP-300 motorized probe slide introduced by Cecil Equipment Co. Inc. is used in conjunction with model CMS-10B, CMS-10A and CMS-9A, automatic guidance systems, to reference from one side wall of a deep groove while a welding head is being repositioned for making multi-pass welds. The probe slide allows: off-setting of the probe while making multi-pass welds; spacing of weld beads while maintaining automatic control of the welding head; final weld passes being made on tanks or vessels by using the probe slide for repositioning the probe to pick-up a new reference point. The slide is also used in a vertical position when welding beams having two or more web thicknesses in a single beam and still maintain automatic control of the welding head.

Circle 168

All-Position Electrode

THE Supercord electrode, marketed by Oerlikon Electrodes Ltd., which is suitable for welding in any position, and for vertically down contact welding, is available in sizes from 12—4 s.w.g. They are of the mild steel medium-coated rutile type and are suitable for general-purpose welding on mild steel applications such as pipework, tank work and sheet metal work. Mechanical properties of Supercord include a U.T.S. of 32 tonf/in.², yield point of 28 tonf/in.² and impact values (Charpy V notch) of 58—75 lbf.

Circle 169

Pressure Welding

Friction Welder—3

A NEW friction welding machine has recently been completed by Blacks Equipment Ltd., Friction Welding Division, for joining high speed tool bits to mild steel shanks in the production of twist drills. A feature of the machine is an automatic cutting head which removes the metal upset after welding. Following the turning operation the head withdraws into a recess below the chuck. With a drill of 1¼ in. diameter, the complete welding and flash removal cycle takes about 45 s. The machine is hydraulically operated through a flow control valve which ensures a constant feed rate during welding. This machine is being delivered to Firth Brown Tools Ltd.

Circle 170

1

2

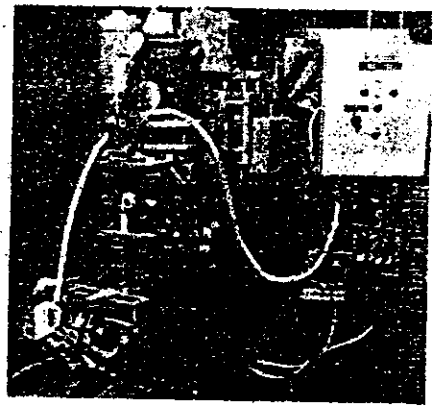

3